انتقال الحرارة بين جسمين في عملية الدرفلة

رسالة
قدمت إلى كليه الهندسة في جامعه بابل وهي جزء
من متطلبات نيل درجه ماجستير علوم في
الهندسة الميكانيكية

أعدت من قبل

محمد يوسف جبار

الجنابي

(حزيران ٢٠٠٤)

١٤٢٥ هـ ٢٠٠٤ م

HEAT TRANSFER BETWEEN TWO BODIES IN ROLLING PROCESS

A THESIS

SUBMITTED TO THE COLLEGE OF ENGINEERING OF THE UNIVERSITY OF BABYLON IN PARTIAL FULFILLMENT OF THE REQUIREMENTS FOR THE DEGREE OF MASTER OF SCIENCE IN MECHANICAL ENGINEERING

BY

Mohammed Yousif Jabbar

Al-Janabi

(B.Sc., ٢٠٠١)

(June ٢٠٠٤)

١٤٢٥ A. ***٢٠٠٤ A. M***

H

بِسمِ اللهِ الرَّحمنِ الرَّحيمِ

﴿وَيَسْئَلُونَكَ عَنِ الرُّوحِ قُلِ الرُّوحُ مِنْ أَمْرِ رَبِّي

وَمَا أُوتِيتُمْ مِنَ الْعِلْمِ إِلاَّ قَلِيلاً﴾

صَدَقَ اللهُ العَلِيِ العَظِيمِ

سورة الإسراء الآية(٨٥)

DEDICATION

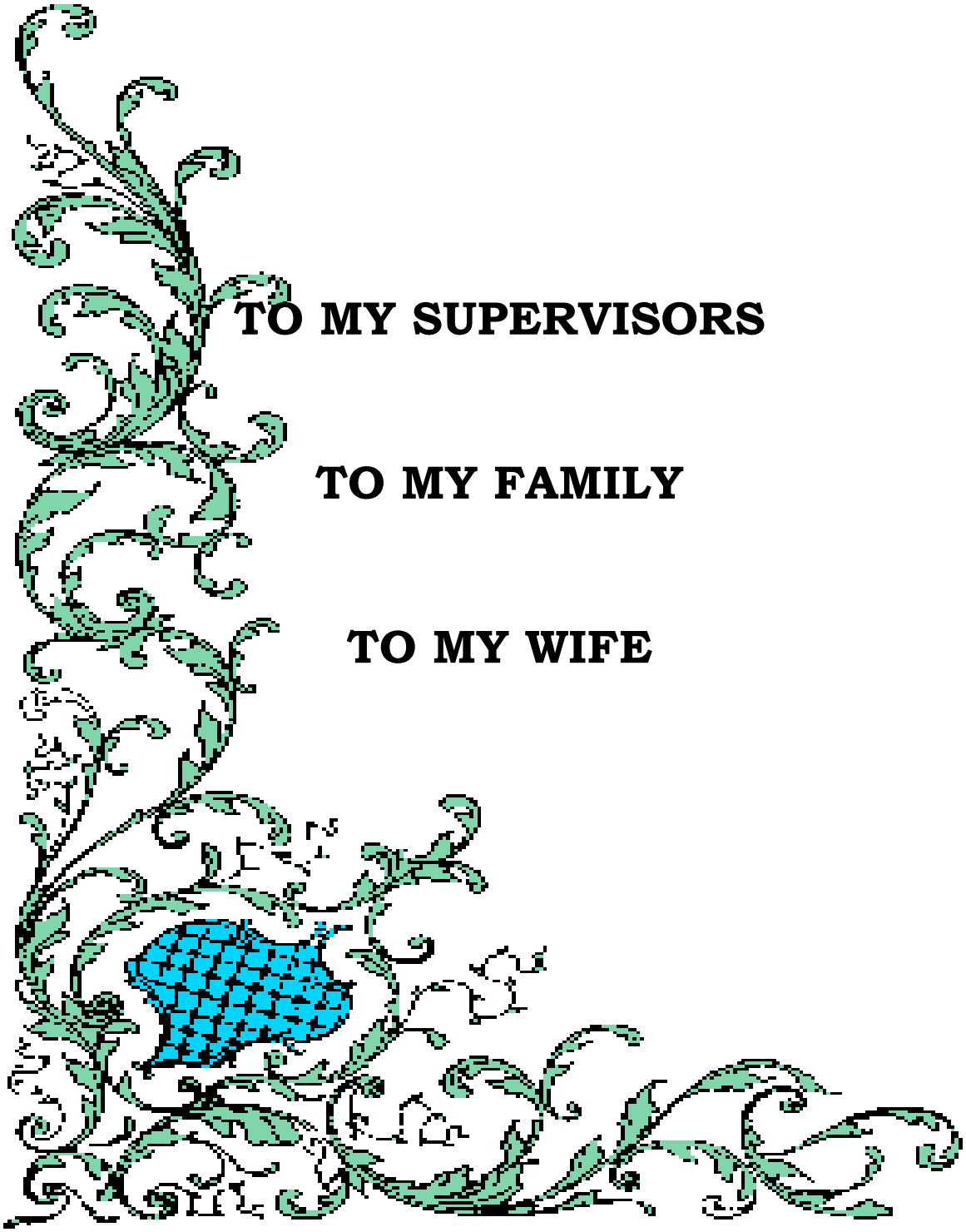

TO MY SUPERVISORS

TO MY FAMILY

TO MY WIFE

خلاصـــــــــــــة

في الدراسة ألحاليه تم عمل نموذج عددي لنمذجه التصرف الحراري لعمليه ألدرفله (Rolling Process). لقد استخدمت صيغه أو لرين (Eulerian Formulation) لتقليل عدد نقاط الشبكه (Mesh) اللازمة للنمذجه. وقد حصلنا على صيغه لحساب كل من عمق انتشار الحرارة (Heat Penetration Depth)، معامل انتقال الحرارة لمائع التبريد (Cooling Heat Transfer Coefficient)، جريان المعدن خلال عمليه الدرفلة (Flow of Metal in Rolling)، الحرارة المتولدة بسبب التشوه اللدن للمعدن والاحتكاك الذي يحصل بين الدرفيل والمعدن عند أسطح التلامس (Heat Generation by Plastic Deformation and Friction)، والظروف الحدودية النموذجية لحل النموذج (Typical Boundary Conditions).

لتسهيل حل المسالة، تم افتراض ثبوت السرعة الدورانيه للدرفيل وان التغيرات التي تطرأ على درجات الحرارة تكون على هيئه قشرة رقيقه (Very Thin Layer) على سطح الدرفيل. بسبب الشكل الدائري للمقطع الجانبي للدرفيل، ستكون الطريقة التقليدية للفروقات المحددة (Conventional Finite Difference Method) المبنية على أساس الإحداثيات القطبية (Polar Coordinates) هي الأكثر ملائمة والتي استخدمت لإيجاد توزيع درجات الحرارة للدرفيل. بالمثل، فأن صيغه الفرو قات المحددة المعمّمة (Generalized Finite Difference Method) قد استخدمت لنمذجه درجات الحرارة للمناطق التي تكون فيها خطوط الشبكه غير متعامدة (Non-orthogonal Mesh) والمتمثلة بالمنطقة التي يتشوه فيها المعدن (أي في داخل المعدن وعند سطح التلامس). لقد اختير نسق الفرو قات للنقاط المواجهة للجريان (Up-wind Differencing Scheme) للتغلب على عدم الاستقرار يه العددية الناتجة من السرع العالية أو عدد بكلت العالي (High Peclet Number) الذي تتضمنه عمليه الدرفلة. يتم إقران الحلين سويه، آي حل المعدن المدرفل (Strip) وحل الدرفيل (Roll) وحلهما آنيا (Simultaneously).

أما بالنسبة لعرض نتائج الدراسة الحالية، عرضت نتائج التصرف الحراري لحالتي الدرفلة على البارد وعلى الساخن ، نتائج توزيع السرع وتوزيع الحرارة المتولدة بالتشوه والاحتكاك بمقتضى الشروط الحدودية النموذجية لإيضاح امكانيه العمل ومقدرة النموذج الذي تم عمله(Developed Model).

وجد في الدراسه الحالية، أثناء تشوه المعدن (Strip)، أن مقدار درجه الحرارة في داخله تزداد بصوره مستمرة، وأن طاقة التشويه تسيطر عليها بصوره كبيره. من ناحية أخرى فأن درجه حرارة سطح المعدن تتغير بصوره أكثر أثاره والتي تكون طاقه الاحتكاك ودرجه الحرارة داخل الدرفيل تسيطر عليها بصوره رئيسيه. أن التبريد العالي الذي يتعرض له الدرفيل, سيكون له أثر كبير أشبه بالمغطس الحراري(Heat Sink). حيث عند اصطدام المعدن بالدرفيل فأن درجه حرارة سطح الدرفيل تهبط. بسبب حرارتي التشوه والاحتكاك اللتان تنشآن على طول سطح التلامس (Interface) أضافه إلى الحرارة المنتقلة من الطبقة المجاورة للمعدن المشوه فأن درجه حرارة سطح المعدن ترتفع بسرعة.

أخيرا، نتائج توزيعات درجه الحرارة والحرارة المتولدة بسبب التشوه والاحتكاك التي تم التوصل لها قورنت بنتائج عمل مسبق للتحقق من مدى صحة الحل العددي. لقد وجد توافق جيد من المقارنة بين النتائج المحسوبة من البحث الحالي والنتائج المحسوبة في عمل مسبق.

ACKNOWLEDGMENTS

(In The Name of Allah, The Gracious, The Merciful)

First of all, I would like to express my deep thanks and gratitude to my supervisors, ***Dr. Ihsan Y. Hussein & Dr. Tahseen A. Al-Hattab*** *especially for* ***Dr. Emad S. Ali*** *for their great support, guidance, advice and assistance throughout the various stages of the present work.*

I would like also to thank all the staff of mechanical engineering and advance computer laboratory for the facilities during my work.

I record my sincere gratitude to my family and to my friends for their encouragement and support during the period of preparing this work.

Finally, I am grateful to all those who have helped me in carrying out this research.

M. Y. Jabbar

ABSTRACT

In the present study, an efficient numerical model has been developed to model the thermal behavior of the rolling process. An Eulerian formulation is employed to minimize the number of grid points required. The approaches to obtain the heat penetration depth, the convection heat transfer coefficient of cooling, the flow of metal through the roll gap, the heat generation by plastic deformation and friction, and the boundary conditions are then discussed.

The roll is rotate at constant speed and the temperature variations are assumed to be cyclically steady state and localized with a very thin layer near the surface. The Conventional Finite Difference Method (CFDM) based on cylindrical coordinate is more convenient and therefore is used to model the roll because of the circular geometry of the roll. Also, A generalized Finite Difference Method (GFDM) is employed to allow use of a non-orthogonal mesh in the deformed strip region and the roll-strip interface area. An up wind differencing scheme is selected to overcome the numerical instability resulting from the high velocity (high Peclet number) involved in the rolling process. The equations of the strip and roll are then coupled together and solved simultaneously.

Both cold and hot rolling heat transfer behaviors, velocity distribution, and heat generation by deformation and friction under typical rolling conditions are presented to demonstrate the feasibility and capability of the model developed.

It has been found that, while the strip is under deformation, the bulk temperatures inside the strip increase continuously; this is largely controlled by the deformation energy. On the other hand, the strip surface temperature changes

much more drastically and it is mainly controlled by the friction heat and the roll temperature. The roll acts like a heat sink, because the coolant heavily cools it.

Thus, as soon as the strip hits the roll its surface temperature drops. Since considerable friction and deformation heat are created along the interface and transferred from the neighboring sub layer, the surface temperature picks up rapidly.

Finally, the results of the temperature distributions for both cold and hot rolling and the heat generation by deformation and friction obtained from the present study are compared with previous study to verify the validity of numerical solution. It has been found that a good agreement is obtained from the comparison between the results of the present study and the results of previous published works.

List of Contents

Subject		*Page*
ACKNOWLEDGEMENTS		**I**
ABSTRACT		**II**
LIST OF CONTENTS		**IV**
NOMENICLATURE		**VII**
CHAPTER ONE-INTRODUCTION		
١.١	General.	١
١.٢	Objectives.	٣
CHAPTER TWO-LITERATURE REVIEW		
٢.١	Theoretical Methods.	٦
٢.٢	Experimental Methods.	١٦
٢.٣	Scope of the Present Work.	١٧
CHAPTER THREE-MATHMATICAL ANALYSIS		
٣.١	Geometry and Coordinate System.	١٨
٣.٢	Assumptions.	١٩
٣.٣	Governing Equations.	٢٠
٣.٣.١	Energy Equations.	٢٠
٣.٣.١.١	Strip Energy Equation.	٢٠
٣.٣.١.٢	Roll Energy Equation.	٢٠
٣.٣.٢	Heat Penetration Depth.	٢١
٣.٣.٣	Cooling Heat Transfer Coefficient.	٢٣
٣.٣.٤	Flow of Metal in Rolling.	٢٥
٣.٣.٥	Heat Generation by Plastic Deformation and Friction.	٣٠
٣.٤	The Boundary Conditions.	٣٤
٣.٥	Methods of Solution.	٣٨

CHAPTER FOUR-NUMERICAL SOLUTION		
٤.١	Grid (Mesh) Generation.	٤٦
٤.٢	Generalized Finite Difference Method (GFDM).	٥٠
٤.٣	Numerical Formulation.	٥٠
٤.٣.١	Governing Equations Representation.	٥١
٤.٣.١.١	Strip Governing Equation Representation.	٥١
٤.٣.١.٢	Roll Governing Equation Representation.	٥٦
٤.٣.٢	Boundary Conditions Representation.	٥٨
٤.٤	Numerical Calculations Algorithm.	٦٠
٤.٥	Computer Program.	٦١
٤.٥.١	Program Input Data.	٦٢
٤.٥.٢	Program Output Data.	٦٣
٤.٥.٣	Program Specifications.	٦٣
CHAPTE FIVE-RESULTS AND DISCUSSION		
٥.١	Numerical Results.	٧٢
٥.١.١	Grid Size.	٧٢
٥.١.٢	Numerical Results of the Program.	٧٣
٥.١.٢.١	Results of the Velocity Distribution.	٧٤

٥.١.٢.٢	Results of the Heat Generation by Deformation and Friction.	٧٤
٥.١.٢.٣	Results of Cold Rolling Temperature Distribution.	٧٦
٥.١.٢.٤	Results of Hot Rolling Temperature Distribution.	٧٨
٥.٢	Verification of Computational Model.	٨٠
٥.٢.١	Comparison with Published Work.	٨٠
٥.٢.١.١	Comparison with the Temperatures of Cold Rolling.	٨٠
٥.٢.١.٢	Comparison with the Temperatures of Hot Rolling.	٨١
٥.٢.٢	The Concluding Remarks from the Comparisons.	٨١

CHAPTER SIX-CONCLUTIONS AND SUGGESTIONS FOR FUTURE WORK		
٦.١	Conclusions.	١٠٠
٦.٢	Suggestions for Future Work.	١٠١
References		١٠٢

Nomenclature

The following symbols are used generally throughout the text.

Others are defined as when used.

Symbol	*Description*	*Unit*
A	Area.	cm^2
Bi	Biot Number.	-
C	Thermal Resistance Parameter.	-
c	Specific Heat.	$KJ/kg.^oC$
d	Jet Diameter.	cm
F	Tangential Force.	N
H	Heat Transfer Coefficient.	$W/cm^2.^oC.$
h	Half Thickness of Strip.	cm
J	Mechanical Equivalent of Heat.	kJ/kcal
k	Thermal Conductivity.	$W/cm.^oC$
L	Length of the Arc of Contact.	cm
l	Distance from Spray Jet to Roll.	cm

n	Out ward normal to the boundary, or refer to the number of divisions.	-
P	Pressure.	N/cm^{2}
Pe	Peclet Number.	-
Q	Heat Generation.	kW
q	Heat Generation Rate, kW per Unit Volume or area.	kW/cm^{3} or kW/cm^{2}
R	Roll Radius.	cm
r	Radial Coordinate.	cm
Re	Reynolds Number.	-
T	Temperature.	^{o}C
t	Thickness.	cm
u	Velocity in *x*-Direction.	cm/s
V	Velocity.	cm/s
v	Velocity in *y*-Direction.	cm/s
W	The Width of the Strip.	cm
x	Horizontal Coordinate.	cm
y	Vertical Coordinate.	cm

Abbreviations

CFDM	Conventional Finite Difference Method.	-
CFDR	Conventional Finite Difference for Roll.	-
Coef.	Coefficient.	-
Dev. %	Deviation Percent.	-
Eq.	Equation.	-
Fig.	Figure.	-
GFDF	Generalized Finite Difference for the Node at the Interface.	-

GFDM	Generalized Finite Difference Method.	-
GFDIN	Generalized Finite Difference for Internal Nodes.	-
ndr	Number of Divisions in the *r*-Direction.	-
ndthbr	Number of Divisions in the θ-Direction in Bite Region for Roll.	-
ndthr	Number of Divisions in the θ-Direction for Roll where the Cooler is Impact.	-
ndy	Number of Divisions in the *y*-Direction.	-
ndxb	Number of Divisions in the *x*-Direction in the Bite Region.	-
ndxl	Number of Divisions in the *x*-Direction in the Billet Region.	-
ndxp	Number of Divisions in *x*-Direction in the Product Region.	-
Ref.	Reference.	-
Temp.	Temperature.	^{o}C
Tran.	Transfer.	-
Vol.	Volume.	cm^{3}

Greek Symbols

α	Thermal Diffusivity.	cm^{2}/s
ρ	Density.	kg/cm^{3}
τ	Time.	s
∇	Laplacian Operator.	-
ω	Roll Angular Velocity.	rad/s
δ	Heat Penetration Depth.	cm
Φ	Bite Angle.	Degree

υ	Kinematics Viscosity.	$cm^{۲}/s$
σ	Plain Strain Yield Stress.	$N/cm^{۲}$
ε	Local Strain Rate.	$۱/s$
η	Efficiency of the Deformation Energy to Converted to Heat.	-
μ	Coefficient of Friction.	-
β	Angle Specified the Direction.	Degree
θ	Circumferential Coordinates.	rad
λ	Weighting Factor.	-

Subscript

b	Boundary.	-
d	Deformation.	-
eff	Effective.	-
f	Final.	-
fr	Friction.	-
i	Neighboring Points or Index.	-
n	Neutral Point.	-
o	Uniform or Original.	-
r	Roll.	-
s	Strip.	-
$slip$	Slip.	-
∞	Coolant or Ambient Conditions.	-

Superscript

*	Dimensionless Quantity.	-

١ *Introduction*

١.١ *General*

The process of plastically deforming metal by passing it between rolls is known as Rolling, Dieter [١]. Rolling is one of the oldest metals working process in industry. In view of tremendous amount, wide variety of rolled products are manufactured and closed control of final product every year. It can be considered as one of the most important of manufacturing process. Numerous investigations, numerical, analytical, and experimental have been carried out on rolling as mentioned by Guo and Kobayashi [٢].

In conventional hot or cold rolling the main objective is to decrease the thickness of the metal. Ordinarily little increase in width occurs, so that decreases in thickness will result in an increase in length.

Then, in deforming metal between rolls, it is subjected to high compressive stresses from squeezing action of the rolls and to surface shear stresses as a result of friction between the rolls and the metal, the frictional forces are also responsible for drawing the metal into the rolls. The cold rolling of metals has reached a position of major importance in industry.

A rolling machine consists of rolls, bearings, a housing for containing these parts, and a drive for applying power to the rolls and controlling their speed as shown in Fig. (١-١). The forces involved in rolling can easily reach large numbers as shown in Table (١-١). Therefore, a very rigid construction is needed,

and very large motors are required to provide the necessary power. When these requirements are multiplied several times for the successive stands of a large continuous machines, it is easy to see why a modern rolling-machine installation demands many millions of dollars of capital investment and many man-hours of skilled engineering design and construction.

In the past, the heat generation during the plastic deformation of the test sample was ignored and initial sample temperature was given to be the test temperature as predicted by Remn [٤].

As predicted by Lahoti and Altan [٥], the energy consumed in plastic deformation is transformed largely into heat while a small portion of the energy is used up in deforming the crystal structure in material. This heat generation coupled with heat transfer within the deforming material and to the environment gives a temperature distribution in the deformed peace.

As mentioned by Karagiozis and Lenard [٦], a ± ١ percent variation of the temperature may well cause ١٠٪ change in strength, which in turn will cause significant change in mill loads. As well as, the adequate cooling of roll and the rolled products is of a considerable concern to rolls designers and operators. Improper or insufficient cooling not only can lead to shorten roll life, due to spalling caused by thermal stresses, but it can also significantly affect the shape or crown of the roll and result in buckled strips or bunted edges.

Also, knowledge of roll and strip temperatures can contribute insights about metalurgical structure of the work-piece, and eventually lead to better control of the material properties and surface conditions.

The lack of practical mathematical model to simulate thermal behavior of the metal rolling process has forced mill operators and designers to rely on plant experience and testing, which is time consuming, not ideal for industrial applications, and expensive. As result from the furthermore simplified

assumptions demanded in the analytical solutions then, it is offer the fastest way to calculate temperatures, but do not provide predictions with sufficient accuracy. On the other hand, numerical models with fine meshes can give detailed information on the temperatures.

In the present study, while the deformation heat generation in the strip and the friction heat generated at the roll strip interface and the heat removed by the coolant to ambient air then, the strip and the roll should be solved simultaneously. A good understanding of the thermal aspects of the process is essential then, the influence of cooling practice on the roll is consider too.

Rolling machines can be conveniently classified with respect to the number and arrangement of the rolls as shown in Fig. (١-٢). In the present study, the simplest and most common type of rolling mill is the two-high roll is considered, see Fig. (١-٣).

The purpose of the present study is to effectively analyze the thermal behavior of rolling process for hot and cold rolling for two cases of rolling conditions, see Fig. (١-٣), by using a suitable numerical methods.

١.٢ *Objectives*

The following are the main objectives of the present work:

١. Developing a mathematical model for the rolling contact heat transfer problem to calculate heat transfer rate and temperature distribution of the solids (strip & rolls).

٢. Numerical solution of the governing equations obtained in (١- above) by using a suitable numerical method.

٣. Parametric study to investigate the effect of a number of parameters of the problem, such rolling speed, environmental conditions and hot and cold rolling.

٤. Verification of the proposed computational algorithm through a comparison with published data.

٥. Discussion of the results for final conclusions and recommendations.

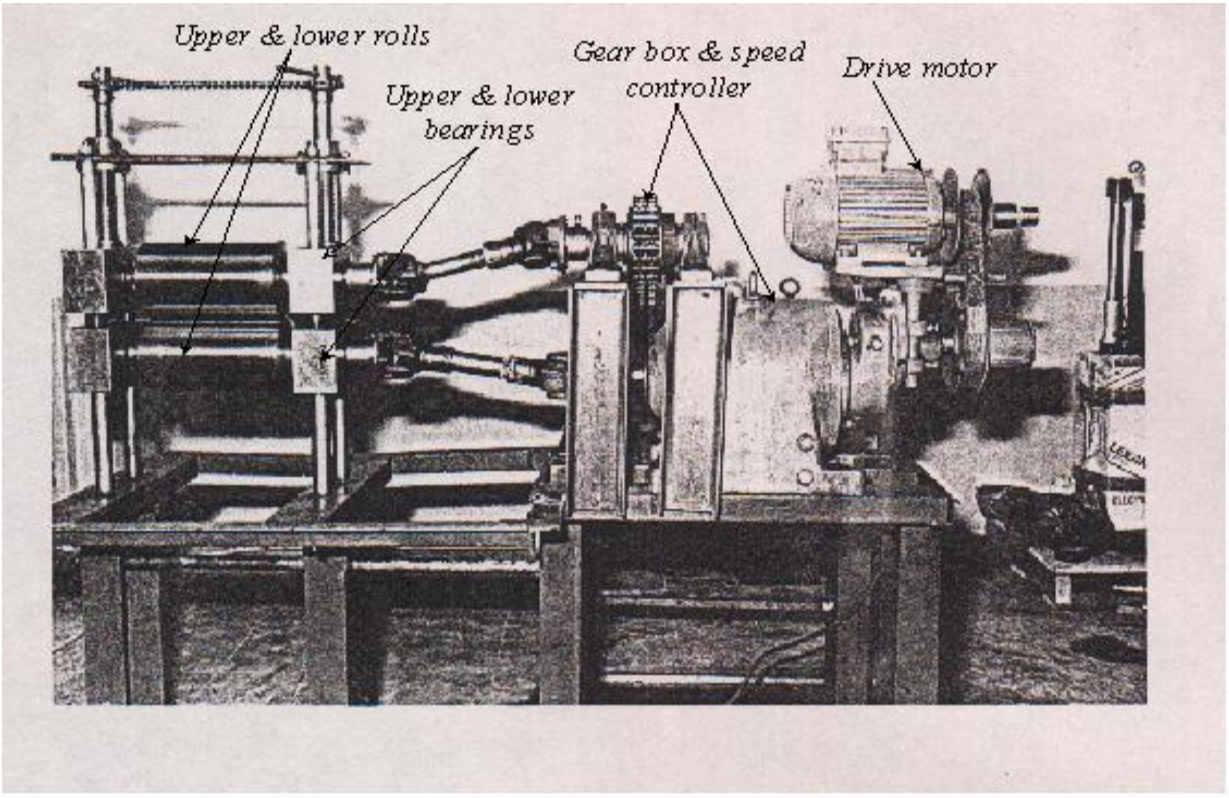

Fig. (1-1): Detail of Strip Rolling Fixture.

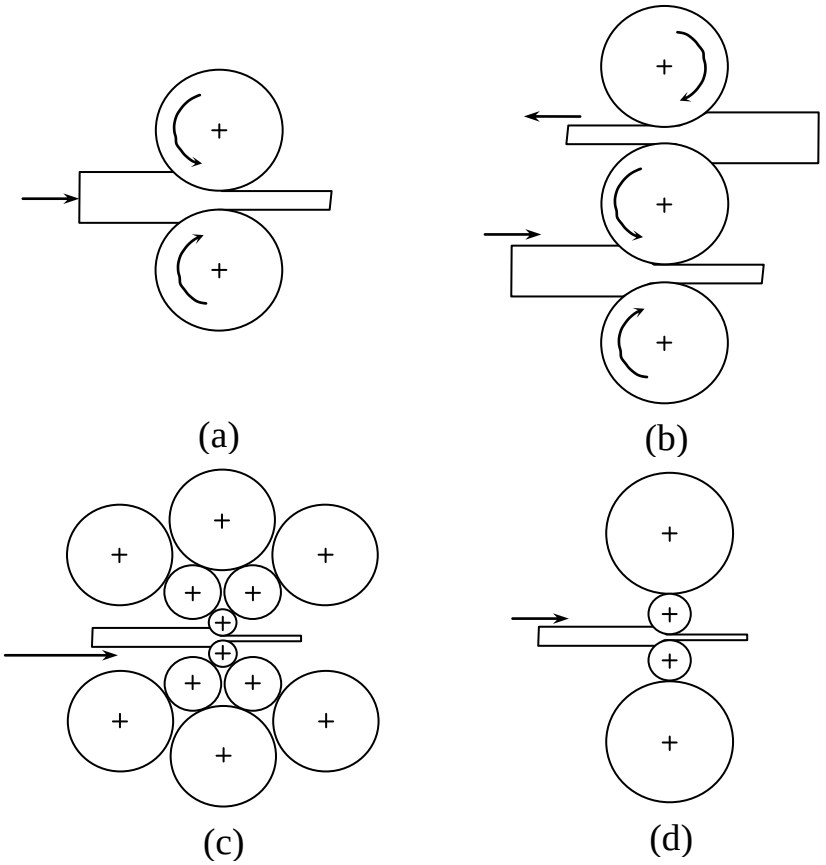

Fig. (١-٢): Typical Arrangements of Rolls for Rolling Process (a) Two High. (b) Three High. (c) Cluster. (d) Four High. Ref. [١].

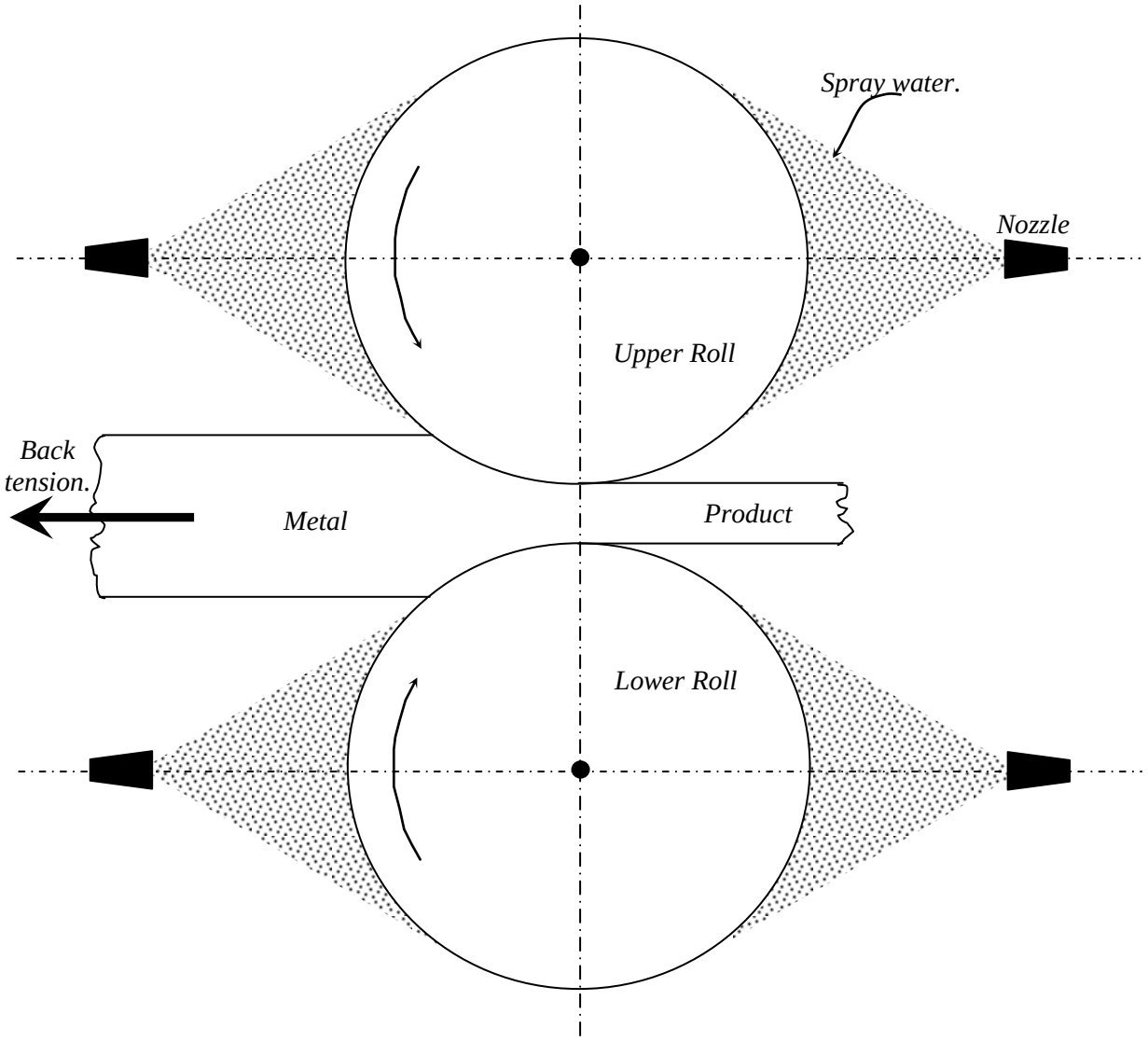

Fig. (١-٣): Typical Arrangement of Rolls for Rolling Process.

Sample Number	Initial Strip Thickness mm	Final Strip Thickness mm	Reduction Percent	Roll Separating Force, KN/m	
				Measured	Calculated
١	٦.٢٧٤	٥.٣٨٥	١٤.١٧	٦٤٧.٣	٧٣٧.٦
٢	٦.٢٧٤	٤.٩٠٠	٢١.٨٦	١٠٦٥.٤	٩٨٩.٣
٣	٦.٢٧٤	٤.٤٤٥	٢٩.٤٠	١٤٩٩.٠	١١٩٧.٥
٤	٢.٠٣٢	١.٣٤٦	٣٣.٧٥	١٢٣٤.٩	٩٩٥.٥

Table (١-١), Measured and Calculated Roll Separating Forces in Cold Rolling, Ref. [٣].

Roll Material: Steel — Strip Material: Aluminum

Roll Radius = ٧٩.٣٧٥ mm — Roll Surface Speed = ٠.١٦ m/s

٢ *Literature Review*

A number of mathematical models of hot or cold rolling have been Published in the literatures. These models have been investigated widely by using a variety of analytical, numerical, and experimental techniques. The review made here in is classified into theoretical and experimental methods.

٢.١ *Theoretical Methods*

These methods include the analytical and numerical methods uses to solve the temperature distribution for different manufacturing process and different boundary conditions. Some of the literature work that used these methods are presented here;

Johnson and Kudo [٧] used upper bound solutions for the determination of the temperature distributions in fast hot rolling and axi-symmetric extrusion process. By using realistic upper bound solutions, it is possible to estimate instantaneous temperature distributions throughout a mass of material, which is being fast plastically deformed. It became possible, by approximating a given slip line field solution and so treating it as an upper bound, to determine the distribution of temperature throughout the deforming mass. This approach is subjected to a certain amount of inexactness, because there is other features at that time. An upper bound solution provides loads, which are overestimated. The upper-bound solutions, which consist of a system of fictional tangential velocity discontinuities, can be made to approximate slip line field solutions as close as

required, and assuming a slip line solution to be the most accurate solution. For particular hot rolling process an estimate of this distribution has been made and in part to justify the use of the method employed. The results of calculations of the deformation of an initially square grid and a calculation of the necessary roll torque and roll pressure distribution are given in this work. Furthermore the method of upper bound solution may be used to calculate the velocity distribution for non-uniform compression of cylinder. Two particular instances of axi-symmetric process are examined, firstly for extrusion through a square die two forms of velocity field are presented and the results predicted there from are compared. Secondly, extrusion through a smooth conical die was examined.

Cornfield and Johnson [٨] studied theoretical predictions of plastic flow in hot rolling including the effect of the various temperature distributions. The three types of the temperature distribution were consider, the first type was hot surface cold interior, second type was cold surface hot interior and third type was non-uniform temperature distribution. The non-uniform temperature distribution were computed for a typical size mild steel slab, using finite difference formulation to the one dimensional heat transfer equation because the thickness of the slab is small compared with its width and length. This work therefore is first concerned with calculation of specific temperature distributions in heat stock. Secondly, an interpretation of the strain and strain rate distribution during rolling deformation is given, and this is combined with the third aspect of this study, namely how particular temperature patterns affect deformational behavior.

Lahoti and Altan [٥] predicted the temperature distribution in axi-symmetric compression and torsion. Two numerical methods were used, one for axi-symmetric compression and the other for axi-symmetric torsion, to predict non-steady state temperature fields in these deformation processes. In compression, the upper bound method has been used to determine the velocity field prior to temperature calculations. In both compression and torsion, the

predicted temperatures agree well with experimental data obtained by other workers. The compression analysis has been also used for investigating the effect of friction upon temperatures and the effect of ram speed upon metal flow and temperatures. The results of these investigations indicate that the numerical approach predicts, within approximations, the trends observed in experimental studies.

Lahoti *et al.* [٣] described the principles and the applications of two models developed for predicting the significant variables of the strip rolling process. The first model is computer program (ROLING) can estimate the roll separating force, roll torque, plastic deformation in the strip, elastic compression and recovery of the strip before and after rolling, and the elastic deformation of the rolls. The second model is computer program (ROLTEM) can estimate the metal flow and temperatures in strip rolling under unsteady state conditions.

At (τ=٠), it was assumed that the strip was fed in up to the exit plane. Then the deformation was approximated as taking place in steps of time interval ($\Delta\tau$) as;

$$\Delta T_d = \frac{\sigma_s \varepsilon_{eff} \Delta\tau}{J c_s \rho_s} \cdot \frac{\eta}{100} \qquad \ldots(٢\text{-}١)$$

where subscript (s) refers to the strip; (ΔT_d) change in temperature due to deformation; (ε_{eff}) is the effective strain rate; (σ_s) is the plain strain yield stress, (c) is the specific heat; (ρ) is the density; (J) is the mechanical equivalent of heat=٤.١٨٥ kJ/kcal and (η) is ($85 \le \eta \le 95$) percent of the deformation energy is transformed to heat. The maximum value of ($\Delta\tau$) is determined from the stability criterion. From the velocity field, it was possible to determine the position of each point before time interval ($\Delta\tau$). These calculated temperatures at each grid point before ($\Delta\tau$), the corresponding temperature increases due to plastic deformation and friction are added then;

$$\Delta T_{fr} = \frac{\mu P_r V_{slip} F \Delta\tau}{Jc_s)_b \gamma_s)_b Vol_s)_b} \qquad \ldots(٢-٢)$$

where the subscript (*b*) refers to the boundary; (ΔT_f) change in temperature due to friction; (V_{slip}) is the slip velocity at the boundary; (γ) is the specific weight; (*Vol*) is the volume of the element at the; (μ) is the coefficient of friction; (P_r) is the roll pressure and (*F*) is the horizontal force act on the boundary.

Using these new calculated values of temperatures as initial temperatures ($T_{i,j}$) heat transfer in the strip and roll is consider during ($\Delta\tau$) and the temperatures ($T_{i,j}^{`}$) are calculated. The repetitions of these sequence of the instantaneous of heat generation by deformation and transportation and static conditions during the time interval ($\Delta\tau$) gives the temperature distribution in strip rolling at any instant (τ). This procedure has been computerized in the system of computer program called (ROLTEM).

Sheppard and Wright [٩] developed a finite difference technique to predict the temperature profile during the rolling of aluminum slabs. The experimental results show substantial agreement with the theory. It was shown that such variations affect the mechanisms determining the development of structure and that structural variations exit throughout the slabs on exit from the roll gap. Qualitatively, these variations agree with predicted variations in temperature compensated strain rate. The effect of (Mg) as an alloying element is to reduce the possibility of formation of equiaxed subgrains resulting in an elongated substructure.

Zienkiewicz *et al.* [١٠] submitted a general formulation for coupled thermal flow of metal for extrusion and rolling process by using the finite element method. A finite element formulation was used to deal with the flow of metals coupled with thermal effects. The deformation process of the metal was

treated using the visco plastic flow approach and the solution technique for the coupled problem implies simultaneous solution for velocities and temperatures.

Some aspects of the numerical solution of the problem are given in the last part of this work. Some steady state extrusion and rolling problems show the applicability of this method.

Patula [١١] attained steady state solution for the temperatures in a rotating roll subjected to surface heat fluxes and convective cooling.

Patula submitted this work to determine the influence of cooling practices on roll temperature. A mathematical model was developed that determines the two dimensional (radial and circumferential) steady state temperature distribution in a rotating roll subjected to constant surface heat input over one portion of the circumference and convective cooling over another portion of the circumference.

The model is analytical in nature, as opposed to a direct numerical simulation, which enables extensive parametric studies to be performed conveniently. The solution technique can be used to solve numerous problems involving any combination of surface boundary conditions that have, at most, a linear dependence with respect to the surface temperature. With the use of the principle of superposition, the present solution can be utilized to solve problems that have various regions of the surface with constant heat fluxes. Results of these analyses indicate that for normal cold rolling situations during steady operation, the (heat penetration depth) heating and cooling that occur during every roll revolution is usually less than (٤) percent of the radius. Furthermore, the bulk of the roll is at a uniform temperature that can be calculated quite accurately by neglecting all internal temperature gradients. The location of the cooling regions relative to the heat-input regions has little effect on the bulk roll temperature in this situation. This approximation would be useful for computing bulk roll temperature, which could be utilized in future models for determining thermal

crowns, but would not be suited for determining accurate temperature at the roll surface.

Bryant and Heselton [١٢] found that the knowledge of heat transfer mechanisms in hot rolling was essential to the study of many areas of the process. This process including roll pacing, slab and strip temperature control, roll thermal camber effects on strip shape, thermally induced stress fatigue in rolls, and temperature dependent yields stress effects on roll force, power, and torque. Mathematical models which can be used to estimate temperature distributions within the rolls and steel strip on a hot roll were described in this work. The roll temperature model is an extension of a theoretical study based on the idea of "rotating line sources of heat", and the slab-strip modeling based on the theory of heat conduction in a "semi infinite body".

Bryant and Chiu [١٤] derived a simple model for the cyclic temperature variation set up within a work roll during the hot rolling process. The equations have been normalized so that they can be used easily for different roll dimensions, strip temperatures, roll cooling coefficients, and roll speeds. The model is sufficiently simple for it to be programmed, and provided solutions typically within (٥) percent of results obtained from more precise equations which can be solved only by using powerful computing facilities. The model is ideally suited for 'real-time' calculations or as part of a hot-roll simulation, providing a rapid solution to equations, which implicitly relate strip and roll temperatures in a train of rougher or finishing roll. The model was derived entirely from physical approximations and arguments, which incidentally provide considerable engineering insight into roll-heating phenomena. The model can be used to calculate internal roll-temperature distributions, and hence to estimate the cyclic stresses which occur within the roll.

Bryant and Chiu [١٤] derived a simple model for the cyclic temperature transients within hot rolling work rolls. The model takes into account variable convective cooling. It is far less demanding in calculation time than, say, models based on finite difference methods, and yet is sufficiently flexible to be applied to a wide range of techniques such as spray cooling, spray geometry, and roll heating phenomena. It can also be used to study temperature transients during cold roll condition, and steady state cyclic phenomena. The model can be used to estimate cyclic stress strain effects near the roll surface which are expected to play an important part in determining roll life and wear. It can be used as part of a larger design suite or for on-line calculations.

Tseng [١٥] submitted a simple but versatile numerical technique using generalized finite difference discretization for heat transfer problems involving high convective heat flow, irregular geometry and high local thermal gradients for roll and strip governing equations respectively;]

$$\frac{\omega}{\alpha_r}\frac{\partial T_r}{\partial \theta}=\frac{\partial^2 T_r}{\partial r^2}+\frac{1}{r}\frac{\partial T_r}{\partial r}+\frac{1}{r^2}\frac{\partial^2 T_r}{\partial \theta^2} \qquad \ldots(٢\text{-}٣)$$

and

$$u\frac{\partial T_s}{\partial x}+v\frac{\partial T_s}{\partial y}=\alpha_s\left(\frac{\partial^2 T_s}{\partial x^2}+\frac{\partial^2 T_s}{\partial y^2}\right)+q_d/\rho_s c_s \qquad \ldots(٢\text{-}٤)$$

where subscript (r) refers to the roll; (r,θ) are the cylindrical coordinate; (x,y) are the Cartesian coordinate; (ω) is the roll angular velocity and (u and v) are the horizontal and vertical velocities of the strip

Upwind differencing was utilized to stabilize the numerical oscillations often induced in convection-dominated heat transfer problems. An arbitrary irregular mesh scheme was adopted to treat the irregular geometry and to achieve high accuracy in zones having high thermal gradients. Then the temperature form of the internal strip nodes was;

$$T_{so}=\frac{q_d/\rho_s c_s-\sum_{j=1}^{2}\left(u_o F_{ij}+v_o F_{2j}-\alpha_s B_{3j}-\alpha_s B_{4j}\right)T_{sj}+\alpha_s\sum_{j=3}^{5}\left(B_{3j}+B_{4j}\right)T_{sj}}{u_o F_{1o}+v_o F_{2o}-\alpha_s\left(B_{3o}+B_{4o}\right)} \qquad \ldots(٢-٥)$$

And the temperature form of the boundary strip nodes was;

$$T_{so}=\frac{\alpha_s\sum_{j=1}^{4}\left(E_{2j}+E_{3j}\right)f_j-\left(u_o+a_2v_o\right)G_1 f_1-a_3v_o+q_d/\rho_s c_s}{\left(u_o+a_2v_o\right)G_o+a_1v_o-\alpha_s\left(E_{2o}+E_{3o}\right)} \qquad \ldots(٢-٦)$$

where subscript (o) refers to the uniform or original quantity; (α) is the thermal diffusivity; (q_d) is the heat generation by deformation and (F,B,E,G,a,f) are constants.

In order to demonstrate the validity of the formulation procedure, result predicted from this scheme was compared with analytical solution for a problem having a regular boundary. Application to atypical metal forming process having curved boundaries is then included such as rolling.

At the same year **Tseng [١٦]** submitted a numerical heat transfer analysis of strip rolling process and used the same finite difference technique that used in Ref. [١٥] but with other rolling dimensions and other cooling conditions. Good correspondence was found when the result of this analysis was compared with analytic solutions.

Dadras and wells [١٧] used a finite different solution for the transient heat transfer during axi-symmetric compression. The interfacial film between the die and the billet has been included in the analysis, and all modes of heat transfer have been taken into account. The result of a parallel experimental study has also been presented. The effects of geometrical and physical characteristics of the billet and the die on the heat transfer process, particularly on die heating, have been systematically investigated.

Tseng *et al.* [١٨] found that the proper roll cooling has been identified as a critical factor in the problem of excessive roll spalling and poor thermal

crowing in modern high speed rolling rolls for the following roll and strip governing equations respectively;

$$\frac{\omega}{\alpha_r}\frac{\partial T_r}{\partial \theta}=\frac{\partial^2 T_r}{\partial r^2}+\frac{1}{r}\frac{\partial T_r}{\partial r}+\frac{1}{r^2}\frac{\partial^2 T_r}{\partial \theta^2} \qquad \ldots(٢\text{-}٧)$$

and

$$\frac{\partial^2 T_s}{\partial y^2}-\frac{V_s)_{average}}{\alpha_s}\frac{\partial T_s}{\partial x}+\frac{q_d}{k_s}=0 \qquad \ldots(٢\text{-}٨)$$

As well as, an analytical model (Forier integral technique) has been developed to determine the temperature profiles of the roll and the strip simultaneously as;

$$\begin{aligned}T_r^*(r^*,\theta)=\frac{\Phi}{2\pi}+\frac{1}{\pi}\sum_{n=1}^{\infty}\{&M_o(A_n)M_o(A_n r^*)/[nD(A_n)]*\{\sin[\,\Theta_o(A_n)-\Theta_o(A_n r^*)\\&-n(\theta-\Phi)]+\sin[\,n\theta-\Theta_o(A_n)+\Theta_o(A_n r^*)]\}+A_n M_1(A_n)M_o(A_n r^*)\\&/[nD(A_n)Bi]*\{\sin[\,\Theta_1(A_n)-\Theta_o(A_n r^*)-n(\theta-\Phi)-\pi/4]\\&+\sin[\,n\theta-\Theta_1(A_n)+\Theta_o(A_n r^*)+\pi/4]\}\}\end{aligned}$$

$$\ldots(٢\text{-}٩)$$

and

$$\begin{aligned}T_s(x,y)=T_o+\frac{A}{3}+\left(q_d-\frac{q_s}{h(x)}\right)\frac{\alpha_s x}{k_s V_s)_{average}}+\frac{q_s h(x)}{2k_s}\left[\frac{1}{3}-\left(\frac{y}{h(x)}\right)^2\right]\\+\frac{4}{\pi^2}\left(\frac{q_s h(x)}{2k_s}+A\right)\sum_{n=1}^{\infty}\frac{(-1)^n}{n^2}\exp\left[-\left(\frac{n\pi}{h(x)}\right)^2\frac{\alpha_s x}{V_s)_{average}}\right]\cos\left(\frac{n\pi}{h(x)}y\right)\end{aligned}$$

$$\ldots(٢\text{-}١٠)$$

where superscript (*) refers to the dimensionless quantity; (T_o) is the strip entering temperature; ($A=(T_\infty-T_o)/[(y/h(x))^2(1+k_s/H_\infty h(x))]$); ($H_\infty$) is the ambient heat transfer coefficient; (k) is the thermal conductivity; ($h(x)$) is the instantaneous strip thickness; (V) is the velocity; (Φ) is the bite angle; (Bi) is the Biot number; ($A_n=\sqrt{nPe}$); (Pe) is the Peclet Number and (M_m and Θ_m) are the modulus and phase of Kelvin function and can be defined as;

$$M_m^2(A_n) = Ber_m^2(A_n) + Bei_m^2(A_n), \qquad m=0 \text{ or } 1 \qquad \ldots(2\text{-}11)$$

and

$$\Theta_m(A_n) = \arctan\left[\frac{Bei_m(A_n)}{Ber_m(A_n)}\right], \qquad m=0 \text{ or } 1 \qquad \ldots(2\text{-}12)$$

Here (Ber_m and Bei_m) are the real and imaginary parts of Kelvin functions respectively. The function of ($D(A_n)$) in Eq. (٢-٩) can be defined as ($D(A_n) = Z_1^2 + Z_2^2$), where

$$Z_1 = Ber_o(A_n) + \sqrt{nPe/2}[Ber_1(A_n) + Bei_1\ (A_n)]/Bi$$
$$Z_2 = Bei_o(A_n) - \sqrt{nPe/2}[Ber_1(A_n) - Bei_1\ (A_n)]/Bi \qquad \ldots(2\text{-}13)$$

This model used basic heat transfer theory and provided the capability of studying the influence of operating parameters on both the work roll and work piece temperatures. Examples on cold and hot rolling of aluminum alloys were given to demonstrate the feasibility and capability of the model developed.

Remn [٤] used the Laplace and inverse transform analytic technique to study the two dimensional unsteady thermal behavior of work rolls in rolling process. This work included the heat generated by the friction at the interface and by the deformation in the strip. It was found that the transient cooling behavior of the roll affects the temperature distribution and the thermal profile.

This article proposed a semi-analytical solution to solve the temperature field of the work roll that is subjected to various cooling and heating boundary conditions during a rolling campaign. The complete solution for various boundary conditions is superimposed by related individual solutions.

Chang [١٩] submitted an efficient way of calculating temperatures in the strip rolling process. Finite difference formulations were used in the rolling direction and analytical solutions were applied normal to this direction, making computational more efficient. Heat transfer in the sticking region was considered.

The influence of real area of contact on heat transfer is also taken into consideration, resulting in a method capable of modeling the strip rolling process

in any of several different lubrication regimes. This method provides good temperature predictions.

٢.٢ *Experimental Methods*

Lee *et al.* [٢٠] used an experimental program for predicting temperatures in continuous hot strip rolls. During the period from November (١٩٦١) to February (١٩٦٢) visits were made to five strip rolls in Britain, two in France, and one each in Belgium and Holland. Of these rolls six were wide strip rolls, two were medium strip rolls, and one askelp roll. All the rolls had continuous finishing trains and all were rolling mild steel strip of various widths and finishing thickness from (٠.١٢٨) in. down to (٠.٠٦٤) in. Measurements were made at each roll to determine the strip temperatures of individual slabs before each stand and to make as many measurements (exit gage, speed and power consumption of each stand) as possible of the roll parameters which were thorough to influence inter stand temperatures.

The experimental work done by **Karagiozis and Lenard [٩]** shows the dependence of the temperature distribution during hot rolling of a steel slab on the speed of rolling, reduction ratio and initial temperature were investigated. It was observed that while the center of the slab cools, the surface loses heat at a rate which significant re-heating occurs. The different parts of the slab receive significantly different thermal mechanical treatments, then it is possibly resulting in a non-homogeneous product.

In the experimental measurements, the measuring of the local temperature change in the bite could be a big challenge [١٦]. For instant, the total time that the strip passes through the bite lasts about (٠.٨) ms. A pyrometer response time less than (١٠٠) microseconds are required to detect this type of temperature changes. Similarly, in numerical analyses, if the mesh used in the bite area is relatively coarse, the temperature drop described before could also be difficult to predict.

٢.٣ *Scope of the Present Work*

Most of the forgoing models such as Zienkiewicz *et al.* [١٠] simulate either the roll or the strip alone. However, the rolling process involves the heat generated by deformation in the strip and friction at the roll-strip interface, and the heat removed from the rolls by coolant and ambient air. Therefore, the strip and the roll should be solved simultaneously.

Although, Lahoti *et al.* [٣] consider the strip and the roll simultaneously, the portion of the roll where cooling impinges was not modeled. So, their model cannot be used to study the influence of changing rolling practices, and artificial boundary conditions must be assumed along the radial boundary of the portion.

Moreover, their finite difference formulation requires an orthogonal type mesh, but the mesh actually was arranged non-orthogonal in the deformed strip region. Current numerical model are, therefore, either inefficient or have distinct limitations.

The present study enables extensive parametric studies to be performed at a reasonable time. It also represents the first step in Iraq up to extent of the present author knowledge, which permits on-line simulation in this field. The model considers some of the major processing parameters and has the capability of studying the influences of cooling practices on both the roll and work piece temperatures.

Finally, considering the heat transfer coefficient for spray cooling, deformation heat generation behavior and the interface friction behavior remain two of the greatest in certainties, the numerical model considered here may be the considered as a good compromise, despite some simplifying assumptions made in the model.

٣ *Mathematical Analysis*

The mathematical formulations of the problem will be presented in this chapter. The geometry, assumptions, governing equations and the boundary conditions, will be derived in terms of a suitable coordinate system.

٣.١ *Geometry and Coordinate System*

In order to solve the governing equations with their auxiliary relations, a proper choice of the coordinate system must first be made. For the problem studied in the present work, the non-orthogonal fixed coordinate system and fixed orthogonal coordinate system in the strip and in the roll is used respectively. In other words, x-y coordinates in the strip and r-θ coordinate in the roll are used in the present study, see Fig. (٣-١).

A metal strip with a thickness (t_o) enters the roll at the entrance. It passes through the roll gap and leaves from exit with a reduced thickness (t_f) as shown in Fig. (٣-١). From symmetry, only the upper half from the system needs to be considered in the present study and the upper and lower rolls were lifted by the bearings.

The roll has a radius (R) and rotates with an angular velocity (ω).

٣.٢ *Assumptions*

In order to solve the problem mathematically and numerically, certain simplifying assumptions were made and used. These are:

١. The strip and roll are long; therefore compared with the strip thickness; axial heat conduction can be neglected.

٢. The thermal properties (k&α) are uniform (isotropic) throughout the roll and strip and independent of temperature.

٣. The roll rotational speed is constant then, the steady state conditions are considered for both strip and roll.

٤. Since tremendous rolling pressure builds up in the interface then, the surface roughness became insignificant, and the film is very thin, on the order of micron, therefore, the thermal resistance of the film can be neglected.

٥. The roll has rigid circular geometry, in other words, neglects the flatness of the arc of contact.

٦. The interface friction follows the coulomb friction law with constant coefficient of friction, i.e., assuming constant friction coefficient.

٧. No increase in width, so that the vertical compression of the metal is translated into an elongation in the rolling direction.

٨. Uniform entry temperature.

٩. The deformation through any vertical section is assumed to be uniform in the strip.

٣.٣ *Governing Equations*

٣.٣.١ *Energy Equations*

٣.٣.١.١ *Strip Energy Equation*

The temperature field (T) of a moving body with homogenous and isotropic properties is governed by the partial differential equation expressing the conservation of energy, i.e.

$$\frac{DT}{D\tau} = \frac{\partial T}{\partial \tau} + V\nabla T = \alpha \nabla^2 T + q/\rho c \qquad \ldots(٣\text{-}١)$$

where ($D/D\tau$)is the substantial derivatives; (∇^2)is the Laplacian operator; (q) is the rate of heat generation per unit volume; and (α, ρ and c) are the thermal diffusivity, density and specific heat respectively. Many metal-forming problems of engineering interest can be modeled by using two-dimensional steady state representation$\left(\partial T/\partial \tau = 0\right)$. Using an Eulerian description, the above equation for a planer steady state problem as shown in references [١٥ and ١٦] becomes;

$$u\frac{\partial T_s}{\partial x} + v\frac{\partial T_s}{\partial y} = \alpha_s\left(\frac{\partial^2 T_s}{\partial x^2} + \frac{\partial^2 T_s}{\partial y^2}\right) + q_d/\rho_s c_s \qquad \ldots(٣\text{-}٢)$$

where (u) and (v) the velocity component in (x and y)directions respectively, which should satisfy the equation of continuity, the subscript (s) refers to the strip properties.

٣.٣.١.٢ *Roll Energy Equation*

The temperature field (T) of a rotating cylinder with homogenous and isotropic properties is governed by the partial differential equation expressing the conservation of energy, i.e.

$$\frac{DT}{D\tau} = \frac{\partial T}{\partial \tau} + V\nabla T = \alpha \nabla^2 T \qquad \ldots(٣\text{-}٣)$$

The roll rotates at constant speed, so that the temperature variation becomes cyclic steady state, then the Eq. (٣-٣) becomes;

$$V\nabla T = \alpha \nabla^2 T \qquad \ldots(٣\text{-}٤)$$

With respect to a fixed Eulerian reference frame, the governing partial differential equation of the roll temperature (T_r) as shown in [١٦ and ١٨] is:

$$\frac{\omega}{\alpha_r}\frac{\partial T_r}{\partial \theta} = \frac{\partial^2 T_r}{\partial r^2} + \frac{1}{r}\frac{\partial T_r}{\partial r} + \frac{1}{r^2}\frac{\partial^2 T_r}{\partial \theta^2} \qquad \ldots(٣\text{-}٥)$$

where (r) and (θ) are the cylindrical coordinates; (ω) is the roll angular velocity; and the subscript (r) refers to the roll properties.

٣.٣.٢ *Heat Penetration Depth (δ)*

In rolling process, the work roll experiences a considerable increases in temperature and complex cyclic steady-state temperature established within the work rolls, especially near the surface.

Rolls are usually cooled to a void the excessive heating. The cyclic steady-state temperature occurs only in a thin layer near the roll surface, and the centre core of the roll was assumed to be at a constant uniform temperature under steady state condition as shown by Patula [١١], Bryant [١٤] and Tseng [١٥ and ١٦].

This boundary layer behavior plays an important rule in determining the transfer of heat from the hot metal to the rolls and represents the main source of cyclic roll temperature stresses as showed by Patula [١١]. Similar to the boundary layer theory, the thermal boundary layer can be defined as the distance from the roll surface as shown in Fig. (٣-٢).

In fact, many investigators such as Patula [١١] and Gecim and Winer [٢١] discussed this thermal layer, and it was found it has a tremendous influence on the thermal stress pattern.

The concept of the thermal layer has also been applied to a numerical analysis by Tseng [١٦] and in the present study, it has been improved computational accuracy.

According to Tseng [١٦], (δ/R) can be found as a function of the Peclet number ($Pe = R^2\omega/\alpha_r$). Alternately, following Patula [١١], showed that ($\delta/R \le 4.24/\sqrt{Pe}$), when ($\sqrt{Pe} >> ٠$), a condition satisfied in most commercial strip rolling.

Based on a numerical study of Tseng [١٦] the

$$\frac{\delta}{R} = \frac{7}{\sqrt{Pe}} \qquad \ldots(٣\text{-}٦)$$

is large enough for the numerical model.

For rolling situations involving high speeds, the penetration would be significantly less where

$$Pe = \frac{R^2\omega}{\alpha_r} \qquad \ldots(٣\text{-}٧)$$

Then, substitute Eq. (٣-٧) in Eq. (٣-٦), then;

$$\delta = 7\sqrt{\frac{\alpha_r}{\omega}} \qquad \ldots(٣\text{-}٨)$$

Conversely, for lower rotational speeds, the penetration would be greater.

Based on Tseng *et al.* [١٨], the boundary layer thickness can be found as;

$$\delta = \frac{2}{\sqrt{Pe}-1}\ln\left(\frac{200Bi\left(\sqrt{2}Bi/\sqrt{Pe}+2\right)}{\Phi\sqrt{Pe/2}\left(Bi^2/Pe+\sqrt{2}Bi/\sqrt{Pe}+1\right)}\right) \qquad \ldots(٣\text{-}٩)$$

As indicated in Eq. (٣-٩), the thermal layer thickness depend not only on the Peclet number, but also on Biot number (*Bi*), and the bite angle (Φ). This improves the previous layer thickness predictions by Patula [١١] and Tseng [١٦]. Their approximations indicate that the thickness is a function of Peclet number only. In the present study, Eq. (٣-٨) is considered instead of Eq. (٣-٩) because the constant heat transfer coefficient is assumed in Eq. (٣-٩).

٣.٣.٢ *Cooling Heat Transfer Coefficient*

Knowledge of the heat transfer coefficient of cooling is essential in evaluating the process numerically. The change in the temperature distribution occurs when the sprays, atmospheres, and back up roll contact cool the roll. Here the usual practice is followed of representing this component by a convective-cooling parameter that is assumed to be variable through this study; of all the various cooling mechanisms.

It is clear that, in any temperature model, certain coefficients must inevitably be fitted to experimental data (heat transfer coefficients, thermal conductivity, etc.), it would be preferable for such coefficients to have some physical basis. This is especially important when models are used off-line to predict plant behavior, rather than in on-line control applications where coefficients can continuously be adapted from process measurements, this is showed by Bryant [١٣].

As mentioned by Tseng *et al.* [١٨], the heat transfer coefficient is greatly affected by the spray nozzle configuration, spray header arrangement, flow rates, roll speed, roll surface temperature, and other operating factors.

Many investigators have studied the heat transfer coefficient. However, a few qualitative results have been reported from these investigations. With such a simulation, the effect of spray-coolant geometry on the roll-temperature cycle can be studied. General trends from such studies shown in reference [١٤] are: -

- The heat is extracted most efficiently near the roll-gap exit.
- Wide-cooling spray angles tend to be less efficient as the heat flow from the boundary layer rapidly diminishes after the initial contact with the spray.
- Several small coolant sprays are more efficient than one, which is large, especially if time is allowed between contact with each spray for the heat to flow from the roll center into the boundary layer.

It is to be noted that at very high rolling speeds (say, ١٥ m/s) as shown by Tseng [١٨], the temperature variation is localized within a very thin layer near the roll surface as mentioned earlier. As a result, this makes the measurement of heat flux or heat transfer coefficient extremely difficult.

For around jet with diameter (*d*), the heat transfer coefficient can be approximated by Tseng [١٨] as;

$$H = 0.42\left(\frac{k_\infty}{d}\right)\mathrm{Re}^{0.63}\,\mathrm{Pr}^{0.36}\left(\frac{l}{d}\right)^{-0.4} \qquad \ldots(٣\text{-}١٠)$$

where (k_∞) is the thermal conductivity of coolant; (*l)* is the distance from the spray jet to the roll; ($\mathrm{Re}=V_\infty d/v_\infty$) is the Reynolds number of jet flow; ($\mathrm{Pr}=v_\infty/\alpha_\infty$) is the Prandtle number of coolant; (V_∞*)* is the average velocity of the spray; and (v_∞*)* is the kinematics viscosity of the coolant. Eq. (٣-١٠) is an appropriate relationship as long as the value of (*l/d)* is in the range of (٥ to ٦٠) as shown by Tseng [١٨], suitable for most of the water- based cooling systems used in the aluminum industry.

As mentioned by Tseng [١٥], the mean film coefficient of the water cooling spray is about (٣.٤ W/cm^٢.^{o}C) over about ٣٠ degrees of the roll circumference. The secondary cooling produced by water puddling varies from (٠.٢٨ to ٠.٨٥ W/cm^٢.^{o}C) as shown in Fig. (٣-٣). The two peak squares represent the entry and exit cooling. The remaining area is covered by puddling.

The convection heat transfers coefficient for a typical water-cooling spray by two jets as shown in Fig. (٣-٤) impinging on a rotating roll was reported by Tseng [١٦]. The convection heat transfer for typical water cooling spray described in Fig. (٣-٤) varies from (٠.٨٥ W/cm^٢.^{o}C to ٣.٤ W/cm^٢.^{o}C) along the roll circumference as shown in Fig. (٣-٥). The heat transfers coefficient as

presented in Fig. (٣-٥) varies as half sine curve to simulate both the entry and exit coolings. Then for nozzles with a certain dimensions and arrangement in Fig. (٣-٤) the heat transfer coefficient can be approximated by Tseng [١٦] as;

$$H(\theta) = 0.85 + 2.55|\sin(\theta)| \qquad \ldots(٣-١١)$$

where

$$2\pi \le \theta \le \Phi^{o} \qquad \ldots(٣-١٢)$$

Through (Φ) the roll is in contact with the strip (bite angle) as shown in Figs (٣-١), (٣-٣) and (٣-٦).

The Eq. (٣-١١) can be plotted in (x-y) coordinate, as shown in Fig. (٣-٦), where the (y-axis) coordinate represents the heat transfer coefficient ($H(\theta)$; W/cm^{٢}.^{o}C), and the (x-axis) coordinate represents the angular location along the circumference (θ).

Then the final two cases of water cooling spray, Figs. (٣-٣) and (٣-٦) are considered in the present study to simulate the entry and exit coolings during the rolling process.

Some researchers assumed that the heat transfer coefficient is constant such as Refs. [١١,١٣ and ١٦].

٣.٣.٤ *Flow of Metal in Rolling*

The flow of metal under the arc of contact is determined by assuming that the volume flow rate through any vertical section is constant. The first approximation in this section, neglect the increase in width results, so that the vertical compression of metal is translated into elongation in the rolling direction.

A metal strip with a thickness (t_o) enters the roll at the entrance plane (XX) with velocity (u_o). It passes through the roll gap and leaves the exit plane (YY) with a reduction thickness (t_f) and velocity (u_f) as shown in Fig. (٣-١).

Since equal volumes of metal must pass at a given point per unit time, then;

$$Wt_o u_o = Wtu = Wt_f u_f \qquad \ldots(٣-١٣)$$

where (W) is the width of strip; (u) is the velocity at any thickness (t) intermediate between (t_o) and (t_f).

In order that vertical elements remain undistorted, Eq. (٣-١٣) requires that the exit velocity must be greater than entrance velocity. Therefore, the velocity of strip must steadily increase from entrance to exit.

At only one point along the arc of contact between the roll and strip is the surface velocity of the roller (V_r) equal the velocity of the strip. This point is called the neutral point or no-slip point and the plane at this point is known as neutral plane. The thickness of the strip at this point is called neutral thickness (t_n) and the angle is called neutral angle (Φ_n). This point is indicated in Fig. (٣-١) by point (N).

At any point along the arc of contact, such as point (A) in Fig. (٣-١), two forces act on the metal. These are roll pressure (P_r) and tangential force (F).

Between the entrance plane and the neutral point, the strip is moving slower than the roll surface, and the friction force acts in the direction as shown in Fig. (٣-١) to draw the metal into the roll gap. On the exit side of the neutral point the strip moves faster than the roll surface, the direction of the frictional force is then reversed as shown in Fig. (٣-٧), so that it acts to oppose the delivery of the strip from the roll. The locations of the neutral point somewhere between the exit section and halfway point on the contact surface (plane ZZ). The location of the neutral point depends mainly on the friction condition as shown by Guo and Kobayashi [٢].

The above description represents the standard conditions of rolling process, and it was explained how the frictional forces change their direction at the neutral point. However, if large back tension or heavy draught is applied, the neutral point shifts toward the exit of the roll (exit plane) as shown in Fig. (٣-٨) and the metal will slip on the roll surface, this is shown by Robert [٢٢]. This (back tension) condition is considered in the present study.

The usual technological approach to the rolling problem proceeds by first finding the position of the neutral point. For the case of standard conditions of rolling, Johnson [٧] present the equilibrium equation on the exit side of the gap, as shown in Fig. (٣-٩);

$$hdp - \sigma_s(\cot \Phi + 2)dh = 0 \qquad \ldots(٣-١٤)$$

where (σ_s) is the strip yield stress (N/cm^2).

Since half strip thickness is considered i.e., ($h_f = t_f/2$), and;

$$h = h_f + \sigma_s \frac{\Phi^2}{2} \qquad \ldots(٣-١٥)$$

and

$$\tan \Phi \cong \Phi \cong \sqrt{\frac{2(h - h_f)}{R}}$$

or

$$\cot \Phi \cong \Phi \cong \sqrt{\frac{R}{2(h - h_f)}} \qquad \ldots(٣-١٦)$$

Substitution Eq. (٣-١٦) in Eq. (٣-١٤), then;

$$hdp - \sigma_s\left(\sqrt{\frac{R}{2(h - h_f)}} + 2\right)dh = 0$$

or

$$dp = \sigma_s\left[\sqrt{\frac{R}{2}}\frac{1}{h}\frac{dh}{\sqrt{h - h_f}} + 2\frac{dh}{h}\right] \qquad \ldots(٣-١٧)$$

Integrating Eq. (٣-١٧) and noting that ($p = 2\sigma_s$) at ($h = h_f$) as shown by Johnson and Kudo [٧] thus;

$$p_2 = 2\sigma_s \left(\sqrt{\frac{R}{2h_f}} . \tan^{-1} \sqrt{\frac{h - h_f}{h_f}} + \ln \frac{h}{h_f} + 1 \right) \qquad \ldots(٣\text{-}١٨)$$

where (p_2) refers to the pressure distribution from neutral point to exit plane .

A similar procedure on the entry side gives, when ($p = 2\sigma_s$) at ($h = h_o$)

$$p_1 = 2\sigma_s \left(\sqrt{\frac{R}{2h_f}} \left(\tan^{-1} \sqrt{\frac{h_o - h_f}{h_f}} - \tan^{-1} \sqrt{\frac{h - h_f}{h_f}} \right) + \ln \frac{h}{h_o} + 1 \right) \qquad \ldots(٣\text{-}١٩)$$

where (p_1) refers to the pressure distribution from entrance to the neutral point and ($h_o = t_o / 2$).

The neutral point is given by ($p_1 = p_2$) and thus;

$$2\sigma_s \left(\sqrt{\frac{R}{2h_f}} \left(\tan^{-1} \sqrt{\frac{h_o - h_f}{h_f}} - \tan^{-1} \sqrt{\frac{h_n - h_f}{h_f}} \right) + \ln \frac{h_n}{h_o} + 1 \right) =$$

$$2\sigma_s \left(\sqrt{\frac{R}{2h_f}} \tan^{-1} \sqrt{\frac{h_n - h_f}{h_f}} + \ln \frac{h_n}{h_f} + 1 \right)$$

Rearranging and simplifying the above equality, thus;

$$h_n = h_f \tan^2 2 \left(\sqrt{\frac{2h_f}{R}} \ln \frac{h_f}{h_o} + \tan^{-1} \sqrt{\frac{h_o - h_f}{h_f}} \right) + h_f \qquad \ldots(٣\text{-}٢٠)$$

For the case of a large back tension or heavy draught to be applied, the neutral point shifts toward the exit plane as predicted by Robert [٢٢] and Yun *et al*. [٢٣] then;

$$t_f = t_n \qquad \ldots(٣\text{-}٢١)$$

At the neutral point the velocity of the strip (V_s) is equal to the roll surface velocity (V_r) as predicted by Tseng [١٥ and ١٦] and Lahoti [٣].

It was obvious that the particles move on curved streamlines in the deformed region. Then these moving particles have two components of velocity, one of these in *x*-direction is denoted by (*u*) and the other in *y*-direction is denoted by (*v*). Recall Eq. (٣-١٣), then;

$$Wt_o u_o = Wt_f u_f = \underbrace{Wtu = Wt_n V_r} \qquad \ldots(٣-١٣)$$

Thus;

$$u = \frac{t_n}{t} V_r \qquad \ldots(٣-٢٢)$$

When the equation of continuity is satisfied then;

$$\frac{\partial u}{\partial x} + \frac{\partial v}{\partial y} = 0 \qquad \ldots(٣-٢٣)$$

Substitute Eq. (٣-٢٢) in Eq. (٣-٢٣) thus;

$$\frac{\partial}{\partial x}\left(\frac{t_n}{t} V_r\right) + \frac{\partial v}{\partial y} = 0 \qquad \ldots(٣-٢٤)$$

After some arrangement the Eq. (٣-٢٤) gives;

$$dv = \frac{t_n}{t^2} V_r \frac{dt}{dx} dy \qquad \ldots(٣-٢٥)$$

After integration Eq. (٣-٢٥) becomes;

$$v = \frac{t_n}{t^2} V_r \frac{dt}{dx} y \qquad \ldots(٣-٢٦)$$

where (dt/dx) is the slope of the arc of contact at any (*x*).

To check whether the neutral point at the exit plane, see Fig. (٣-١٠), then;

$$V_r = V_s = \sqrt{u^2 + v^2} \qquad \ldots(٣-٢٧)$$

Substitute Eqs. (٣-٢٢), (٣-٢٦) and (٣-٢١) in Eq. (٣-٢٧), then;

$$V_r = \sqrt{\left(\frac{t_n}{t_n} V_r\right)^2 + \left(\frac{t_n}{{t_n}^2} V_r \frac{dt}{dx} t_n\right)^2} \qquad \ldots(٣-٢٨)$$

After the simplifications $(dt/dx = 0)$. Then, the arc of the contact has $(dt/dx = 0)$ at the exit plane, i.e., at $(t=t_f)$ or $(t_n = t_f)$.

Lahoti *et al.* [٣] showed that the above velocity field is kinematically admissible and describes the metal flow with acceptable accuracy. The most popular technique in rolling analyses by Usama and Lenard [٢٤], and also are quite similar to those found by a detailed finite element analysis by Guo and Kobayashi [٢]. A finite element formulation to deal with the flow of metals coupled with thermal effects was presented by Zienkiewiewicz *et al.* [١٠]

٣.٣.٥ *Heat Generation by Plastic Deformation and Friction*

As shown by Barber [٢٥] and Wilson and Sheu [٢٦]. The heat generation during rolling due to the plastic deformation of the strip or at the interface. The distribution of the heat depends on the nature of these interactions.

In the rolling process, most of the power input goes to deform the strip and overcome the friction resistance along the roll-strip interface. The remaining power is dissipated as friction energy in the mill stand, particularly in the back up bearing.

In the present study, the deformation heat is distributed in the strip in proportion to the local effective strain rate and same as that distributed in Ref. [١٥];

$$\varepsilon_{eff} = \sqrt{(\varepsilon_x)^2 + (\varepsilon_y)^2} \qquad \ldots(٣-٢٩)$$

or

$$\varepsilon_{eff} = \sqrt{\left(\frac{\partial u}{\partial x}\right)^2 + \left(\frac{\partial v}{\partial h}\right)^2} \qquad \ldots(٣-٣٠)$$

In general, the deformation heat is proportional to both the strain rate and the flow stress, then;

$$Q_d \propto \varepsilon_{eff}\, \sigma_s)_{flow} \qquad \ldots(٣-٣١)$$

where (Q_d) is the deformation heat generation (Kw); (ε_{eff}) is the strip effective strain rate (١/s) and ($\sigma_s)_{flow}$) is the strip flow stress (N/cm^٢).

The distribution assumed in Eq. (٣-٣١) implies that the flow stress variation is small compared with very large strain rate as showed by Zienkiewicz *et al.* [١٠] and Tseng [١٦] then;

$$Q_d \propto \varepsilon_{eff} \qquad \ldots(٣-٣٢)$$

Recall Eqs. (٣-٢٢) and (٣-٢٣) respectively;

$$u = \frac{h_n}{h} V_r \qquad \ldots(٣-٢٢)$$

$$\frac{\partial u}{\partial x} + \frac{\partial v}{\partial y} = 0 \qquad \ldots(٣-٢٣)$$

At ($y=h$) the Eq. (٣-٢٣) becomes;

$$\frac{\partial v}{\partial h} = -\frac{\partial u}{\partial x} \qquad \ldots(٣-٣٣)$$

Substitute the Eq. (٣-٣٣) in Eq. (٣-٣٠), then;

$$\varepsilon_{eff} = \sqrt{2}\,\frac{\partial u}{\partial x} \qquad \ldots(٣-٣٤)$$

Substitute Eq. (٣-٢٢) in Eq. (٣-٣٤), then;

$$\varepsilon_{eff} = \sqrt{2}\,\frac{\partial}{\partial x}\left(\frac{h_n}{h} V_r\right) \qquad \ldots(٣-٣٥)$$

After differentiation the Eq. (٣-٣٥), then

$$\varepsilon_{eff} = -\sqrt{2}\,\frac{h_n}{h^2} V_r \frac{dh}{dx} \qquad \ldots(٣-٣٦)$$

where (h_n) is the half thickness of the strip at the neutral point.

In principle, information on heat generation by friction can be analytically predicted or directly measured. However, the greatest uncertainty in the analytic approach is in modeling the friction behavior, which still is not completely understood, as shown by Tseng [١٥ and ١٦]. This uncertainty greatly affects predicting not only the friction energy but also the neutral point and consequently the velocities and the deformation heat generation rate.

The study of aluminum rolling by Usama and Lenard [٢٤] is based on coulomb friction law with constant coefficient that exists between the rolls and

strip. As shown by Tseng [١٥ and ١٦], these numerical predictions of the roll separating force can match the measured data reasonably well, but there is more than a (١٠٠ percent) difference in predicted and measured torque because of the allocation in the total energy measured to the various sources of energy consumption. On the other hand, if the torque matches well the difference in predicted and measured forces may be more than (١٠٠ percent) for the same reason.

In the present study, the friction heat is distributed along the interface in proportion to the magnitude of the slip (relative velocity) between the roll and the strip as shown in Fig. (٣-١١). Which suggests that the interface friction follows either the Coulomb-type friction or constant shear stress friction as studied by Usama and Lenard [٢٤] and Guo and Kobayashi [٢], then;

$$Q_{fr} \propto V_{slip} \qquad \ldots(٣-٣٧)$$

where (Q_{fr}) is the heat generation by friction (kW).

It is well known from Fig. (٣-١١) that the slip velocity is;

$$V_{slip} = |V_r - V_s| \qquad \ldots(٣-٣٨)$$

Substitute Eq. (٣-٢٧) but at any (t) in Eq. (٣-٣٨) then;

$$V_{slip} = \left| V_r - \sqrt{u^2 + v^2} \right| \qquad \ldots(٣-٣٩)$$

where (V_{slip}) is the slip velocity (cm/s) between the roll surface velocity and the velocity of the strip at the interface, i.e., at ($y = h(x)$).

The input data of the heat generation by deformation and friction will be obtained from direct measurement of the power and it is considered in the present study, because of the mentioned uncertainty.

In order to calculate the rate of heat generation by plastic deformation (q_d) (kW/cm^٣) and the rate of heat generation by friction (q_{fr}) (kW/cm^٢). It should be

divided the deformation heat by deformation volume (cm^3) and the frictional energy by apparent contacting area (cm^2) as shown in Fig. (٣-١٢) then;

$$A_1 = \left(\frac{h_f + h_o}{2} \right) x_o \qquad \ldots(٣-٤٠)$$

where (A_1) is the trapezoidal area (cm^2) as shown in Fig. (٣-١٢) and;

$$A_2 = \frac{\sqrt{x_o^2 + (h_o - h_f)^2}}{2} \sqrt{R^2 - \frac{x_o^2 + (h_o - h_f)^2}{4}} \qquad \ldots(٣-٤١)$$

where (A_3) is the triangular area (cm^2) as shown in Fig. (٣-١٢) and;

$$A_3 = \frac{\Phi}{360} \pi R^2 \qquad \ldots(٣-٤٢)$$

where (A_4) is the pie area (cm^2) as shown in Fig. (٣-١٢) then;

$$A_4 = A_3 - A_2$$

where (A_5) is the piece area (cm^2) as shown in Fig. (٣-١٢).

Thus, the area of deformed volume ($A_d = 2(A_1 - A_4)$) or;

$$A_d = 2\left\{ \left(\frac{h_f + h_o}{2} \right) x_o - \left(\frac{\Phi}{360} \pi R^2 \right) + \left(\frac{\sqrt{x_o^2 + (h_o - h_f)^2}}{2} \sqrt{R^2 - \frac{x_o^2 + (h_o - h_f)^2}{4}} \right) \right\} \qquad \ldots(٣-٤٣)$$

the number (٢) refers to the upper and lower halves.

The deformation volume ($Vol_d = A_d . W$) then;

$$Vol_d = 2W\left\{ \left(\frac{h_f + h_o}{2} \right) x_o - \left(\frac{\Phi}{360} \pi R^2 \right) + \left(\frac{\sqrt{x_o^2 + (h_o - h_f)^2}}{2} \sqrt{R^2 - \frac{x_o^2 + (h_o - h_f)^2}{4}} \right) \right\} \qquad \ldots(٣-٤٤)$$

and the apparent contact area (area of friction) ,($A_{fr} = L_o W$) then;

$$A_{fr} = W\left(\sqrt{R(t_o - t_f) - \frac{(t_o - t_f)^2}{4}}\right) \quad \ldots(٣-٤٥)$$

There is another method that can be used to calculate the area of deformation. This method includes the integration of the arc of contact equation from (٠ to x_o), but this method was more complex than the above used method then it was neglected.

٣.٤ *The Boundary Conditions*

The ability to influence all other points in the domain from an interior point implies that the boundary conditions are required on all the boundaries. The boundary conditions can be any combination of the following: -

- Dirichlet condition, e.g. *T=constant*.
- Neumann (derivative) condition, e.g. $\partial T/\partial n = constant$.
- Mixed or Robin condition, e.g. $\partial T/\partial n = constant_١ \pm constant_٢ * (\partial T/\partial n)$.

As shown by Tseng [١٥ and ١٦], before entering and after exit the strip into and from the roll bite respectively, the strip loses heat to the ambient air or coolant by convection, see Fig. (٣-١٣), an important effect, especially in hot rolling then;

$$-k_s \frac{\partial T_s}{\partial n} = H_\infty (T_s - T_\infty) \quad \ldots(٣-٤٦)$$

The strip entry temperature with a parabolic variation in the thickness direction is often observed and can be expressed as mentioned by Ref. [١٨] as;

$$T_s(0, y) = T_o + \left(\frac{T_\infty - T_o}{1 + \frac{k_s}{H_\infty . h_o}}\right) \quad \ldots(٣-٤٧)$$

where (T_o) is the strip entry temperature at center; (T_∞) is the strip ambient temperature and (H_∞) is the ambient heat transfer coefficient.

In the present study and in Refs. [١٥ and ١٦], since the strip velocity (or, more precisely, the strip Peclet number ($V_r\, t_n/\alpha_s$)) is high, the conduction term, ($\partial^2 T_s / \partial x^2$) becomes small in comparison with the convection term, ($u\, \partial T_s / \partial x$). Thus the temperature at a short distance upstream of the initial contact point should be the initial strip temperature (T_o).

The boundary condition as shown by Tseng [١٥ and ١٦] at some distance downstream (e.g., the contact length) from the exit contact point may be assumed to be;

$$\frac{\partial T_s}{\partial x} = 0 \qquad \ldots(٣\text{-}٤٨)$$

i.e., the temperature variation in the (x-direction) should be no longer sensitive to the location of the boundary as shown in Fig. (٣-١٣).

As showed by Tseng [١٥ and ١٦], because of the symmetry, the lower horizontal boundary having;

$$\frac{\partial T_s}{\partial y} = 0 \qquad \ldots(٣\text{-}٤٩)$$

The boundary condition for the roll circumference is;

$$-k_r \frac{\partial T_r(R,\theta)}{\partial r} = H(\theta)\{T_r(R,\theta) - T_\infty\} \qquad \ldots(٣\text{-}٥٠)$$

where ($H(\theta)$) is the heat transfer coefficient explained previously, the Eq. (٣-٥٠) represents the heat loss by convection to the coolant.

Since the roll is rotate rapidly, and all temperatures vary within a very thin layer near the surface, only a thin layer needs to be modeled. The interior boundary condition as shown by Tseng [١٦] becomes;

$$\frac{\partial T_r\left((R-\delta),\theta\right)}{\partial r}=0 \qquad \ldots(٣\text{-}٥١)$$

where (δ) is the depth of the skin layer.

For the boundary condition at the interface, specific care is required. As an example, a typical boundary condition frequently encountered in the metal forming process is considered here. The body (strip) analyzed is assumed to be in contact with another body (roll) and each moves relative to the other, creating the friction heat along the interface. In addition, as mentioned by Tseng *et al.* [١٨], the heat flux out of the strip plus the friction energy must be equal to the heat flux into the roll;

$$q_s + q_{fr} = q_r \qquad \ldots(٣\text{-}٥٢)$$

Mathematically, as shown by Tseng [١٥ and ١٦] the above boundary condition (Eq. (٣-٥٢)) may be expressed as;

$$k_s\left(\frac{\partial T_s}{\partial n}\right)_b + k_r\left(\frac{\partial T_r}{\partial n}\right)_b - q_{fr} = 0 \qquad \ldots(٣\text{-}٥٣)$$

where ($\partial/\partial n$) represents differentiation along the normal of the boundary (positive outward); see Fig. (٣-١٤); and (q_{fr}) is the friction heat generated along the interface. All special derivatives for the points at the interface must be formulated using points located in their respective sides as follows;

$$k_s\left(\frac{\partial T_s}{\partial n}\right)_b = q_1 + q_2 \qquad \ldots(٣\text{-}٥٤)$$

Then, from Fig. (٣-١٤);

$$\sin\beta_o = \frac{q_2}{k_s\left(\frac{\partial T_s}{\partial y}\right)_b}$$

$$\cos\beta_o = \frac{q_1}{k_s\left(\frac{\partial T_s}{\partial x}\right)_b} \qquad \ldots(٣\text{-}٥٥)$$

Substituting Eq. (٣-٥٥) in Eq. (٣-٥٤), thus:

$$k_s\left(\frac{\partial T_s}{\partial n}\right)_b = k_s\left(\frac{\partial T_s}{\partial x}\right)_b \cos\beta_o + k_s\left(\frac{\partial T_s}{\partial y}\right)_b \sin\beta_o \qquad \ldots(٣-٥٦)$$

where the angle (β_o) specifies the direction as shown in Fig. (٣-١٤).

In the rolling process, tremendous pressure built up in the roll-strip interface results in a very thin film layer on order of micron (about $١٠^{-٧}$ m) according to Tseng [١٦] and Kanel and Dow [٢٧], then the roll and strip come into intimate contact. However, some coolant film or scale might also be accumulated in the interface and the thermal resistance of this film or flame should be considered.

Refs. [٨, ١٥ and ١٦], the interface resistance can be considered as a function of the magnitude of the interface heat flux and if the average assumption is also applied, the interface conduction can be expressed as;

$$\frac{(T_s)_b}{(T_r)_b} = C_i \qquad \ldots(٣-٥٧)$$

where (C_i) is the thermal resistance parameter. If the interface heat flux toward the roll, then (C_i >١) and vice versa. The magnitude of (C_i) should be determined experimentally.

In the present study, the interface thermal resistance is assumed to be insignificant. In other words, the surface temperature of the roll and strip approach to the same value, i.e., (C_i=١), this showed by Tseng [١٥ and ١٦] and Tseng *et al.* [١٨].

If the roll is also to be analyzed by finite difference method thus;

$$\left(\frac{\partial T_r}{\partial n}\right)_b = \left(\frac{\partial T_r}{\partial r}\right)_b = f\left(T_o, T_r, q_{fr}\right) \qquad \ldots(٣-٥٨)$$

where $(T_s)_b = T_r)_b$) as indicated in Eq. (٣-٥٧).

Replacing $(\partial T_s/\partial n)_b$ by the directional derivatives and $(\partial T_r/\partial n)_b$ by the above expression and from Fig. (٣-١٤), Eq. (٣-٥٣) becomes;

$$\left(\frac{\partial T_s}{\partial x}\right)_b \cos\beta_o + \left(\frac{\partial T_s}{\partial y}\right)_b \sin\beta_o + \frac{k_r}{k_s}\left(\frac{\partial T_r}{\partial r}\right)_b - \frac{q_{fr}}{k_s} = 0 \qquad \ldots(٣-٥٩)$$

٣.٥ *Methods of Solution*

The governing equation, Eq. (٣-٢), and its associated boundary conditions described the problem suitable for solution by the Generalized Finite Difference Method (GFDM) in the bite region (internal and interface nodes). The strip has a curved boundary associated with a very complicated interface condition, and here a non-orthogonal mesh is convenient. Therefore, (GFDM) is used.

After bite region (product), the mesh return to become orthogonal, then, the solution of GFDM like their central finite difference counterpart in the Conventional Finite Difference Method (CFDM).

Similarly, because of the circular geometry of the roll, the CFDM formulation based on cylindrical coordinate is more convenient to solve the energy equation, Eq. (٣-٥), and therefore is used to solve the roll.

As a result from the study of Tseng [١٦], Murli *et al.* [٢٨], and Roach [٢٩] the solution of the GFDM and CFDM displays non-physical oscillation at high Peclet number, then in the present study, the up-wind scheme is employed to achieve the numerical instability.

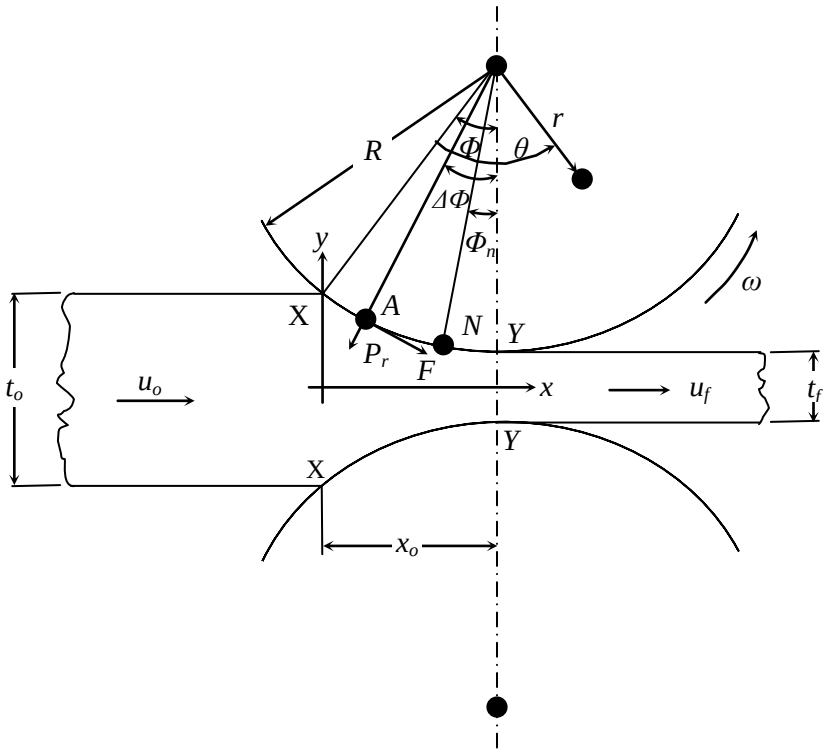

Fig. (٣-١): Forces Acting During Rolling, Ref. [١].

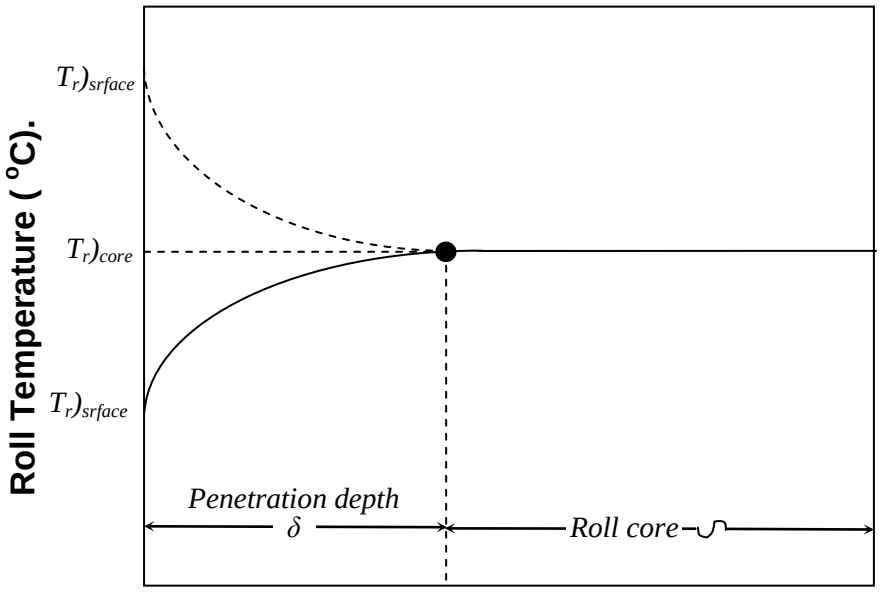

Fig. (٣-٢): The Relationship Between (δ) and Roll Temperature, Ref. [١٤].

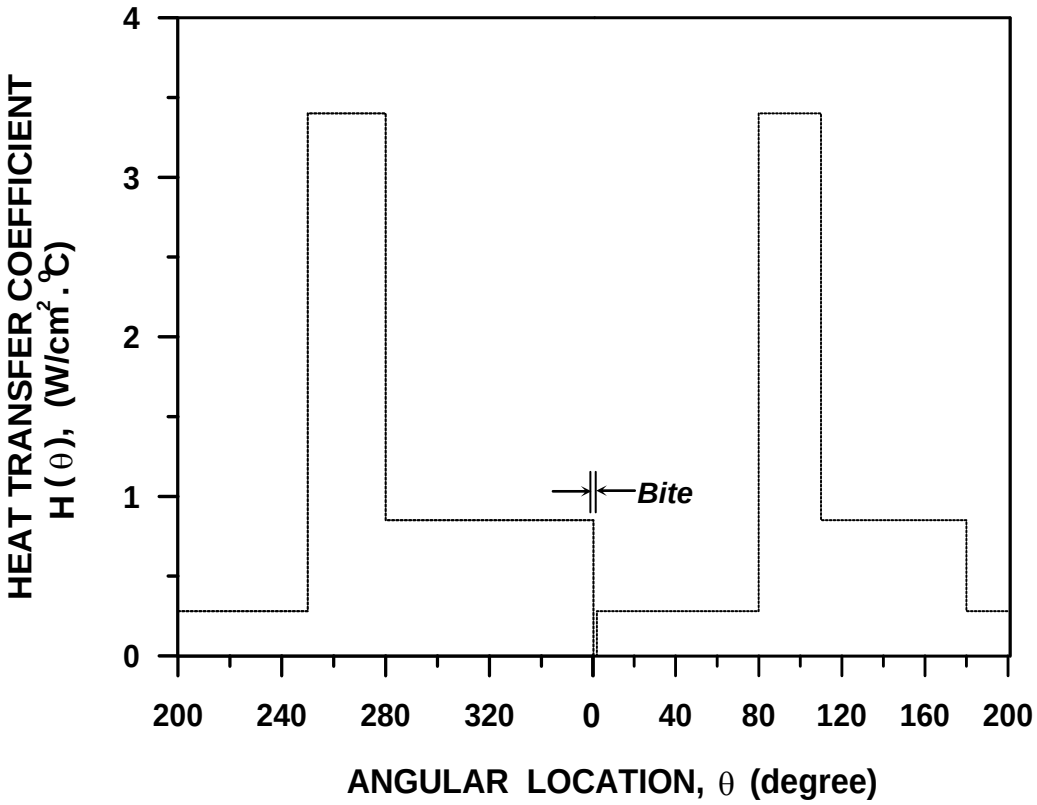

Fig. (٣-٣): Cooling Heat Transfer Coefficient, Ref.

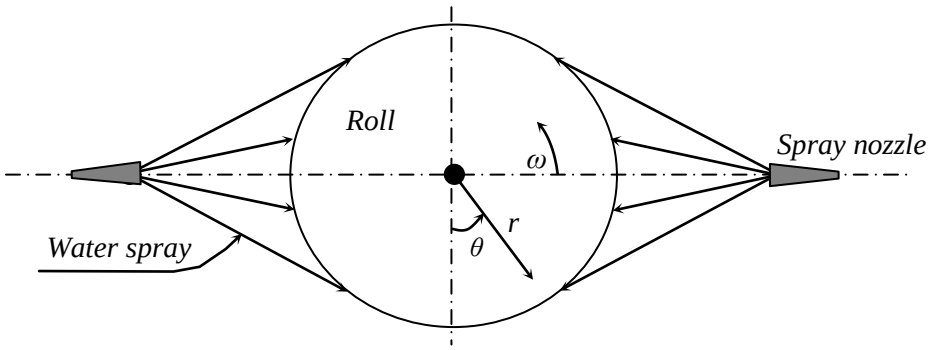

Fig. (٣-٤): Roll Cooling System.

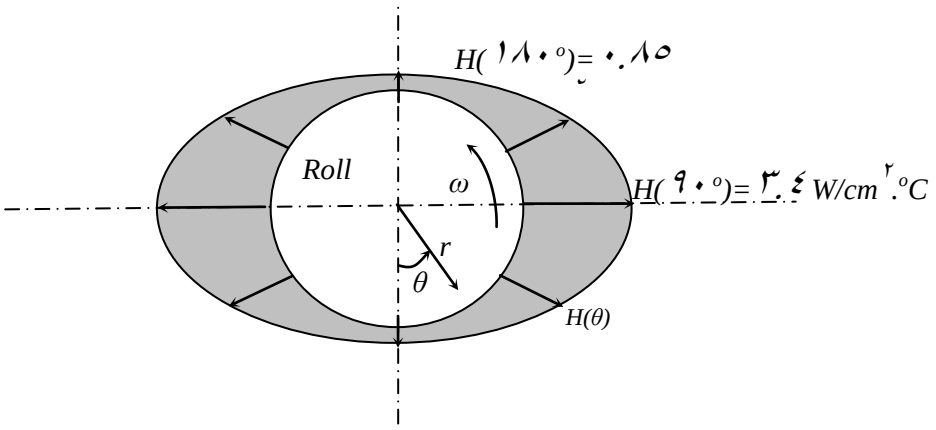

Fig. (٣-٥): Roll Heat Transfer Coefficient Variation Representation.

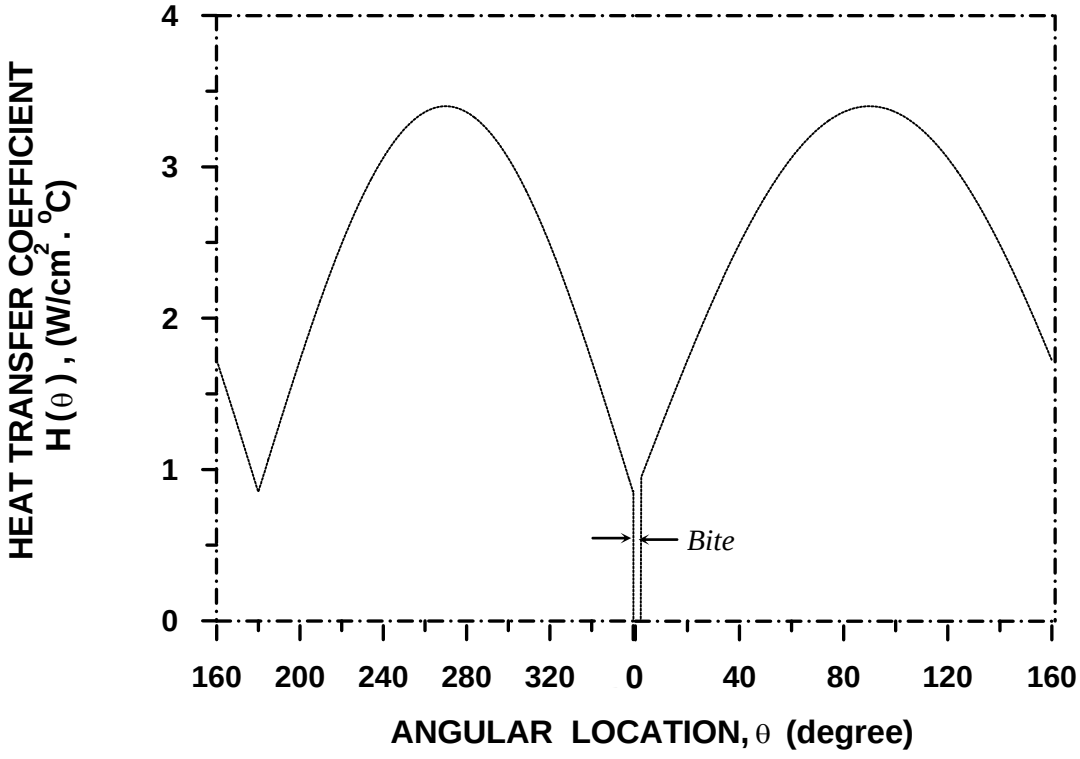

Fig. (٣-٦): Heat Transfer Coefficient that Varies as A Half Sine Curve, Ref. [١٦].

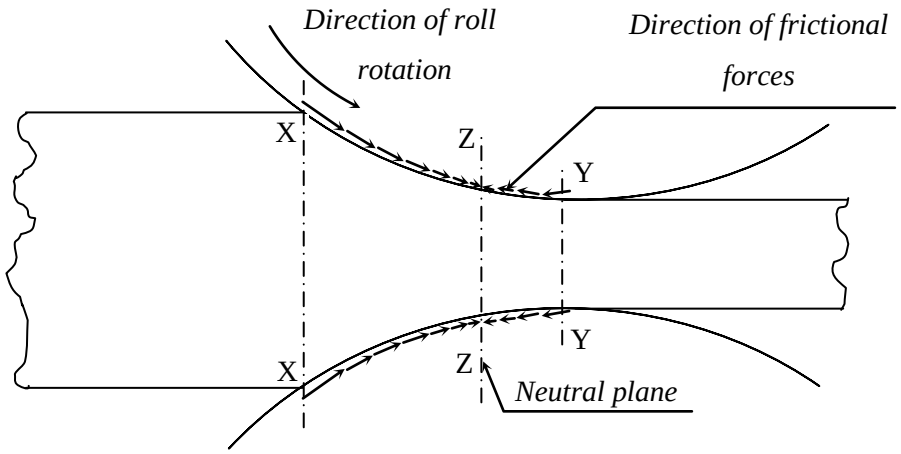

Fig. (٣-٧): Distribution of Frictional Forces in Rolling at Standard Condition, Ref. [٢٢].

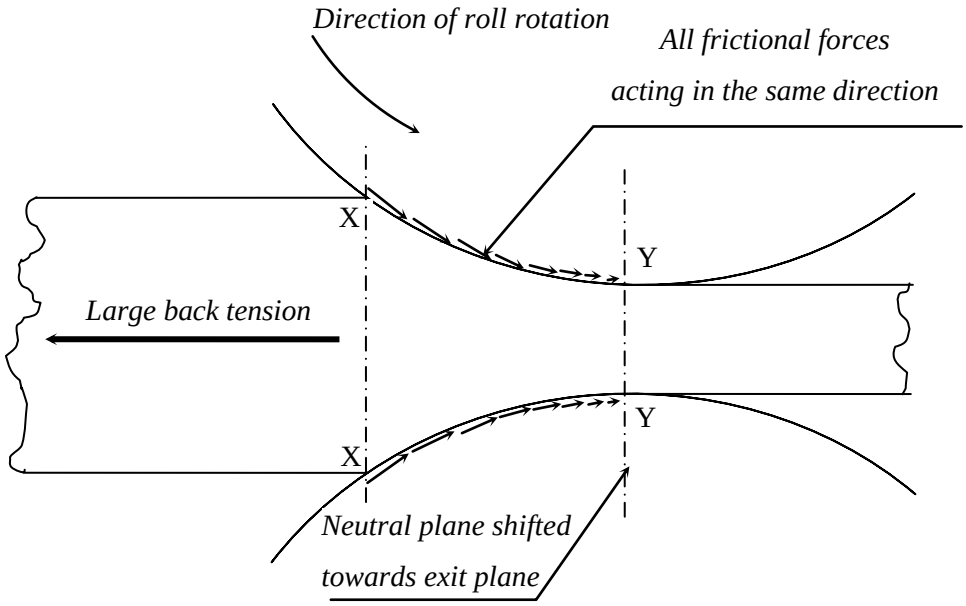

Fig. (٣-٨): Influence of Large Tension in Rolling, Ref. [٢٢].

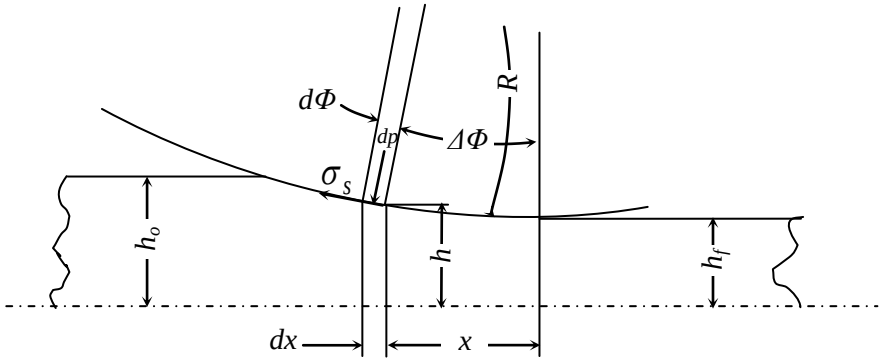

Fig. (٣-٩): For Approximate Analysis of Rolling, Ref. [٧].

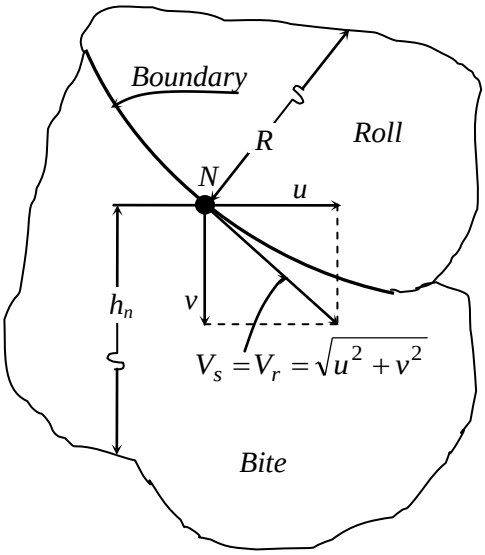

Fig. (٣-١٠): The Equality of the Roll Surface and Strip Velocities at the Neutral Point.

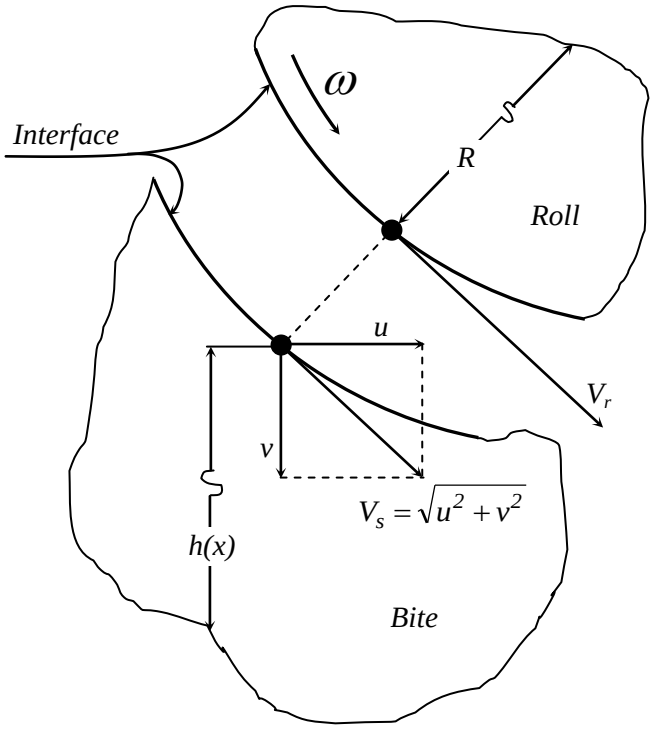

Fig. (٣-١١): The Relative Velocity Between the Roll and Strip.

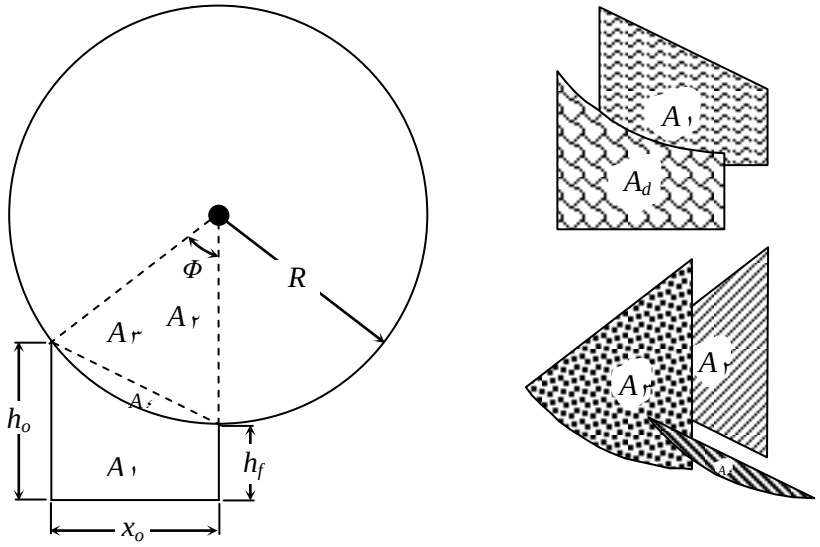

Fig. (٣-١٢): The Method of Calculation of the Deformation Area.

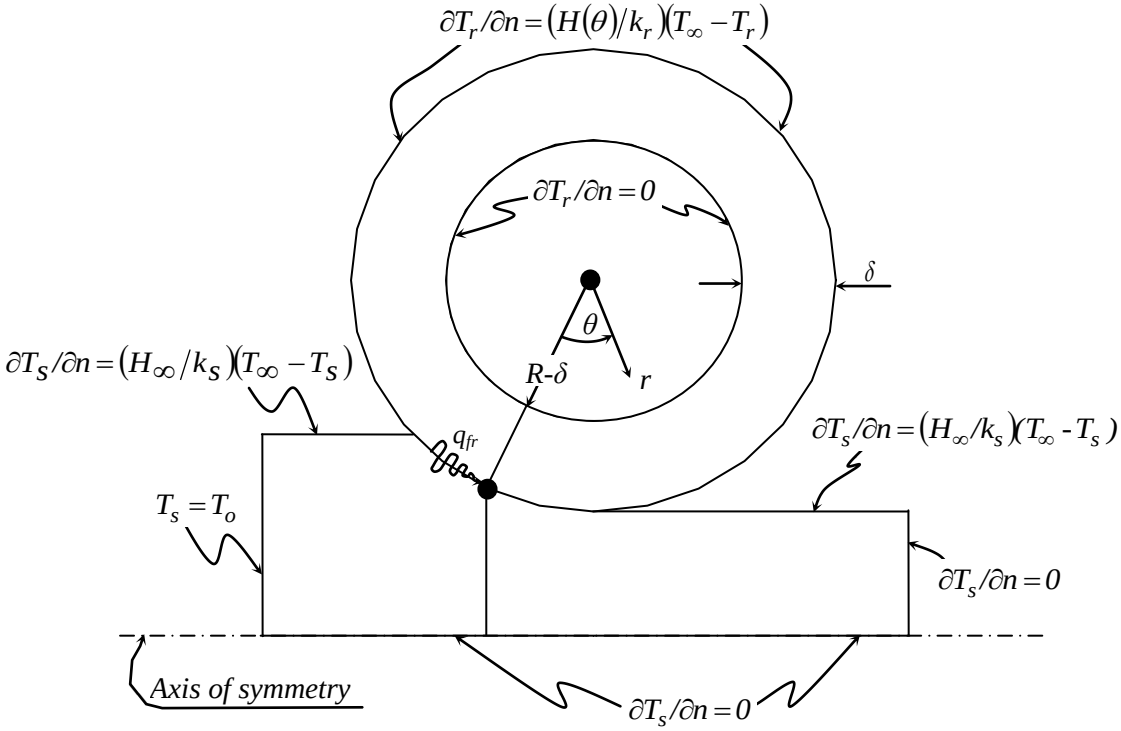

Fig. (٣-١٣): Typical Boundary Conditions for Strip, Roll and

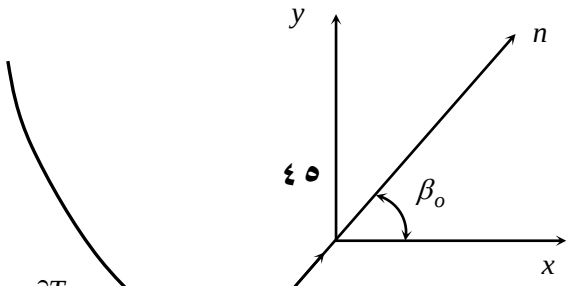

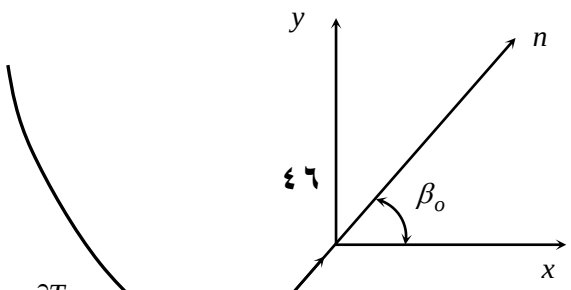
y
n
٤٦
β_o
x

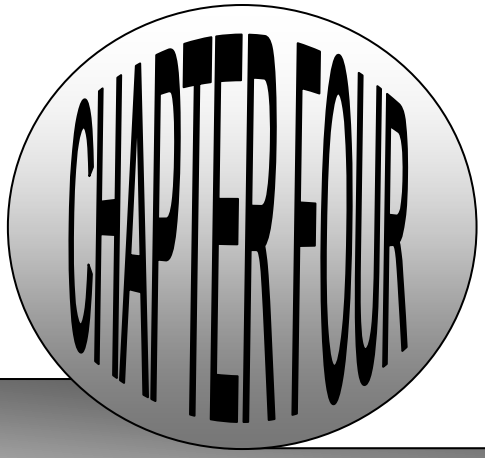

٤ *Numerical Solution*

Mostly heat conduction problems involving simple geometries with simple boundary conditions had been considered because only such simple problems can be solved analytically. But many problems encountered in practice involving complicated geometry with complex boundary conditions or variable properties cannot be solved analytically. In such case, sufficiently accurate approximate solutions can be obtained by computers using a numerical method.

In this chapter, the task of constructing the grid generation, a numerical method for solving the governing partial differential Eqs. (٣-٢) and (٣-٥) which governs the physical process of interest, the boundary conditions representation, the numerical calculation algorithm and the computer program.

٤.١ *Grid (Mesh) Generation*

The solution of system of partial differential equations can be greatly simplified by a well-constructed grid. It is also true that a grid, which is not well suited to the problem, can lead to an unsatisfactory result. In some applications, improper choice of grid point locations can lead to apparent instability or lack of convergence. One of the central problems in computing numerical solutions to partial differential equations is that of grid generation as illustrated by Anderson *et al.* [٣٠].

The first step in the calculation of the mesh generation is to find the equation of the arc of contact. By ignoring the elastic deformation (flattening) of the roll at the surface of contact and considering half strip thickness. Therefore, the arc of contact can be assumed as a[٤٦] portion from circle circumference with radius (R) and (x_o, $(R+h_f)$) as center, as shown in Fig. (٤-١).

$$(x - x_o)^2 + \left(y - \left(h_f + R\right)\right)^2 = R^2 \qquad \ldots(٤\text{-}١)$$

Rearranging Eq. (٤-١) and taking the square root for the two sides, thus;

$$y - \left(h_f + R\right) = \pm\sqrt{R^2 - (x - x_o)^2} \qquad \ldots(٤\text{-}٢)$$

$+$ and $-$ signs for the right hand side of Eq. (٤-٢) refer to the lower and upper semi circles respectively.

During the rolling process the lower semi circle is in contact with the strip as shown in Fig. (٤-١), then it is to be considered in the calculations, then;

$$y = h(x) = \left(h_f + R\right) - \sqrt{R^2 - (x - x_o)^2} \qquad \ldots(٤\text{-}٣)$$

where $h\,(x)$, is the arc of the contact equation.

The grid system used for calculating temperature in strip rolling includes half of the strip thickness. The upstream (billet) and down stream (product) regions have uniformly spaced grid lines in both x and y directions, but the roll gap (bite) region have non-uniformly spaced grid lines (non-orthogonal mesh) in both x and y directions.

The arc of contact is divided in a specified number of divisions of equal lengths as shown in Fig. (٤-٢). With the same procedure, the half-thickness of the deforming strip is also divided into elements of equal height at a certain location in the roll gap. In general, the mesh in y-direction is uniformly distributed over the local thickness of the strip as reported by Tseng [١٥].

To represent the previous description analytically, from Fig. (٤-٢) and from trigonometric substitutions it can be written;

$$\Phi = \tan^{-1}\left(\frac{\sqrt{R^2 - \left(R - h_o + h_f\right)^2}}{R - h_o + h_f}\right) \qquad \ldots(٤-٤)$$

and

$$x_o = R\sin\Phi \qquad \ldots(٤-٥)$$

The arc of contact is then divided into a specific number of divisions of equal lengths, therefore, let us assume that the number of divisions is (n), then;

$$\Delta\Phi = \frac{\Phi}{n} \qquad \ldots(٤-٦)$$

The problem becomes how to find the x and y coordinates for the points from ٠, ١,...,n on the arc of contact.

where $x_o, x_١, \ldots\ldots, x_n$ and $x_o`, x_١`, \ldots\ldots, x_n`$ are shown in Fig. (٤-٢), then;

$$\begin{aligned} x_5` &= R\sin(0\Delta\Phi) \\ x_4` &= R\sin(1\Delta\Phi) \\ x_3` &= R\sin(2\Delta\Phi) \\ x_2` &= R\sin(3\Delta\Phi) \\ &\vdots \\ x_{(n-i)}` &= R\sin(i\Delta\theta) \end{aligned} \qquad \ldots(٤-٧)$$

where, i= ٠, ١, ..., n.

It becomes well obvious from Fig. (٤-٢) that the;

$$x_i = x_o - x_i` \qquad \ldots(٤-٨)$$

After substitution Eq. (٤-٧) in Eq. (٤-٨), then;

$$\begin{aligned} x_5 &= x_o - \grave{x}_5 \\ x_5 &= x_o - R\sin(0\Delta\Phi) \\ x_4 &= x_o - \grave{x}_4 \\ x_4 &= x_o - R\sin(1\Delta\Phi) \\ x_3 &= x_o - \grave{x}_3 \\ x_3 &= x_o - R\sin(2\Delta\Phi) \\ &\vdots \\ x_{(n-i)} &= x_o - R\sin(i\Delta\Phi) \end{aligned} \quad \ldots (٤-٩)$$

After calculating the values of *x*-coordinates for these points, to get the values of *y*-coordinates for the same points. By substituting the Eq. (٤-٩) in the arc of contact Eq. (٤-٣), then;

$$h(x_{(n-i)}) = (h_f + R) - R\sqrt{1-\sin^2(i\Delta\Phi)} \quad \ldots (٤-١٠)$$

Since

$$\sin^2(i\Delta\Phi) = 1 - \cos^2(i\Delta\Phi) \quad \ldots (٤-١١)$$

After substitution Eq. (٤-١١) in Eq. (٤-١٠), thus;

$$h(x_{(n-i)}) = h_f + R(1-\cos(i\Delta\Phi)) \quad \ldots (٤-١٢)$$

An angular and radial mesh is used for the roll. The grid lines in the roll in the radial direction are distributed uniformly within a thin layer of thickness (δ) as shown in Fig. (٤-٣).

Lahoti *et al.* [٣] assumed that the grid lines in the roll in the radial direction are distributed logarithmically within a thin layer with a certain thickness. In order to solve the problem simultaneously, the roll mesh is refined near the bite region to match that use in strip (i.e., non-uniform mesh in θ

direction are adopted). The mesh generation obtained for the strip and roll can be shown in Figs. (٤-٣) and (٤-٤).

As reported by Tseng [١٥], Liszka and Orkisz [٣١] and Sienkiewicz *et al.* [١٠], no difficulty was expected when the mesh generation codes developed for the finite element shemes were used.

٤.٢ *Generalized Finite Difference Method (GFDM)*

Applying the finite difference methods to heat transfer problems has become an established practice. In the past, much effort has been spent on developing techniques to cope with the difficulties involved, e.g. the irregular boundaries and the inaccuracies in region having rapidly change in temperature gradients. Among the most successful of these schemes is the arbitrary irregular mesh approach or the Generalized Finite Difference Method (GFDM).

The GFDM was initiated in ١٩٥٠. Development proceeded from the mesh being partially regular in subdomains; to its being irregular, but with restricted topology; to its being fully arbitrary irregular. This method has had recent successful application to heat transfer problems.

The GFDM, like its centre difference counter part in the CFDM, is extremely used in the problems involving both conduction and convection, where convection is dominant or more precisely, the Peclet number is high. When the Peclet number becomes very large, the conduction term will be very small, thereby enabling the convection terms to induce a numerical instability.

٤.٣ *Numerical Formulation*

The numerical methods for solving differential equations are based on replacing the differential equations by algebraic equations. In the case of the popular finite difference method, this is done by replacing the derivatives by differences. Below the demonstration of this with both (GFDM) and (CFDM).

٤.٣.١- *Governing Equations Representation*

٤.٣.١.١- *Strip Governing Equation Representation*

The essence of GFDM is its ability to obtain the needed derivative expression at a given point as a function of arbitrarily located neighboring points.

As reported by Tseng [١٥ and ١٦] for any sufficiently differentiable function, *T (x,y)*, in a given domain has Taylor series expansion about a point (x_o,y_o) up to second order terms can be written as;

$$T_i = T_o + m_i\left(\frac{\partial T}{\partial x}\right)_o + n_i\left(\frac{\partial T}{\partial y}\right)_o + \frac{m_i^2}{2}\left(\frac{\partial^2 T}{\partial x^2}\right)_o + \frac{n_i^2}{2}\left(\frac{\partial^2 T}{\partial y^2}\right)_o + m_i n_i\left(\frac{\partial^2 T}{\partial x \partial y}\right)_o \qquad \ldots(٤-١٣)$$

where $(T_i=T(x_i,y_i),\ T_o=T(x_o,y_o),\ m=x-x_o)$and $(n= y-y_o)$. Five independent equations, similar to Eq. (٤-١٤), can be obtained by using five arbitrarily located neighboring points (x_i,y_i), $i=$ ١,..., ٥, as shown in Fig. (٤-٥).

Let $(T_s = T_{si}(x_i, y_i))$, then $(m_i = x_i - x_o)$ and $(n_i = y_i - y_o)$, then;

$$T_{si} = T_{so} + m_i\left(\frac{\partial T_s}{\partial x}\right)_o + n_i\left(\frac{\partial T_s}{\partial y}\right)_o + \frac{m_i^2}{2}\left(\frac{\partial^2 T_s}{\partial x^2}\right)_o + \frac{n_i^2}{2}\left(\frac{\partial^2 T_s}{\partial y^2}\right)_o + m_i n_i\left(\frac{\partial^2 T_s}{\partial x \partial y}\right)_o \qquad \ldots(٤-١٤)$$

or

$$T_{s1} = T_{so} + m_1\left(\frac{\partial T_s}{\partial x}\right)_o + n_1\left(\frac{\partial T_s}{\partial y}\right)_o + \frac{m_1^2}{2}\left(\frac{\partial^2 T_s}{\partial x^2}\right)_o + \frac{n_1^2}{2}\left(\frac{\partial^2 T_s}{\partial y^2}\right)_o + m_1 n_1\left(\frac{\partial^2 T_s}{\partial x \partial y}\right)_o$$

$$T_{s2} = T_{so} + m_2\left(\frac{\partial T_s}{\partial x}\right)_o + n_2\left(\frac{\partial T_s}{\partial y}\right)_o + \frac{m_2^2}{2}\left(\frac{\partial^2 T_s}{\partial x^2}\right)_o + \frac{n_2^2}{2}\left(\frac{\partial^2 T_s}{\partial y^2}\right)_o + m_2 n_2\left(\frac{\partial^2 T_s}{\partial x \partial y}\right)_o$$

$$T_{s3} = T_{so} + m_3\left(\frac{\partial T_s}{\partial x}\right)_o + n_3\left(\frac{\partial T_s}{\partial y}\right)_o + \frac{m_3^2}{2}\left(\frac{\partial^2 T_s}{\partial x^2}\right)_o + \frac{n_3^2}{2}\left(\frac{\partial^2 T_s}{\partial y^2}\right)_o + m_3 n_3\left(\frac{\partial^2 T_s}{\partial x \partial y}\right)_o$$

$$T_{s4} = T_{so} + m_4\left(\frac{\partial T_s}{\partial x}\right)_o + n_4\left(\frac{\partial T_s}{\partial y}\right)_o + \frac{m_4^2}{2}\left(\frac{\partial^2 T_s}{\partial x^2}\right)_o + \frac{n_4^2}{2}\left(\frac{\partial^2 T_s}{\partial y^2}\right)_o + m_4 n_4\left(\frac{\partial^2 T_s}{\partial x \partial y}\right)_o$$

$$T_{s5} = T_{so} + m_5\left(\frac{\partial T_s}{\partial x}\right)_o + n_5\left(\frac{\partial T_s}{\partial y}\right)_o + \frac{m_5^2}{2}\left(\frac{\partial^2 T_s}{\partial x^2}\right)_o + \frac{n_5^2}{2}\left(\frac{\partial^2 T_s}{\partial y^2}\right)_o + m_5 n_5\left(\frac{\partial^2 T_s}{\partial x \partial y}\right)_o$$

...(٤-١٥)

If the first special derivatives ($\partial T_s/\partial x \ldots \partial^2 T_s/\partial x\partial y$)at point ($x_o$, y_o) can computed in terms of the functional values at five neighboring points, see Fig. (٤-٥). In matrix form, as mentioned in Ref. [١٥ and ١٦];

$$\begin{bmatrix} m_1 & n_1 & m_1^2/2 & n_1^2/2 & m_1 n_1 \\ m_2 & n_2 & m_2^2/2 & n_2^2/2 & m_2 n_2 \\ m_3 & n_3 & m_3^2/2 & n_3^2/2 & m_3 n_3 \\ m_4 & n_4 & m_4^2/2 & n_4^2/2 & m_4 n_4 \\ m_5 & n_5 & m_5^2/2 & n_5^2/2 & m_5 n_5 \end{bmatrix} \begin{Bmatrix} \partial T_s/\partial x \\ \partial T_s/\partial y \\ \partial^2 T_s/\partial x^2 \\ \partial^2 T_s/\partial y^2 \\ \partial^2 T_s/\partial x\partial y \end{Bmatrix} = \begin{Bmatrix} T_{s1} - T_{so} \\ T_{s2} - T_{so} \\ T_{s3} - T_{so} \\ T_{s4} - T_{so} \\ T_{s5} - T_{so} \end{Bmatrix} \qquad \ldots(٤-١٦)$$

or

$$[A_{i,j}]\{DT_{sj}\} = \{T_{si} - T_{so}\} \qquad i, j = ١,٢,\ldots,٥ \qquad \ldots(٤-١٧)$$

Inverse of the matrix $[A_{i,j}]$ leads to;

$$\{DT_{si}\} = [B_{i,j}]\{T_{si} - T_{so}\} \qquad i, j = ١,٢,\ldots,٥ \qquad \ldots(٤-١٨)$$

where $[B_{i,j}]$ is the inverse of $[A_{i,j}]$. If matrix $[A_{i,j}]$ is ill conditioned or singular, a technique developed by Perron and Kao [٣٢] can be used to obtain acceptable derivative approximations $\{DT_i\}$.

Rearranging Eq. (٤-١٨), then;

$$\{DT_{si}\} = [B_{i,j}]\{T_{sj}\} \qquad i = ١,\ldots,٥,\ j = ٠,\ldots,٥ \qquad \ldots(٤\text{-}١٩)$$

where;

$$B_{io} = -\sum_{j=1}^{5} B_{ij} \qquad \ldots(٤\text{-}٢٠)$$

Finally the special derivatives at point (x_o, y_o) can be found as reported by Tseng [١٥] as;

$$\left(\frac{\partial T_s}{\partial x}\right)_o = \sum_{j=o}^{5} B_{1j}\ \ T_{s\,j} \qquad \ldots(٤\text{-}٢١a)$$

$$\left(\frac{\partial T_s}{\partial y}\right)_o = \sum_{j=o}^{5} B_{2\,j}\ \ T_{s\,j} \qquad \ldots(٤\text{-}٢١b)$$

$$\left(\frac{\partial^2 T_s}{\partial x^2}\right)_o = \sum_{j=o}^{5} B_{3j}\ \ T_{s\,j} \qquad \ldots(٤\text{-}٢١c)$$

$$\left(\frac{\partial^2 T_s}{\partial y^2}\right)_o = \sum_{j=o}^{5} B_{4j}\ \ T_{s\,j} \qquad \ldots(٤\text{-}٢١d)$$

Substituting the Eqs. (٤-٢٠), (٤-٢١a), (٤-٢١b), (٤-٢١c) and (٤-٢١d) in the strip governing Eq. (٣-٢), an algebraic approximation for each internal point was as reported by Tseng [١٥];

$$T_{so} = \frac{q_d / \rho_s c_s - \sum_{j=1}^{5}\left(u_o B_{1j} + v_o B_{2\,j} - \alpha_s\, B_{3j} - \alpha_s\, B_{4\,j}\right) T_{sj}}{u_o B_{1o} + v_o B_{2o} - \alpha_s\left(B_{3o} + B_{4o}\right)} \qquad \ldots(٤\text{-}٢٢)$$

For the boundary points, spatial care is required. Substituting Eq. (٣-٥٩) with $\left(\partial T_r/\partial r\right)_b = \left((T_{ro} - T_r)/\Delta r\right)$ and ($\Delta r = r_o - r_j$) into Eq. (٤-١٤), from equation (٣-٥٩) after the final substitution, eliminate $\left(\partial T_s/\partial x\right)_o$ or $\left(\partial T_s/\partial y\right)_o$. If ($\beta_o \neq 0$ or $\neq \pi$), keep $\left(\partial T_s/\partial x\right)_o$ and find;

$$T_{si} = (1+a_1 n_i)T_{so} + (m_i + a_2 n_i)\left(\frac{\partial T_s}{\partial x}\right)_o + a_3 n_i + \frac{1}{2}\left(\frac{\partial^2 T_s}{\partial x^2}\right)_o m_i^2 + \frac{1}{2}\left(\frac{\partial^2 T_s}{\partial y^2}\right)_o n_i^2 + \left(\frac{\partial^2 T_s}{\partial x \partial y}\right)_o m_i n_i \quad \text{...(٤- ٢٣)}$$

where

$$a_1 = \frac{k_r}{k_s \Delta r \sin \beta_o} \quad \text{...(٤- ٢٤)}$$

$$a_2 = -\cot \beta_o \quad \text{...(٤- ٢٥)}$$

$$a_3 = -\frac{1}{k_s \sin \beta_o}\left(\frac{k_r}{\Delta r} T_r + q_{fr}\right) \quad \text{...(٤- ٢٦)}$$

As reported by Tseng [١٥], upon providing four arbitrary selecting neighboring points, Fig. (٤-٦), four independent equations similar to Eq. (٤-٢٣) can be obtained by following the procedure similar to that for treating the internal points, then;

$$[D_{ij}]\ \{DT_{sj}\} = \{f_i - T_{so}\} \qquad i, \quad \text{...(٤- ٢٧)}$$

$j = ١, \ldots\ldots, ٤$

where

$$D_{i1} = \frac{m_i + a_2 n_i}{1 + a_1 n_i}, \qquad D_{i2} = \frac{m_i^2}{2(1 + a_1 n_i)}, \qquad D_{i3} = \frac{n_i^2}{2(1 + a_1 n_i)}$$

$$D_{i4} = \frac{m_i n_i}{1 + a_1 n_i}, \qquad f_i = \frac{T_{si} - a_3 n_i}{1 + a_1 n_i}$$

and $\{DT_{si}\}$ is column matrixes containing the four derivatives of Eq. (٤-٢٣).

Again, inversion of $[D_{ij}]$ leads to

$$\{DT_{si}\} = [E_{ij}]\{f_j\} \qquad i = ١, \ldots, ٤,\ j = ٠ \ldots,\ ٤ \quad \text{...(٤- ٢٨)}$$

where $[E_{ij}]$ is the inverse of $[D_{ij}]$, $f_o = T_{so}$, and $E_{io} = -\sum_{j=1}^{4} E_{ij}$. Thus, the special derivatives at the boundary points, (x_o, y_o) become;

$$\left(\frac{\partial T_s}{\partial x}\right)_o = \sum_{j=0}^{4} E_{1j} f_j \qquad \text{...(٤-٢٩a)}$$

$$\left(\frac{\partial^2 T_s}{\partial x^2}\right)_o = \sum_{j=0}^{4} E_{2j} f_j \qquad \text{...(٤-٢٩b)}$$

and

$$\left(\frac{\partial^2 T_s}{\partial y^2}\right)_o = \sum_{j=0}^{4} E_{3j} f_j \qquad \text{...(٤-٢٩c)}$$

Substituting Eq. (٤-٢٩a) in Eq. (٣-٥٦) and determining $(\partial T_s/\partial y)_o$, then;

$$\left(\frac{\partial T_s}{\partial y}\right)_o = a_2 \sum_{j=0}^{4} E_{1j} f_j + a_1 f_o + a_3 \qquad \text{...(٤-٢٩d)}$$

Substituting the Eqs. (٤-٢٩a), (٤-٢٩b), (٤-٢٩c) and (٤-٢٩d) into strip governing Eq. (٣-٢), an algebraic relationship for the boundary point (x_o,y_o) was as reported by Tseng [١٥];

$$T_{so} = \frac{\sum_{j=1}^{4}\left[\alpha_s\left(E_{2j}+E_{3j}\right)-\left(u_o+a_2 v_o\right)E_{1j}\right]\left(T_{sj}-a_3 n_j\right)/\left(1+a_1 n_j\right)-a_3 v_o+q_d/\rho_s c_s}{\left(u_o+a_2 v_o\right)E_{1o}+a_1 v_o-\alpha_s\left(E_{2o}+E_{3o}\right)} \qquad \text{...(٤-٣٠)}$$

As expected, when (x_o,y_o) is a central point, Fig. (٤-٥), the solution of the GFDM equations, like their central difference counterpart in the CFDM, displays non-physical oscillation at high Peclet number.

Following remedy similar to that used in CFDM, upwind scheme was employed to achieve numerical stability. One-sided approximations were used for the convection terms and central differences for the conduction terms. For the first order upwind scheme;

$$T_{si} = T_{so} + m_i\left(\frac{\partial T_s}{\partial x}\right)_o + n_i\left(\frac{\partial T_s}{\partial y}\right)_o \qquad \text{...(٤-٣١)}$$

Two simultaneous equations were obtained by using two neighboring points ($x_١$, $y_١$) and ($x_٢$, $y_٢$).

The convective derivatives can be computed in terms of functional values at the selected neighboring points, (T_{s1} and T_{s2}), i.e.;

$$\left(\frac{\partial T_s}{\partial x}\right)_o = \left[(n_1 - n_2)T_{so} + n_2 T_{s1} - n_1 T_{s2}\right]/(m_1 n_2 - m_2 n_1) \quad \text{... (٤-٣٢a)}$$

$$\left(\frac{\partial T}{\partial y}\right)_o = \left[(m_2 - m_1)T_{so} - m_2 T_{s1} + m_1 T_{s2}\right]/(m_1 n_2 - m_2 n_1) \quad \text{...(٤-٣٢b)}$$

or

$$\left(\frac{\partial T_s}{\partial x}\right)_o = \sum_{j=0}^{2} F_{1j} T_{sj} \quad \text{...(٤-٣٣a)}$$

$$\left(\frac{\partial T_s}{\partial y}\right)_o = \sum_{j=0}^{2} F_{2j} T_{sj} \quad \text{...(٤-٣٣b)}$$

Substitute the Eqs. (٤-٣٣a) and (٤-٣٣b), and those in Eqs. (٤-٢١c) and (٤-٢١d) to the strip governing Eq. (٣-٢), the first upwind GFDM equation for each internal point was as reported by Tseng [١٥];

$$T_{so} = \frac{q_d / \rho_s c_s - \sum_{j=1}^{2}\left(u_o F_{ij} + v_o F_{2j} - \alpha_s B_{3j} - \alpha_s B_{4j}\right)T_{sj} + \alpha_s \sum_{j=3}^{5}\left(B_{3j} + B_{4j}\right)T_{sj}}{u_o F_{1o} + v_o F_{2o} - \alpha_s\left(B_{3o} + B_{4o}\right)} \quad \text{...(٤-٣٤)}$$

For the typical boundary condition described in Eq. (٣-٥٩), and using the same notations as in Eqs. (٤-٢٣) and (٤-٢٧) for (a_i and f_j), respectively, point (١) is again to be an upwind point, Fig. (٤-٦) then;

$$T_{si} = (1 + a_1 n_i)T_{so} + (m_i + a_2 n_i)\left(\frac{\partial T_s}{\partial x}\right)_o + a_3 n_i + (all\ terms = 0) \quad \text{...(٤-٣٥)}$$

or

$$\left(\frac{\partial T}{\partial x}\right)_o = \sum_{j=0}^{1} G_j f_j \quad \text{...(٤-٣٦)}$$

and

$$\left(\frac{\partial T}{\partial y}\right)_o = a_2 \sum_{j=0}^{1} G_j f_j + a_1 f_o + a_3 \quad \text{...(٤-٣٧)}$$

where $G_1 = -G_o = (1 + a_1 n_1)/(m_1 + a_2 n_1)$

Substitute the Eqs. (٤-٣٦), (٤-٣٧), (٤-٢٩b) and (٤-٢٩c) into strip governing Eq. (٣-٢), an upwind GFDM relationship for a boundary point (x_o,y_o) was as reported by Tseng [١٥];

$$T_{so} = \frac{\alpha_s \sum_{j=1}^{4} (E_{2j} + E_{3j}) f_j - (u_o + a_2 v_o) G_1 f_1 - a_3 v_o + q_d / \rho_s c_s}{(u_o + a_2 v_o) G_o + a_1 v_o - \alpha_s (E_{2o} + E_{3o})} \qquad \ldots(٤-٣٨)$$

٤.٣.١.٢- *Roll Governing Equation Representation*

An upwind CFDM based on cylindrical coordinates is more convenient and therefore is used to model the roll, because of the circular geometry of the roll.

The roll governing Eq. (٣-٥), is approximated by using second order central differencing for the conduction terms (right side) and first order up wind differencing for the convection terms (left side), the later eliminate the numerical instability resulting from high Peclet number as reported by Tseng [١٥] and Roach [٢٩].

The temperature profile becomes identical in a plot of normalized temperature, $T_r^* = H_o (T_r - T_\infty)/q_o$, against, $r^* = r/R$, which will certainly simplify further parametric study and high accuracy can be achieved by including the normalized temperature distribution.

Then, in dimensionless form the roll governing Eq. (٣-٥) becomes;

$$\frac{1}{r_o^*} \frac{\partial T_r^*}{\partial r^*} + \frac{1}{r_o^{*2}} \frac{\partial^2 T_r^*}{\partial \theta^2} + \frac{\partial^2 T_r^*}{\partial r^2} = Pe \frac{\partial T_r^*}{\partial \theta} \qquad \ldots(٤-٤٨)$$

where the superscript (*) refers to the dimensionless quantity.

In addition, as mentioned by Tseng *et al.* [١٨] the corresponding normalized boundary conditions should be transformed into dimensionless form too, then Eqs. (٣-٥٠), (٣-٥١) and (٣-٥٣) become Eqs. (٤-٤٠), (٤-٤١) and (٤-٤٢) respectively, thus;

$$\frac{\partial T_r^*(1,\theta)}{\partial r^*} = -Bi(\theta) T_r^*(1,\theta) \qquad \ldots(٤-٤٠)$$

$$\frac{\partial T_r^*\left(\frac{R-\delta}{R},\theta\right)}{\partial r^*} = 0 \qquad \ldots(٤-٤١)$$

and

$$k_s\left(\frac{\partial T_s}{\partial n}\right)_b + k_r \frac{q_o}{H_o}\left(\frac{\partial T_r^*}{\partial n}\right)_b - q_{fr} = 0 \qquad \ldots(٤-٤٢)$$

By using four arbitrary located neighboring points as shown in Fig. (٤-٧), then the roll governing Eq. (٣-٥) becomes;

$$\frac{T_{r4}^* - 2T_{ro}^* + T_{r2}^*}{\Delta r^{*^2}} + \frac{1}{r_o^*}\frac{T_{r4}^* - T_{r2}^*}{2\Delta r^*} + \frac{1}{r_o^{*^2}}\frac{T_{r3}^* - 2T_{ro}^* + T_{r1}^*}{(2\Delta\theta)^2} = Pe\frac{T_{ro}^* - T_{r1}^*}{\Delta\theta} \qquad \ldots(٤-٤٣)$$

Rearranging the above equation, an algebraic approximation for roll internal nodes was;

$$T_{ro}^* = \frac{a_{r1}T_{r1}^* + a_{r2}T_{r2}^* + a_{r3}T_{r3}^* + a_{r4}T_{r4}^*}{a_{ro}} \qquad \ldots(٤-٤٤)$$

where

$$a_{r1} = \frac{1}{(2r_o^*\Delta\theta)^2} + \frac{Pe}{\Delta\theta} \quad , \qquad a_{r2} = \frac{1}{(\Delta r^*)^2} + \frac{1}{2r_o^*\Delta r^*}$$

$$a_{r3} = \frac{1}{(2r_o^*\Delta\theta)^2} \quad , \qquad a_{r4} = \frac{1}{(\Delta r^*)^2} + \frac{1}{2r_o^*\Delta r^*}$$

$$a_{ro} = \frac{Pe}{\Delta\theta} + 2\left(\frac{1}{\left(2r_o^* \Delta\theta\right)^2} + \frac{1}{\left(\Delta r^*\right)^2} \right)$$

٤.٣.٢ *Boundary Conditions Representation*

The general relation for obtaining the GFDM and CFDM equations, for each interior node of strip and roll developed before. These relations were not applicable to nodes on the boundaries, however, since the boundary node does not have neighboring nodes on at least one side. Therefore, to obtain the finite differences equations of boundary nodes separately. Applying an energy balance to the volume elements of the boundary nodes. The energy balance is expressed as;

$$\sum Q_{all\ sides} + Q_{generation} = 0 \qquad \text{...(٤-٤٥)}$$

Boundary conditions most commonly encountered in practice are the specified temperature, specified heat flux, convection and radiation boundary conditions, and below the developed finite difference formulations for them for case of steady one-dimensional heat conduction as shown in Fig. (٤-٨).

The node a and d. the nodes of the strip that locate on this boundaries are subjected to a convection boundary condition, then the energy balance to this boundaries nodes, Eq. (٣-٤٦), gives;

$$T_s)_{i,j} = \frac{T_s)_{i,j-1} + \left(\frac{H_\infty \Delta y}{k_s} \right) T_\infty}{1 + \left(\frac{H_\infty \Delta y}{k_s} \right)} \qquad \text{...(٤-٤٦)}$$

Similarly, the roll nodes such as (f) are subjected to a convection boundary condition, Eq. (٣-٥٠), then, the energy balance to these boundary nodes, Eq. (٣-٥٠), gives;

$$T_r)_{i,j} = \frac{T_r)_{i,j-1} + \left(\frac{H(\theta)\Delta r}{k_r}\right)T_\infty}{1+\left(\frac{H(\theta)\Delta r}{k_r}\right)} \qquad \ldots(٤-٤٧)$$

Return back to Eq. (٣-٥٠) the Eq. (٤-٤٧) can be written in a dimensionless form as;

$$T_r^*)_{i,j} = \frac{T_r^*)_{i,j-1}}{1+Bi(\theta)\Delta r^*} \qquad \ldots(٤-٤٨)$$

where $Bi(\theta)$; is the Biot number $(H(\theta)R/k_r)$.

The node b and c. the nodes of the strip that locate on these boundaries are on the insulated boundaries, the energy balance at these boundaries gives;

For node b.

$$T_s)_{i,j} = T_s)_{i-1,j} \qquad \ldots(٤-٤٩)$$

For node c.

$$T_s)_{i,j} = T_s)_{i,j+1} \qquad \ldots(٤-٥٠)$$

Similarly, for the roll nodes such as (*e*), Eq. (٣-٥١)), becomes;

$$T_r)_{i,j} = T_r)_{i,j+1} \qquad \ldots(٤-٥١)$$

In the dimensionless form the above boundary condition becomes;

$$T_r^*)_{i,j} = T_r^*)_{i,j+1} \qquad \ldots(٤-٥٢)$$

Finally, the interface boundary condition was included previously in the numerical formulation and the billet region was assumed previously has a uniform temperatures of $T_s = T_o$.

٤.٤ *Numerical Calculations Algorithm*

The numerical calculations described in the previous article had transformed to a numerical calculation algorithm from which a computer

program (described later) was developed. The steps of this numerical algorithm are as follows:

١. Calculate the grid generation for the strip and roll. The strip grid generation in bite region was determined from Eqs. (٤-٩) and (٤-١٢). Then, the grid for billet and product are uniformly divided in *x* and *y* directions after assuming a certain lengths for the billet and product.

In the roll, the value of (δ) calculated from Eq. (٣-٨) is divided equally in (r) direction and the divisions in (θ) direction are refined during the contacting surfaces to match that used in (strip) bite region.

٢. Calculate the velocity distribution for the strip (u) and (v) in (x) and (y) direction from Eqs. (٣-٢٢) and (٣-٢٦) respectively.

The billet and the product regions have velocity (u) in the (x) direction only (i.e., v= ٠) and calculated respectively as follows;

$$u = \frac{t_n}{t_o} V_r \qquad \ldots(٤-٥٣)$$

and

$$u = \frac{t_n}{t_f} V_r \qquad \ldots(٤-٥٤)$$

In the present study ($t_n = t_f$), then the Eq. (٤-٥٤) becomes;

$$u = V_r \qquad \ldots(٤-٥٥)$$

٣. Calculate the distribution of the heat generation by plastic deformation from Eqs. (٣-٣٢) and (٣-٣٦).

٤. Calculate the distribution of the heat generation by friction from Eq. (٣-٣٩).

٥. Calculate the heat transfer coefficient $H(\theta)$ from Eq. (٣-١١) and from Fig. (٣-٣).

٦. Assign the initial temperature distribution for the strip and roll to start with the solution of the Gause-Seidel iteration with under relaxation technique.

٧. Investigations of the boundary nodes to define the boundary conditions for the strip and the roll from Eqs. (٤-٤٢), (٤-٤٦), (٤-٤٨), (٤-٤٩), (٤-٥٠) and (٤-٥٢). The entering temperatures were assumed to have (T_o).

٨. Investigation of the interior nodes to calculate the temperature distribution for the strip (billet, bite, and product) and the roll from Eqs. (٤-٣٤), (٤-٣٨) and (٤-٤٤).

٩. Calculate the heat transfer to the roll, and the heat transfer from the strip from the Eq. (٤-٤٢).

٤.٥ *Computer Program*

A computer program was written in Quick Basic to perform the mathematical solution and numerical solution formulated previously.

The program consists of six main parts. The first is for the grid generation. The second deals with the velocity distribution of the strip. The third deals with the deformation heat generation distribution, friction heat generation distribution and heat transfer coefficients. The fourth is to calculate the temperature distribution for both strip and roll simultaneously. The fifth is to calculate the heat flux from strip and heat flux to roll and the sixth part is for output results arrangements.

In the first part of the program, the grid generation for both strip and roll was generated simultaneously. The (x-y and r-θ) coordinates was developed to locate the position of each point in the strip and roll.

In the second part, the velocity distribution, (u) and (v) in (x and y) directions respectively was developed for the strip (billet, bite and product) regions.

In the third part, the deformation and friction heat generation distribution was calculated from the input data of the direct measurements of power. Moreover, the heat transfers coefficient calculations $H(\theta)$.

In the fourth part, the temperature distribution for both strip and roll was solved simultaneously by GFDM and CFDM by using Gause-Seidel iteration method.

In the fifth part, the heat flux to roll is calculated and equals to the sum of interface heat flux and the heat flux transferred from the strip.

In the last part of the program, the output results were arranged in order to be printed-out or saved in output files for further presentations.

٤.٥.١ *Program Input Data*

The input data of the program may be classified as follows;

١. The strip and roll dimensions, which include the entry thickness (t_o), exit thickness (t_f), billet length, product length, strip width (W), work roll-diameter (D) and constants using for dimensionless roll calculation (q_o, H_o).

٢. The number of divisions in both (x and y, r and θ) directions for the strip and roll respectively, for both mathematical and numerical calculations. Where (*ndxbl, ndxb* and *ndxp*) are the numbers of divisions in the billet, bite and product regions respectively in the (x) direction. (*ndy*) is the number of divisions in the strip in the (y) direction. (*ndthbr* and *ndthr*) are the numbers of divisions for roll in the bite and in the cooling region respectively in the (θ) direction.

٣. The strip and roll thermal properties, thermal conductivity (k_s, k_r), and thermal diffusivity (α_s, α_r).

٤. Ambient influences, these are represented by the temperature of the circumference (T_∞), cooling heat transfer coefficients (H_∞ and $H(\theta)$), roll speed (V_r), strip entry temperature (T_o), and the input data from the direct measurements of power.

٥. Gause-Seidel iteration input data, this included the damping factor (λ=٠.٩٨) and error limits (*ER*=٠.٠٠٠١). Some times (λ) called weighting factor that is assigned a value between (٠ and ٢), the choice of a proper value for (λ) is highly problem specific and is often determined empirically as mentioned by Chapra and Canale [٣٣].

٤.٥.٢ *Program Output Data*

The output data of the program include the following;

١. The strip grid generation and roll grid generation.

٢. The strip velocity distribution for the billet, bite and product regions.

٣. The heat generation distribution of the plastic deformation and friction.

٤. The distribution of the heat flux from strip and the distribution of the heat flux to roll.

٥. The strip temperature distribution and roll temperature distribution.

٤.٥.٣- *Program Specifications*

The program was written in Quick Basic and designed for Pentium (II) (PERSONAL COMPUTER) of ١٢٨ MB RAM. Using operation system Dos to run the program. The execution time of the program was less than (١:٢٠) hours.

When the (*ndxb*=٢٠, *ndxp*=٢٠, *ndxbl*=٥, *ndy*=١٥ and *ndthr*=٥٢), the program takes ٢٨٨٠ iteration to reach to the convergence of criterion. The convergence of criterion is the different in temperatures between the current and previous nodal values of strip or roll and is equal or less than (٠.٠٠٠١). The total number of nodes of the strip and roll is (١٧٥٥) nodes.

The strip initial temperature distribution is (٦٥.٦ ^{o}C) (entrance temperature) and the roll initial normalized temperature distribution is (٠.٤٥).

The flowchart of the program is given below;

The Main Program

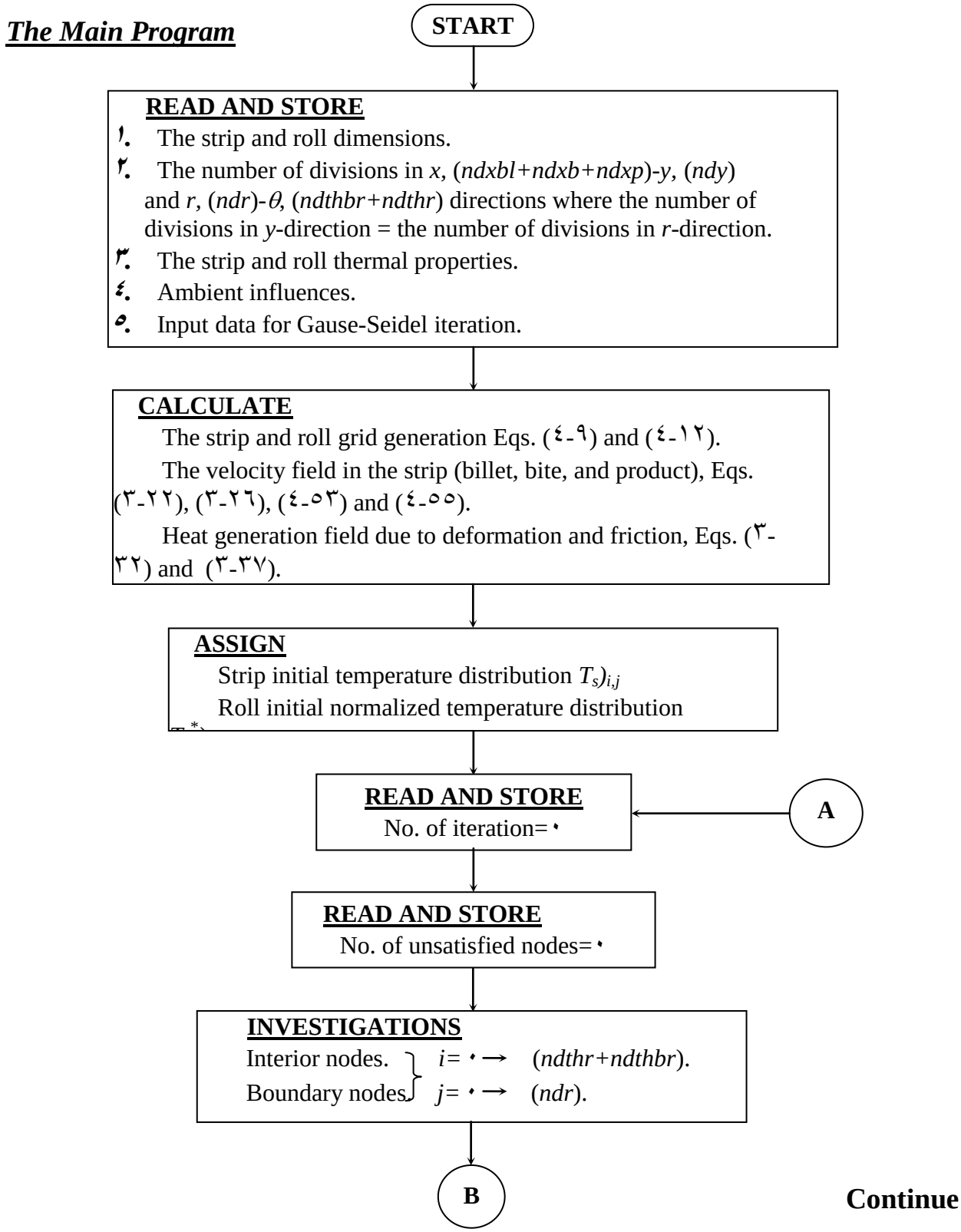

Continue

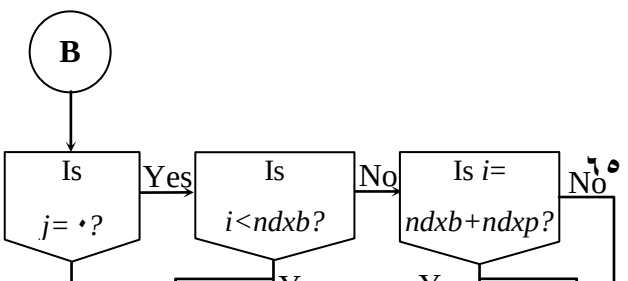

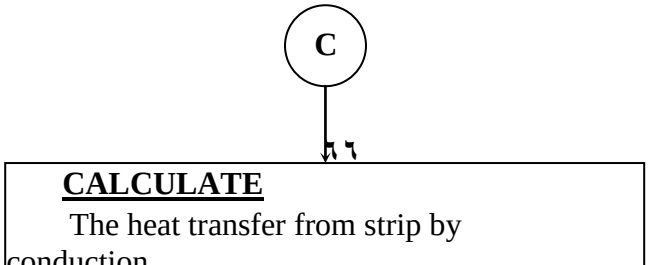
C
CALCULATE
The heat transfer from strip by
conduction

The CFDR Subroutine

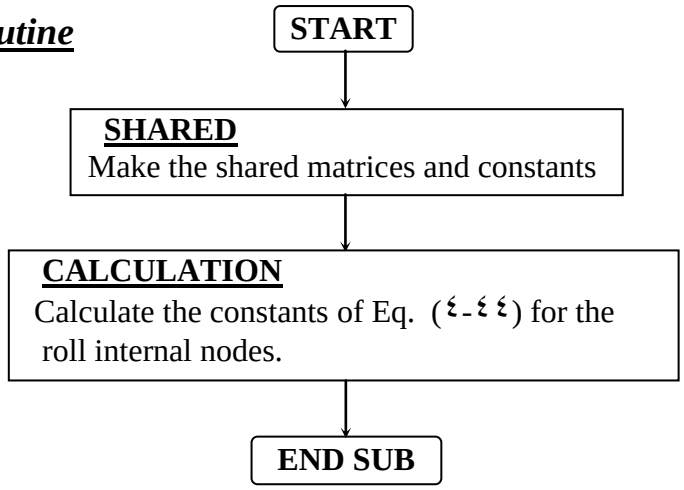

Continue

The GFDIN Subroutine

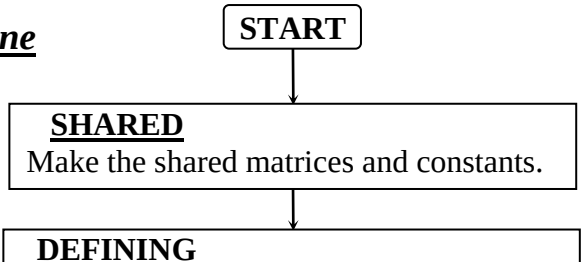

The GFDF Subroutine

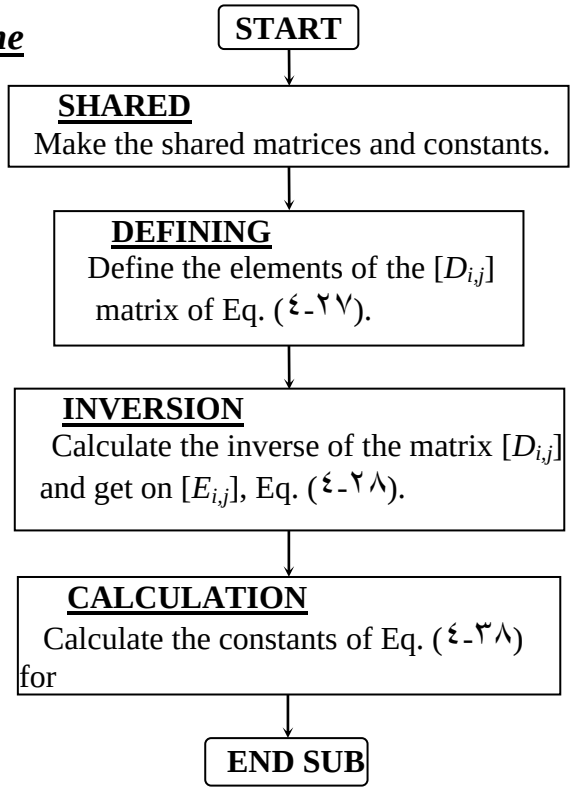

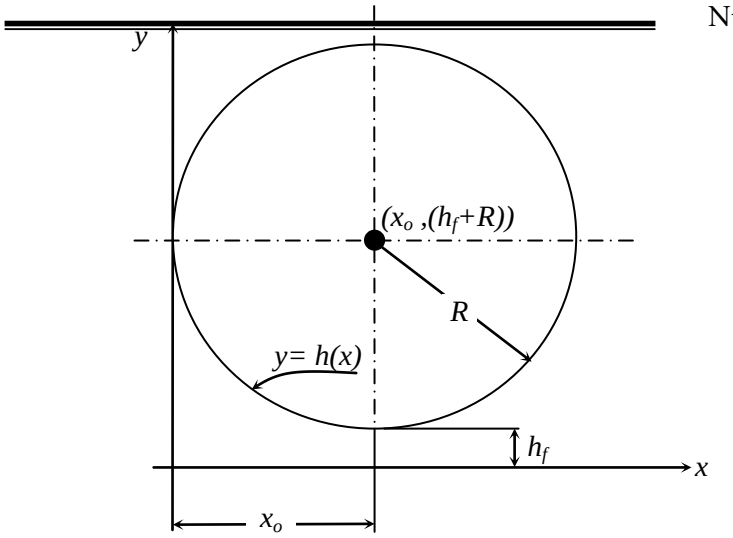

Fig. (٤-١): Representation of the Roll Coordinates.

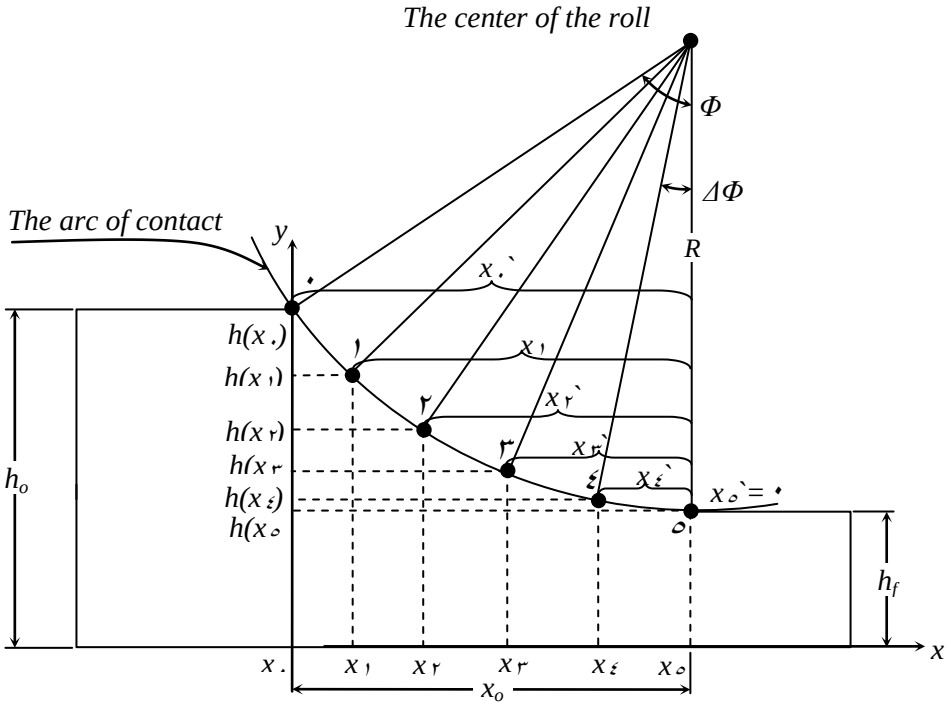

Fig. (٤-٢): Explains the Method was used to Calculate the Strip Grid Generation.

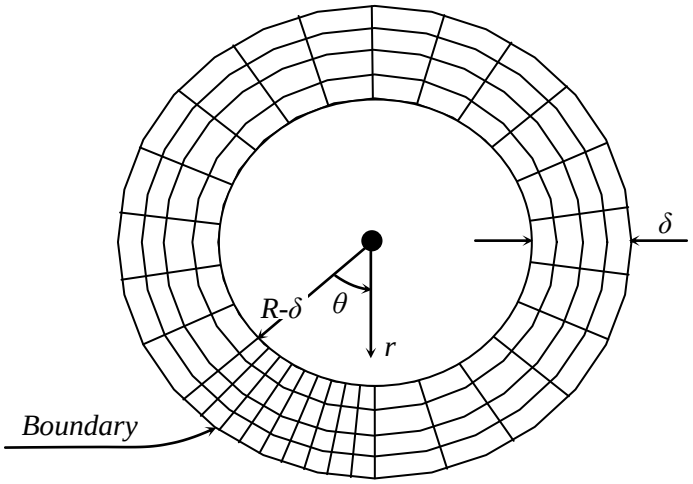

Fig. (٤-٣): Typical Mesh for the Roll, Ref. [١٥ and

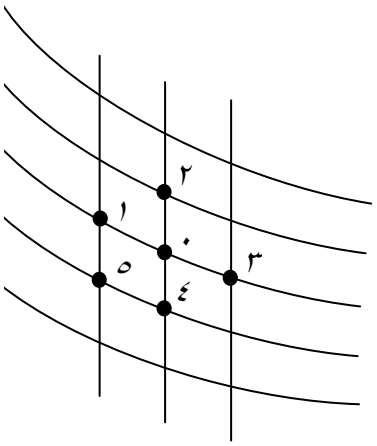

Fig. (٤-٥): The Grid Arrangement for the Strip Internal Nodes, Ref. [١٥ and ١٦].

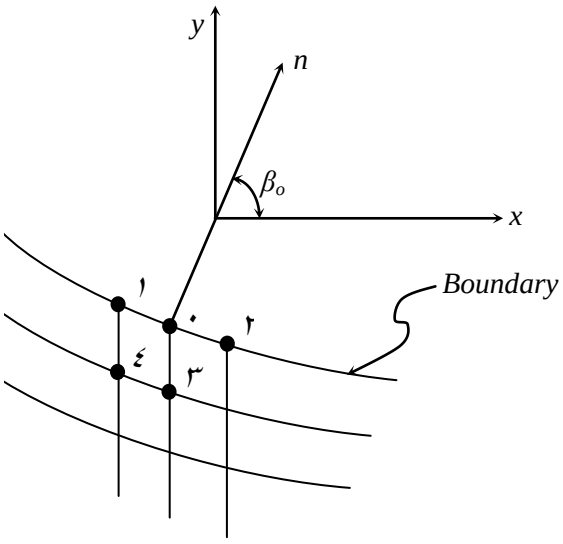

Fig. (٤-٦): The Grid Arrangement for the Strip Boundary (Interface) Nodes, Ref. [١٥].

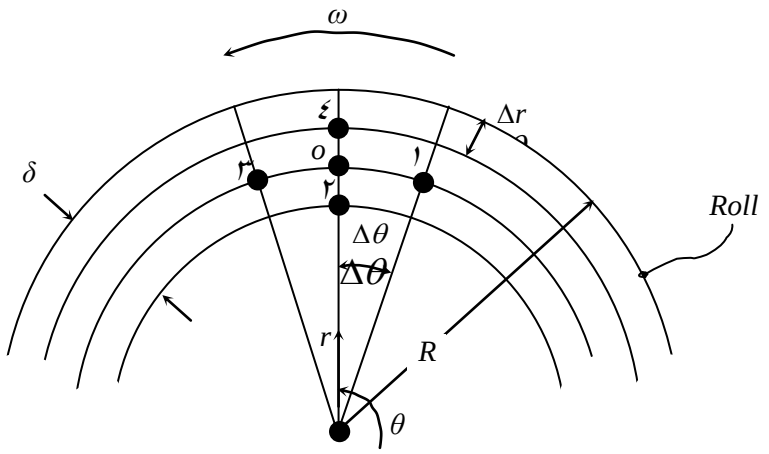

Fig. (٤-٧): Neighboring Points Arrangement for Roll Internal Nodes.

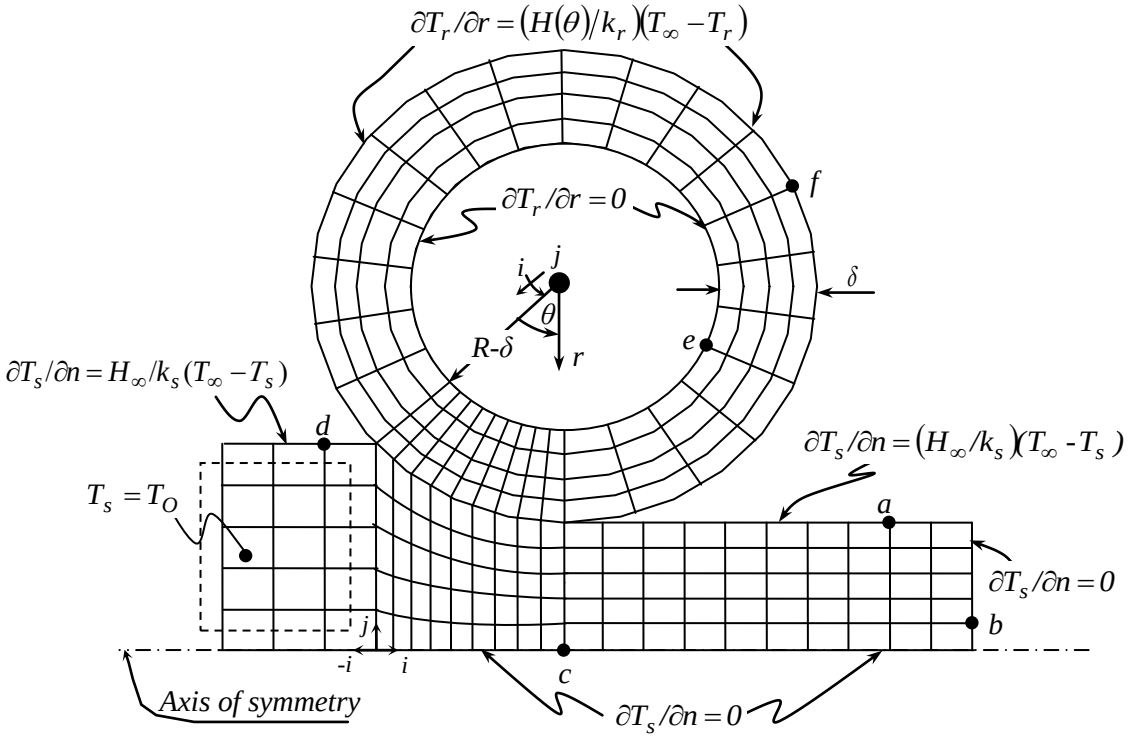

Fig. (٤-٨): Typical Boundary Conditions and Mesh for Strip and Roll, Refs. [١٥ and ١٦].

٥ Results and Discussion

This chapter presents the numerical results of the present work. Besides, a verification of the computational model will be made through a comparison between the numerical results of the present work and published papers [١٥ and ١٦].

٥.١ Numerical Results

The results obtained from the developed computer program described in chapter four will be shown in this section. These numerical results are for cold and hot rolling.

٥.١.١ Grid Size

The developed computer program deals with a grid having a number of divisions in strip in the bite region equal to (*ndxb,ndy*) divisions in the (*x-y*) directions respectively. Similarly, a number of divisions in roll in bite the region equal to (*ndr,ndthbr*) divisions in the (r-θ) directions respectively, where (*ndxb=ndthbr*) and (*ndy=ndr*) are input values specified by the user.

To investigate the effects of the grid sizes on the numerical solution, these divisions are set at different values and the steadiness of the solution are observed. During the investigation, the calculated value of the strip temperature (T_s) at the exit plane (at the surface) was considered, i.e., at ($x=x_o$ and $y=h_f$). The procedure is described below;

At first the values of (*ndxb*×*ndy*) where changed from (٥×٥ to ٤٠×٣٠). The value of calculated (T_s) from Eq. (٤-٣٨) at the exit plane was constant beyond (٢٠×١٥), as shown in Figs. (٥-١) and (٥-٢) for the first and second case study (Tables (٥-١) and (٥-٢)) respectively.

As a result from the above investigations, a ٤٥ (divisions in *x*-direction, (*ndxbl*=٥)+(*ndxb*=٢٠)+(*ndxp*=٢٠))×١٥ (divisions in the *y*-direction) mesh was selected for the strip in which ٢٠×١٥ were within the bite region. The mesh in (*y* and *r*) directions are uniformly distributed over the local thickness of the bite and explorer depth respectively, and the mesh is also chosen to match the uniform spacing along the circumference of the roll. In the billet and the product regions the mesh uniform in *x* and *y* directions.

A ٧٢ (circumferential ((*ndthbr*=٢٠)+ (*ndthr*=٥٢)) × ١٥(radial (*ndr*)) mesh was used for the roll. The roll mesh was refined near the bite region to match that used in the strip (i.e., *ndxb*=*ndthbr*). Based on this mesh arrangement, the computed temperatures of the strip at the exit plane for different grid sizes are shown in Figs. (٥-١) and (٥-٢).

٥.١.٢ *Numerical Results of the Program*

The numerical results of the program will be presented in this article for the velocity distribution, heat generation by deformation and friction, and the results of the temperature distribution for both cold and hot rolling. The results will be presented along different lines used in the numerical calculations. Two different cases has been investigated, the first case for roll speed of (١١٤٦.٦ cm/s) and the second case for roll speed of (١٢١٩ cm/s).

٥.١.٢.١- *Results of the Velocity Distribution*

Figs. (٥-٣) and (٥-٤) show the calculated velocity (u) in the (x) direction (horizontal component) for the first and second case study. Before the bite region (billet) the strip has velocity (u) only, i.e., (v=٠). Since equal volumes of metal must pass at any vertical section through the roll gap and the vertical elements remain undistorted (no increase in width), Eq. (٣-١٣) requires that the exit velocity must be greater than entrance velocity, therefore, the velocity (u) of the strip must be steadily increased from entrance to exit. At the exit plane ($t= t_f= t_n$), as shown in Eq. (٣-٢١), this plane (product region) having (u) velocity only, i.e., (v=٠) as shown in Eq. (٤-٥٥).

The calculated velocity (v) in the (y-direction) (vertical component) for the first and second case study and for different lines are shown in Figs. (٥-٥) and (٥-٦). Before the bite region (billet), the streamlines are horizontal and having horizontal component of velocity (u) only and (v=٠). After entering the roll gap (bite) the streamlines have curved shapes and the slopes of these curves gradually decrease from entrance to exit and from the arc of contact to the axis of symmetry. Then the velocity (v) gradually diminishes from entrance to exit and from the arc of contact to the axis of symmetry as shown in Eq. (٣-٢٦) and in Figs. (٥-٥) and (٥-٦).

٥.١.٢.٢ *Results of the Heat Generation by Deformation and Friction*

As mentioned by many authors such as Tseng [١٥ and ١٦], Lahoti *et al.* [٣], and Zienkiewicz *et al.* [١٠], rolling a mild steel at the speed presently considered as shown in Tables (٥-١) and (٥-٢), consume about (٩٠) percent of the total power in the deformation of the work piece and in the friction loss at the interface.

Moreover, according to Zienkiewicz *et al.* [١٠] and Tseng [١٥ and ١٦] measured both the plastic work and the temperature rise in a tensile experiment. It was found that for steels, copper and aluminum, the heat rise represents

(٨٦.٥, ٩٠.٥-٩٢ and ٩٥) percent, respectively, of the deformation energy which is converted into heat.

In the present study, this (٩٠) percent estimated is used, i.e., that (٦.٥) percent of (٩٠) percent of total power is dissipated as friction heat along the interface.

The remainder of plastic work is stored as internal energy associated with the non-homogeneous deformations that are inherent characteristics of plastic flow. This energy can be recovered during heat treatment.

Using forgoing numbers, the resulting values of the heat generation by deformation and friction were summarized in the Table (٥-٣) for the first and second case study. In the first case study, the heat generation by deformation and friction are assumed to be uniformly distributed in the deformed region (bite) and the interface as shown in the Figs. (٥-٧) and (٥-٨) respectively where x and x_o have been defined in Fig. (٣-١).

In the second case study, the heat generation by deformation is then distributed to the strip in proportion to the local effective strain rate as shown in Eqs. (٣-٣٢) and (٣-٣٦) and Fig. (٥-٩). Note that the highest strip deformation (strain rate) occurs near the bite entry and diminishes monotonically toward the end of the bite, then the highest strain rate occurs near the bite entry as shown in Fig. (٥-١٠). Thus, the highest heat generation by deformation occurs near the bite entry too and diminishes monotonically toward the end of the bite as shown in Eq. (٣-٣٩) and Fig. (٥-٩).

Also, the strip is to be moved relative to the other (roll) creating friction heat along the interface as recorded in Eq. (٣-٣٨), i.e., the friction heat is then distributed in proportion to the slip velocity (relative velocity between the strip and roll) as recorded in Eq. (٣-٣٧) and in Fig. (٥-١١). The maximum slip occurs at the first point of contact at the strip-roll interface because the roll draws the thick

strip into the roll gap. Then, the slip velocity decreases gradually until sticking (no slip) at the final point of contact as shown in Fig. (٥-١٢).

Finally, since the deformation starts at the entrance plane, then there is no deformation occurs in billet region that leads to no heat generation by deformation that takes place in this region.

Similarly for the product, the deformation terminals at the exit plane, then there is no heat generation by deformation in this region.

٥.١.٢.٣ *Results of Cold Rolling Temperature Distribution*

As an illustration, a rolling condition recorded from one of the Bethlehem steel's cold tandem mills is analyzed by the present finite difference scheme. The operational parameters recorded and summarized in Tables (٥-١) and (٥-٢).

Figs. (٥-١٣) and (٥-١٤), indicate that the roll temperature variations (with different heat transfer coefficient, $H(\theta)$, distribution and with different heat generation distribution (q_{fr} and q_d) for the first and second case study respectively) are limited within a very thin layer, about ١ percent of the radius, which consistent with the associated boundary condition Eq. (٣-٥١). The surface temperature rapidly increases at the bite due to great heat generated by the friction and transferred from the strip. As the roll leaves the bite, the roll surface temperature immediately decreases due to heat convected to the coolant and heat conducted into the immediate sub surface layer. In general the results of the present study are similar to the results of Refs. [١٥ and ١٦].

As well as, as shown in Figs. (٥-١٣) and (٥-١٤) the different in temperatures between the final and initial points of contact for the first case study is less than for the second case. This means, using several small coolant sprays (second case) is more efficient than one large spray (first case).

Figs. (٥-١٥) and (٥-١٦) indicate that while the strip is under deformation (uniform and non-uniform distribution of (q_{fr} and q_d), the bulk temperatures

inside the strip increase continuously; this is largely controlled by the deformation energy. On the other hand, the strip surface temperature changes much more drastically and it is mainly controlled by the friction heat and the roll temperature.

The coolant heavily cools the roll, it acts like a heat sink. Thus, as soon as the strip hits the roll its surface temperature drops as shown in Figs. (٥-١٥) and (٥-١٦). Since considerable friction and deformation heat are created along the interface and transferred from the neighboring sub layer, the surface temperature picks up rapidly.

Beyond the bite, Figs. (٥-١٥) and (٥-١٦), the strip temperature tends to be uniform. In this region, the heat convected to the air has been assumed to be negligible. For high-speed rolling (rather than the considered limits), the strip (product) temperature behaves parabolically rather than elliptically as implied by Eq. (٣-٢). In other words, the boundary conditions that are assumed in the downstream region (product) should not have a noticeable effect on the bite region.

The interface heat fluxes results for uniform and non-uniform heat generation distributions are shown in Figs. (٥-١٧) and (٥-١٨). At the initial contact stage, as anticipated, a very large amount of heat is transferred to the roll. In fact, the roll surface temperature is about (٢٥ ^{o}C and ١١.٠٣٦٢ ^{o}C) lower than that of the strip as shown in Figs. (٥-١٣), (٥-١٤), (٥-١٥) and (٥-١٦), respectively.

To satisfy the boundary condition Eq. (٣-٥٧), a step change of surface temperatures are expected to occur at the initial contact point (x=٠). The induced heat flux to the roll at (x=٠) as shown in Figs. (٥-١٧) and (٥-١٨), also ensure the above findings that a large amount of heat is transferred to the roll from strip and the interface friction at the initial contact stage. The heat flux transferred to the roll equals the sum of the friction heat and the heat flux transferred from the strip. In the rest of contact area, the heat flow from the strip to the rolls obeys

an inverse law with distance (or time) into the roll gap. This is similar to the theoretical heat transfer variation with time that occurs between two semi-infinite bodies brought together when they are initially at different temperatures.

The theoretical heat transfer between two semi-infinite bodies varies as the inverse square root of time.

It is believed that in the previous studies, the strip initial temperatures were close to that of the roll. Therefore, the strip is not expected to have a temperature drop at the initial contact stage. However, it is note worthy that at very high rolling speeds, measuring the local temperature change in the bite could be a big challenge as mentioned previously in Refs. [١٥ and ١٦].

٥.١.٢.٤ *Results of Hot Rolling Temperature Distribution*

In hot rolling, the strip is normally rolled at elevated temperatures at which re-crystallization proceeds faster than work hardening. In addition, the hot strip is generally rolled at thicker gages and lower speed than that of the cold strip.

Since the gages specified in the first case study (Table (٥-١)) are still suitable for hot rolling, these gages are used for the hot rolling analysis. Two focuses are considered. The first focuses on the effect of changing the working temperature by raising the strip entry temperature to (٩٠٠ ^{o}C), which is frequently encountered in hot rolling. The second focus shows the effect of changing velocity by slowing the roll speed from (١١٤٦.٦ to ٥٧٣.٣ cm/s). The other operating conditions are similar to those discussed for cold rolling.

Fig. (٥-١٩) depicts the roll temperature distribution for the two hot rolling cases consider (V_r=١١٤٦.٦ and ٥٧٣.٣ cm/s). A comparison of Fig. (٥-١٩) with Fig. (٥-١٣) indicates that the temperature profile between the hot and cold rolling is mainly in magnitude but not in shape.

Both the interface heat flux and speed govern the temperature magnitude. As shown in Fig. (٥-٢٠) at speed of (١١٤٦.٦ cm/s), the heat flux increases about

four times for the hot to cold rolling. The corresponding increase of temperature is also found to be about four time too as shown in Figs. (٥-١٩) and (٥-٢١).

Fig. (٥-١٩) shows except in the bite region, the roll temperature is reducing about ١٥ percent with the speed slowed to (٥٠) percent. As indicated in Fig. (٥-٢١) the different in the bite region is much smaller and the maximum temperature occurs at the end the arc of contact. For example, the corresponding decrease of the peak temperature is less than (٢) percent. The temperature decrease due to slowing the speed is mainly due to decrease of the heat flux Fig. (٥-٢٠).

Actually, when keeping constant heat flux, slowing the speed will increase the temperature because at a lower speed where the time of the flowing through roll gap becomes larger, conduction in the radial direction will be dominant and the local temperature rise will be more. Figs. (٥-٢١) and (٥-٢٢) also show that near the bite, very large temperature variations are within a very thin layer. The layer thickness (δ), consistent with the previous finding, is dependent on the speed, or more precisely, the roll Peclet number as shown in Eq. (٣-٦).

The strip temperatures for the two hot rolling cases are presented in Fig. (٥-٢٣). In the bite region, the strip temperature, similar to the roll temperatures, is not noticeably affected by changing the speed within the range consider. In the down stream region ($x>x_o$), the strip centre temperature drops faster in the slower strip. By contrast, the surface temperatures are not sensitive to the speeds considered. This figure also indicates the temperature drop in the initial contact stage is much large than its counterpart for the clod strip, as shown in Fig. (٥-٢٣). When the strip entry temperature rises from (٦٥.٦ ^{o}C) to (٩٠٠ ^{o}C) from cold to hot rolling, the temperature drop increases approximately from (٢٥ ^{o}C) to (٦٤٩ ^{o}C), reflecting the great increase in the temperature different between the strip and roll a head of the bite.

The shape of the heat input distribution to the roll (q_r) governs the roll and strip temperatures in the roll gap region. As shown in Figs. (٥-١٦) and (٥-٢٢)

with a parabolic distribution of (q_r) of the second case study, the location of the maximum temperature shifts to the interior of the arc of contact (heating zone). Although, the cumulative energy input is still increasing beyond ($\Phi/2$), the flux is decreasing, yet the effect of the type of heat distribution on the temperature distribution away from the roll gap should be minimal as shown in Figs (٥-٢١) and (٥-٢٢).

Finally, note that for the same amount of thickness reduction, the power requirement for hot rolling generally less than that for cold rolling. However, in view of uncertainty of the friction behavior and the deformation energy publications noted before, in the present study, it is not worth while to explore the effects of changing friction energy of variability due to deformation energy.

٥.٢ *Verification of Computational Model*

A verification of the proposed computational model of the present work is made here through a comparison between the numerical results of the present work and with those calculated by Tseng [١٥ and ١٦].

٥.٢.١ *Comparison with Published Works*

In order to check the accuracy of the present computations, the numerical results of the present work will be compared with numerical results of Refs. [١٥ and ١٦]. The comparison will be made along the surface line and centre line of the strip temperatures.

٥.٢.١.١ *Comparison with the Temperatures of Cold Rolling*

A verification of the proposed numerical scheme is made here through a comparison between the calculated temperatures of the cold rolling case with the temperatures calculated by Tseng [١٥ and ١٦] for the same case along line of study. Figs. (٥-٢٤) and (٥-٢٥) show typical examples of such comparison for the temperature distribution.

٥.٢.١.٢ *Comparison with the Temperatures of Hot Rolling*

Similarly, the calculated temperatures of the hot rolling case are compared with its counterpart that is calculated by Tseng [١٦]. Fig. (٥-٢٦) shows typical example of such comparison for the temperature distribution. A similar trend of verifications to that of Figs. (٥-٢٧), (٥-٢٨), (٥-٢٩), (٥-٣٠) and (٥-٣١) respectively was obtained.

٥.٢.٢ *The Concluding Remarks from the Comparisons*

It is clear from all the comparisons mentioned previously that larger deviation for the second case study occurs at the first point of contact, i.e., at (x= ٠ and $h=h_o$) and this deviation decreased gradually until reach its minimum value at exit, i.e., at ($x=x_o$ and $h=h_f$) as shown in Table (٥-٤). The main reasons for this deviation are the amount of (q_{fr}) at the first contact point and (q_d) near the entrance of the bite that have values larger than its values that are calculated by Tseng [١٥] as shown in Figs. (٥-٢٧), (٥-٢٨) and (٥-٢٩).

But with respect to the first case study, the amount of deviation is less than deviation that occurs in the second case study. The main reasons for this small deviation are the small difference between calculated (q_{fr} and q_d) in the present study and with those calculated by Tseng [١٦] as shown in Figs. (٥-٣٠) and (٥-٣١). This deviation was calculated from the following equation;

$$Dev.\ \% = \frac{T_s)_{pres.\ study} - T_s)_{cal.\ [15\ and\ 16]}}{T_s)_{cal.\ [15\ and\ 16]}} \qquad \textbf{...(٥.١)}$$

The main reasons for the deviation between the calculated (q_{fr} and q_d) in the present study and those calculated by Tseng [١٥ and ١٦] are;

١. Tseng [١٥ and ١٦] mentioned, there is no difficulty to be expected when the mesh generation codes are used, i.e., he may use this codes to perform the grid, but in the present study an mathematical equations in chapter four are used to generate the grid for the strip and roll.

٢. Tseng [١٥] mentioned, the deformation heat is distributed in proportion to the effective strain rate and the friction heat is distributed in proportion to the

slip velocity at the interface. Ref. [١٥] did not give a detailed description for the method used to calculate (q_{fr}) and (q_d,) but in the present study the (q_{fr}) and (q_d)are calculated from mathematical equations described in chapter three.

٣. In the present study, the environment temperatures (T_∞) are (٣٠ m^{o}C and ٥٠ ^{o}C) for the first and second case study respectively, but in the Refs. [١٥ and ١٦] the used (T_∞) are not recorded.

Finally, the present study also shows by comparing the present results with published findings by Tseng [١٥ and ١٦] that the computational scheme used is effective and reliable. However, it is believed that the greatest uncertainty in analysis will arise not from the numerical scheme, but from the input data, in particular, the friction energy, the location of the neutral point (or the forward slip), and the heat transfer coefficient of coolant.

Strip Material.	Mild Steel.
Roll Material.	Cast Steel.
Coolant.	Water.
Entry Gauge.	٠.١٥ cm (٠.٠٥٨٩ in).
Exit Gauge.	٠.١١٤ cm (٠.٠٤٥ in.).
Roll Speed.	١١٤٦.٦ cm/s (٢٢٥٧ fpm).
Roll Angular Speed	٢٢.٧٥ rpm
Forward Slip.	٠
Strip Width.	٦٣.٥ cm (٢٥ in).
Work-Roll Diameter.	٥٠.٨ cm (٢٠ in).
Total Input Energy.	٣٦٩٤ kW (٤٩٥٤ HP).
Strip Entry Temperature.	٦٥.٦ ^{o}C (١٥٠ ^{o}F).

Table (٥-١), (First Case) Operational parameters for Coil ٤٥, Ref. [١٦].

Strip Material.	Mild Steel.
Roll Material.	Cast Steel.
Coolant.	Water.
Entry Gauge.	٠.٠٨٥ cm (٠.٠٣٣ in).
Exit Gauge.	٠.٠٥٧ cm (٠.٠٢٢٦ in).
Roll Speed.	١٢١٩ cm/s (٢٤٠٠ fpm).
Roll Angular Speed	٢٤.١٨٦ rpm
Forward Slip.	٠
Strip Width.	٨١.٣ cm.
Work-Roll Diameter.	٥٠.٨ cm (٢٠ in).
Total Input Energy.	٣٣٤٠ kW (٤٥١٥ HP).
Strip Entry Temperature.	٦٥.٦ ^{o}C (١٥٠ ^{o}F)

Table (٥-٢), (Second Case) Operational parameters for Coil ٣٢, Ref. [١٥].

Both the roll and the strip have the following thermal properties: -

Thermal conductivity (k_r, k_s); ٠.٤٥٧٨ W/cm.^{o}C

Thermal diffusivity (α_r ,α_s); ٠.١٢٦٧ cm^{٢}/s

Case Number	Heat Generation by Plastic Deformation Q_d (kW)	Heat Generation by Friction Q_{fr} (kW)
١st	٢٤٥٠	١٩٨
٢nd	٢٦٨٩	٢١٧

Table (٥-٣), Amounts of the Heat Generation by Deformation and Friction.

Case Number	The Strip Cold Temp. at x= ٠ and $h=h_o$		Dev. % at x= ٠ and $h=h_o$	The Strip Cold Temp. at $x=x_o$ and $h=h_f$		Dev. % at $x=x_o$ and $h=h_f$	Average of Dev.%
	T_s cal. [١٥ , ١٦]	T_s Present Study		T_s cal. [١٥ , ١٦]	T_s Present Study		
١st	٤٠.٦	٤٣.١	٦.١٥٪	١١٠.٤	١١٣.٣٢	٢.٦٤٪	٤.٤٪
٢nd	٥١.٨١	٥٦.١٧	٨.٤٢٪	١٢٤	١٢٨.٤٨	٣.٦٢٪	٦.٠٢٪

Table (٥-٤), Comparison between the Present Study and those Published in Refs. [١٥ and ١٦].

٦ Conclusions and Suggestions for Future Work

The following are the conclusions drawn from the present investigation and suggestions for the future work are given.

٦.١ Conclusions

The heat transfer behavior of the rolling process has been studied for cold and hot rolling conditions and the conclusions are as follows:

١. While the heat generation by deformation occurs in the strip or by friction at the strip-roll interface and the heat removal is at the roll surface then, both strip and roll should be considered together and solved simultaneously.

٢. The highest heat generation by the deformation and friction occurs at the entrance to the bite and diminishes gradually toward the end of the bite.

٣. The results show that the extremely large temperature drop at the interface and large temperature variation in both roll and strip are found. Such high temperature variations could create very large (δ) thermal stresses within the thin layer and this stresses lead to the roll wear or roll failure, then proper control of this stresses could significantly extend the roll life.

٤. Several small coolant sprays (second case) are more efficient than one large spray (first case).

٥. The temperature decreases due to slowing the roll speed, this is mainly due to decrease the total input power that led to decrease of the heat flux at the interface.

٦. The shape of the heat input distribution (uniform or parabolic heat input) to the roll governs the location of the peak temperature.

٧. Knowledge of roll and strip temperatures can contribute to insights about the metallurgical structure of the strip, and eventually lead to better control of the material properties and surface conditions.

٨. The heat input rate (q_o) can also be eliminated by defining a dimensionless roll temperature consequently, information concerning the shape and behavior of the temperature distributions can be obtained without specific knowledge of the heat transfer coefficient, H_o, or the heat input rate, q_o. However, these quantities would have to be determined and specified if actual roll temperatures were desired.

٦.٢ *Suggestions for Future Work*

As related to the present work, the following suggestions for future developments forward;

١. Treating the problem as three-dimensional problem, however, the effect of axial heat flow or axial temperature variations is significant and should be taken into account.

٢. Considering the time effect, the inclusion of the unsteady-state term in the governing equations should be considered.

٣. Suggest mathematical expression to consider the thermal resistance (roughness of the surface and lubricant scale layer at the interface) in the calculations and its effect on the interfaces heat fluxes and on the temperature distribution.

٤. Suggestion a method for obtaining the shape of an elastic deformation of the roll (arc of contact equation) and its effect on the calculations especially on the grid generation.

٥. The location of the neutral point variation may be taken into account and determining its effect on the behavior of heat generation by friction and deformation and on the temperature distribution.

٦. Suggestion a method to study the method experimentally.

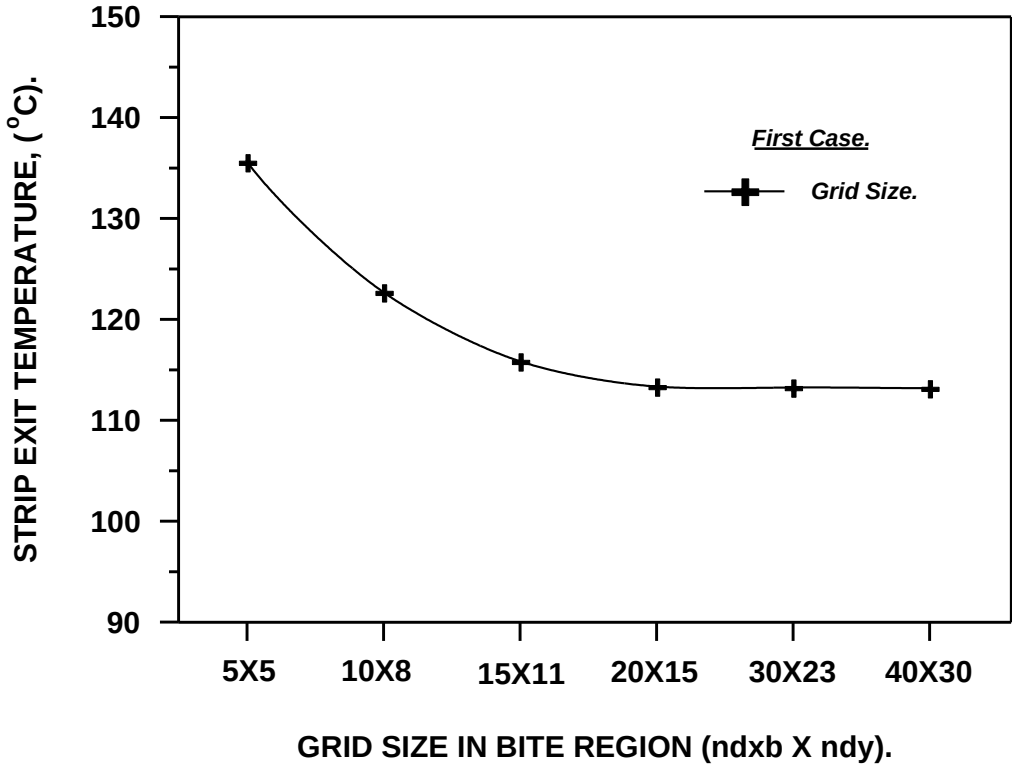

Fig. (٥-١): Effect of the Grid Size on the Numerical Solution.

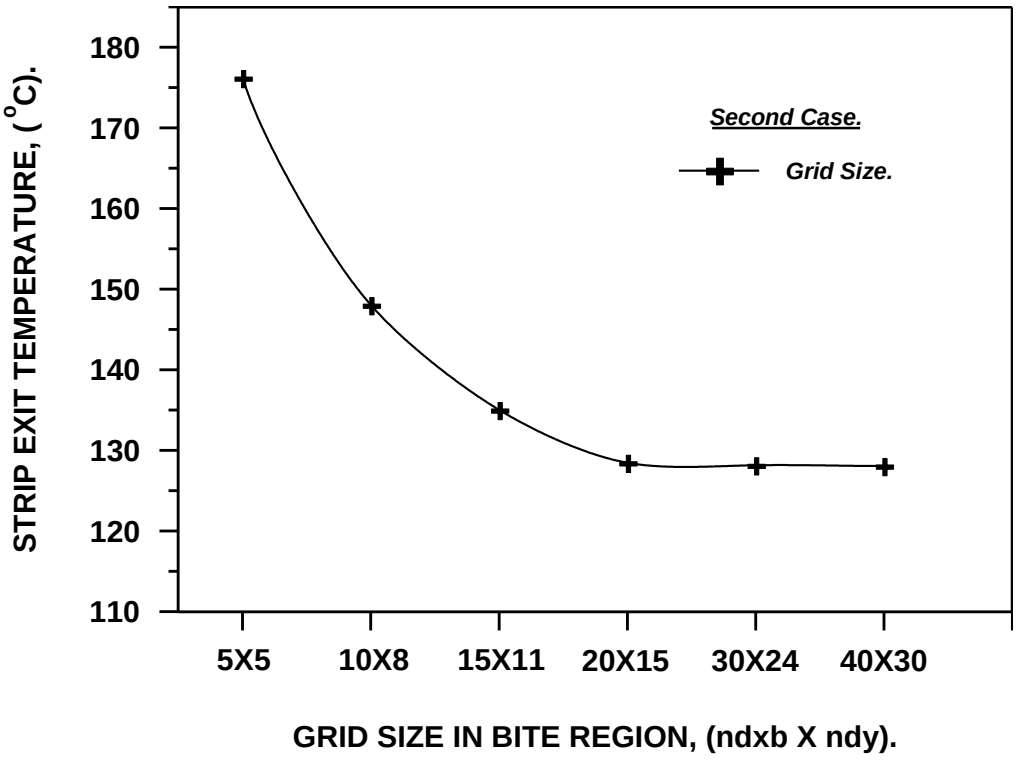

Fig. (٥-٢): Effect of the Grid Size on the Numerical Solution.

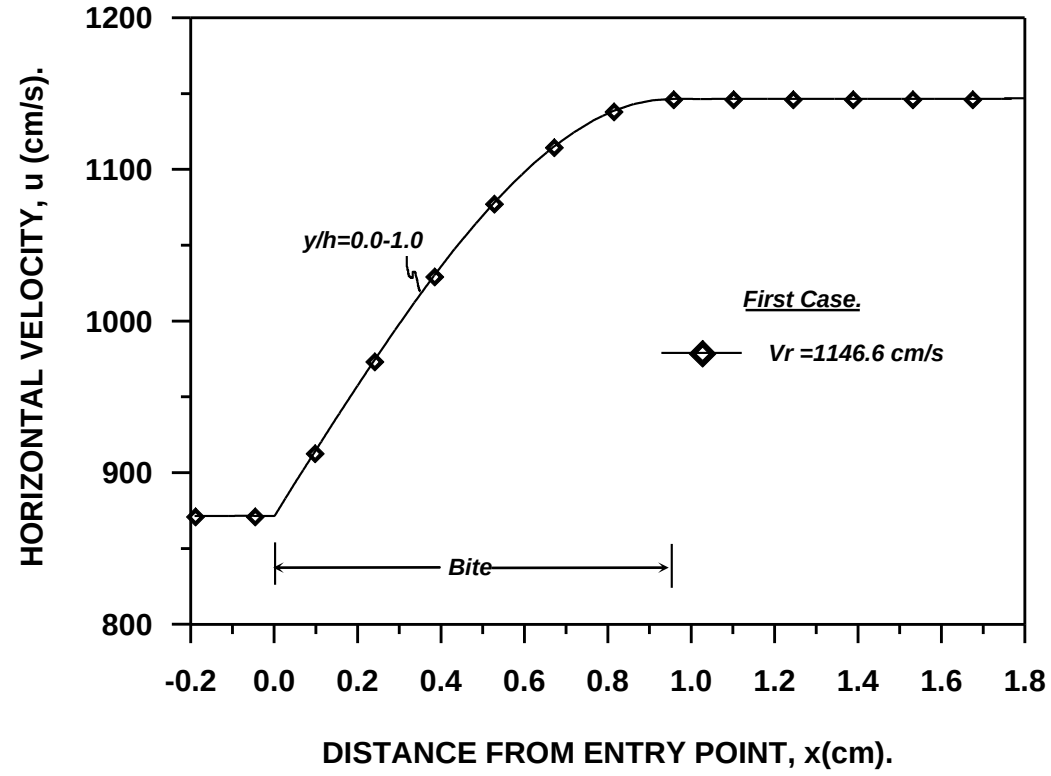

Fig. (٥-٣): Horizontal Component of Strip Velocity.

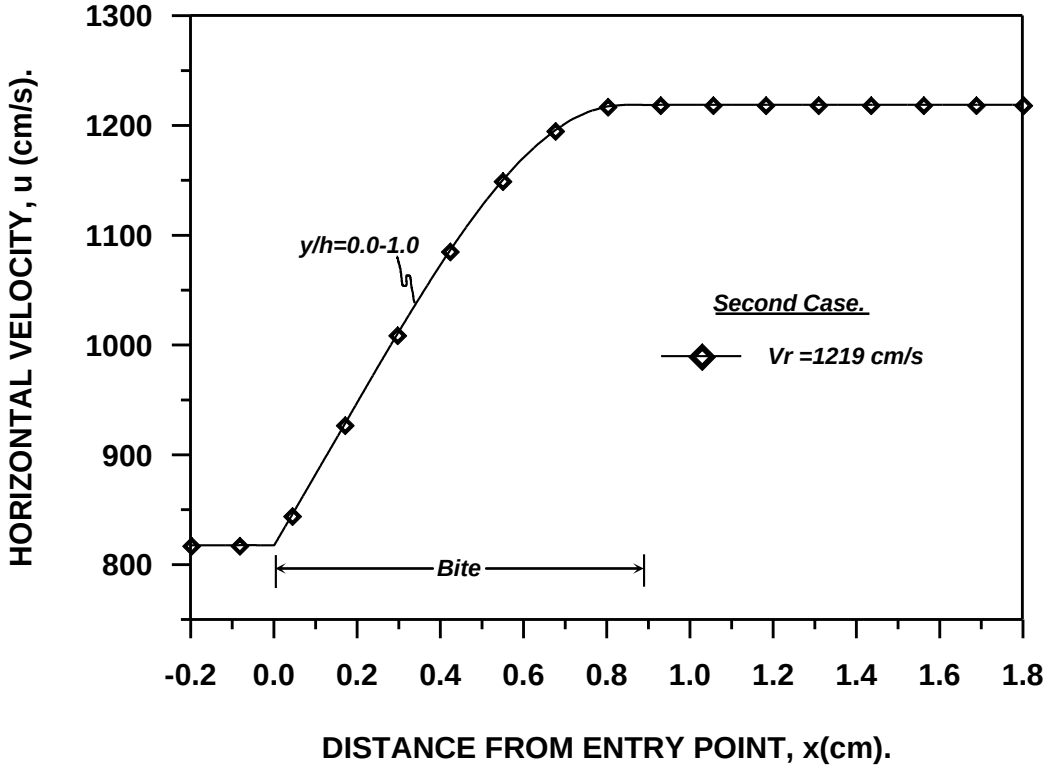

Fig. (٥-٤): Horizontal Component of Strip Velocity.

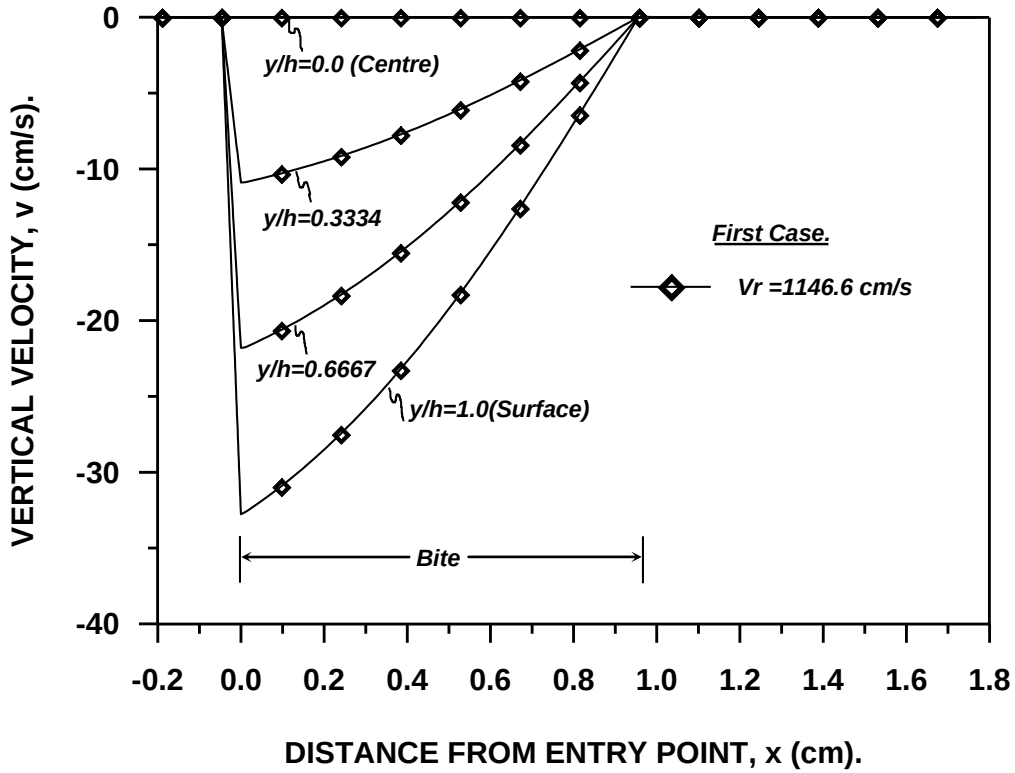

Fig. (٥-٥): Vertical Component of Strip Velocity.

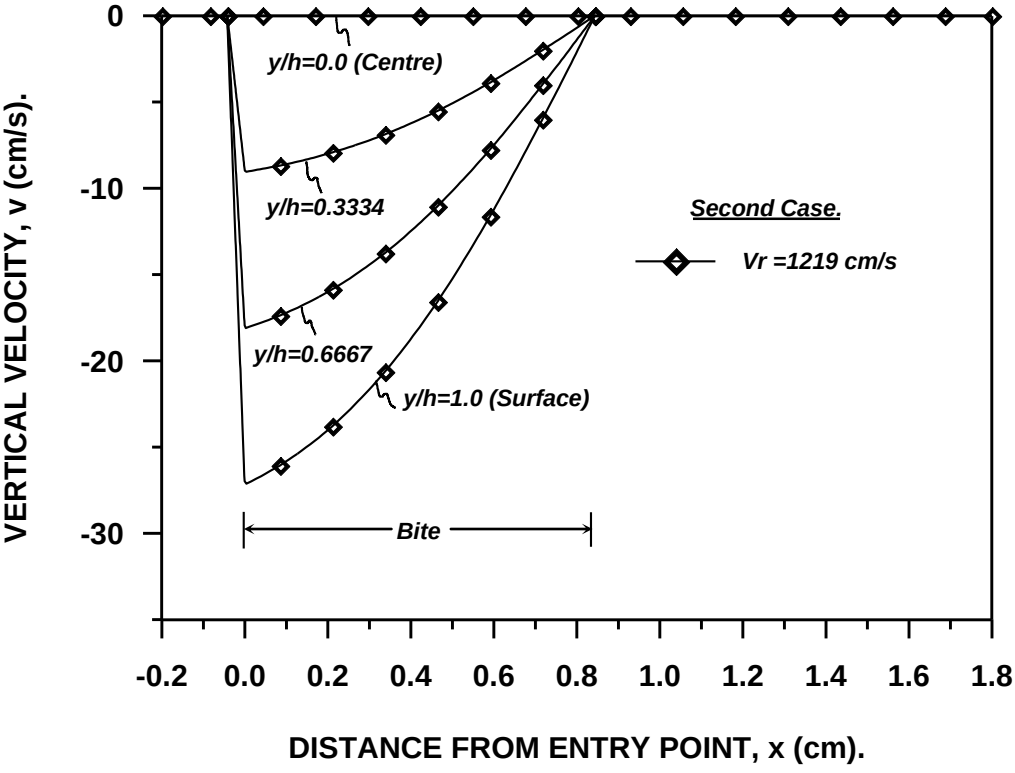

Fig. (٥-٦): Vertical Component of Strip Velocity.

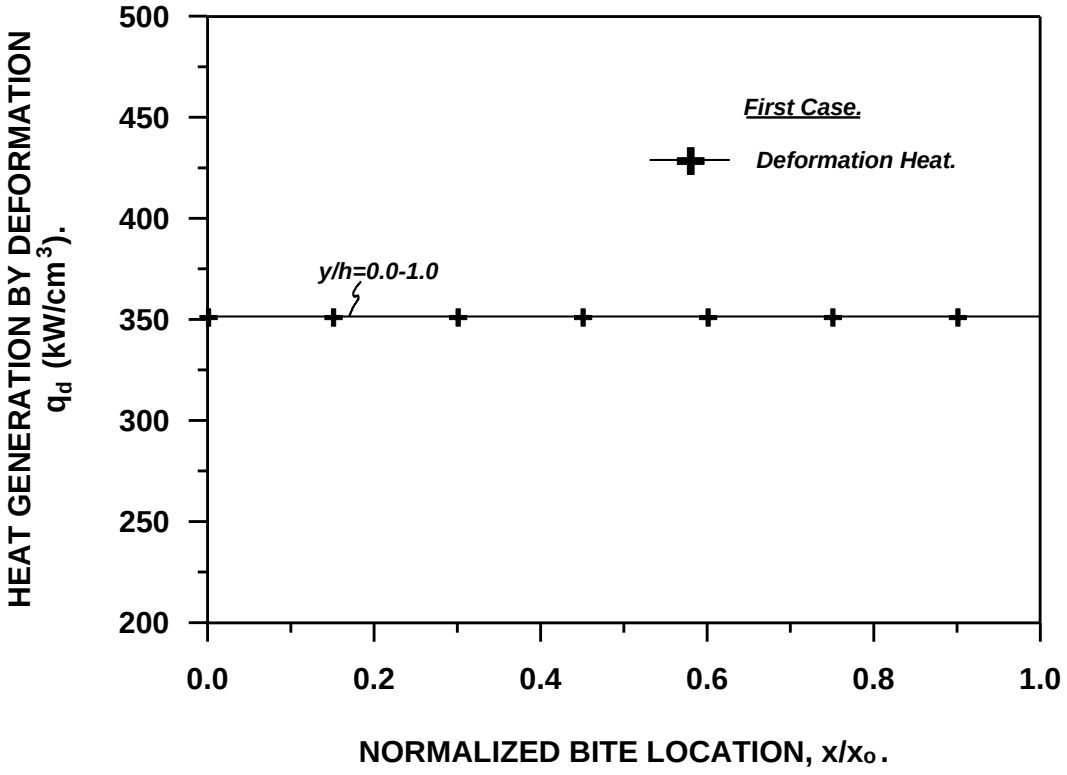

Fig. (٥-٧): Uniform Heat Generation by Deformation.

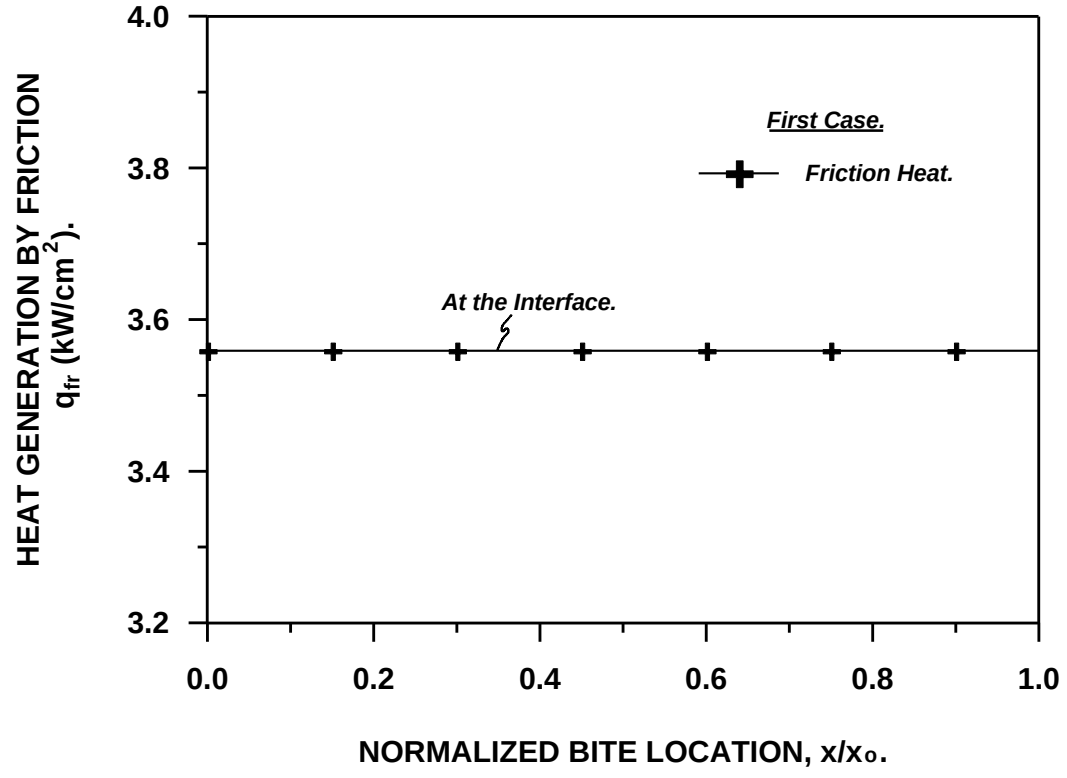

Fig. (٥-٨): Uniform Heat Generation by Friction.

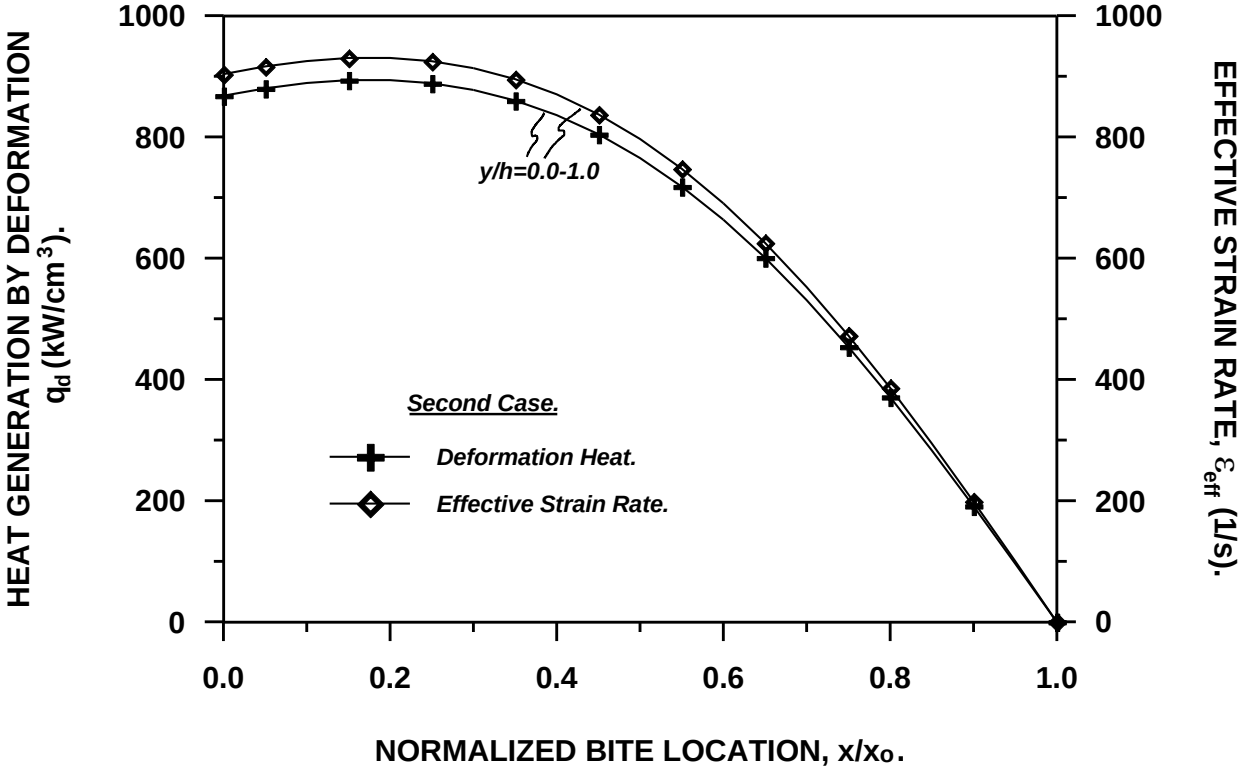

Fig. (٥-٩): Effective Strain Rate and Heat Generation by Deformation.

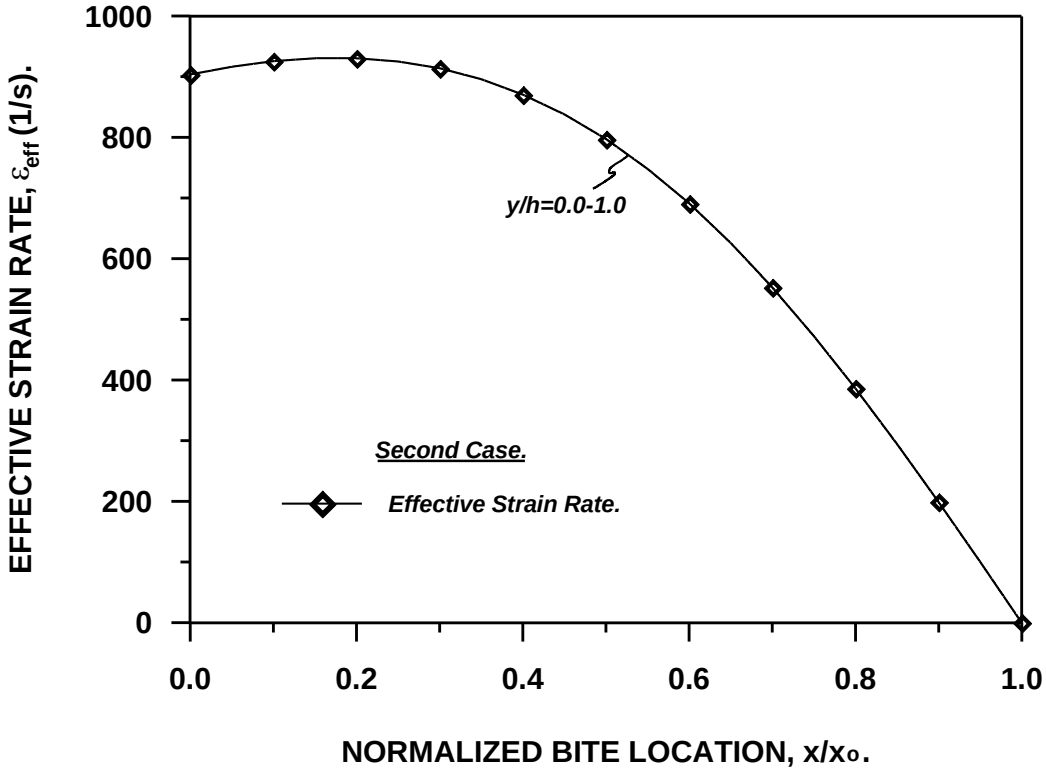

Fig. (٥-١٠): Effective Strain Rate.

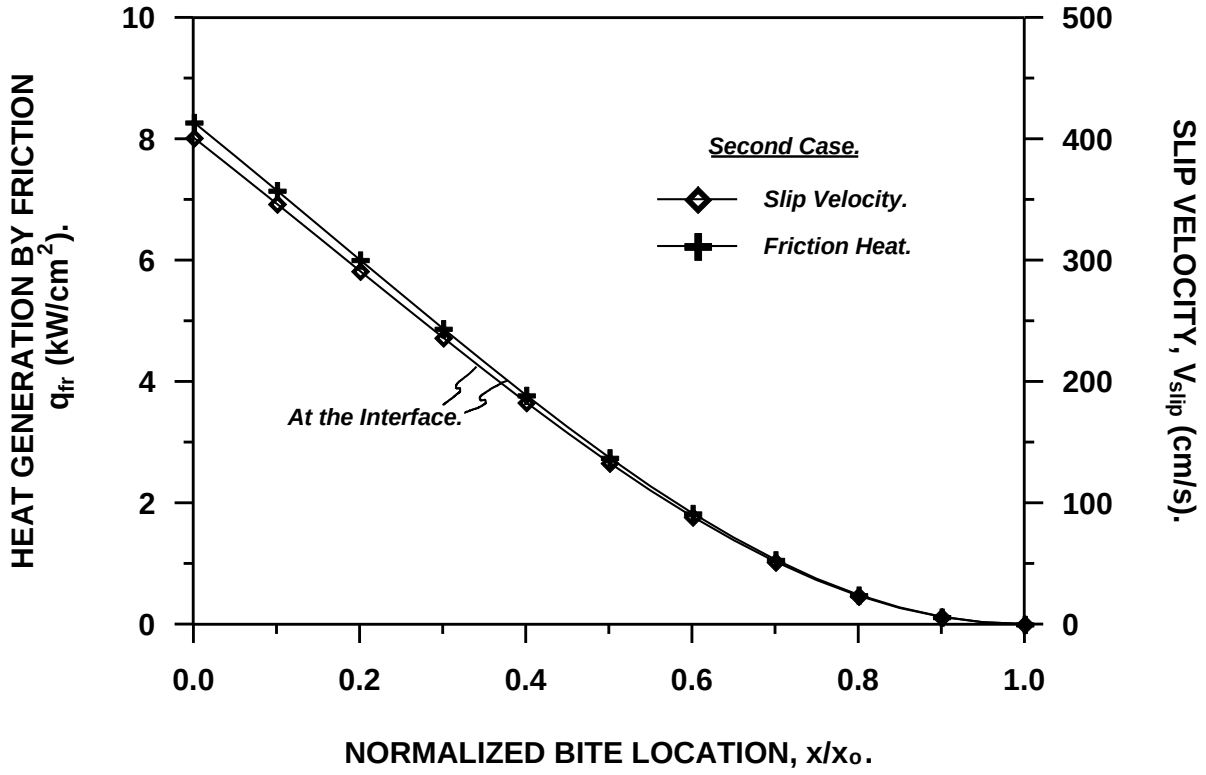

Fig. (٥-١١): Slip Velocity and Heat Generation by Friction.

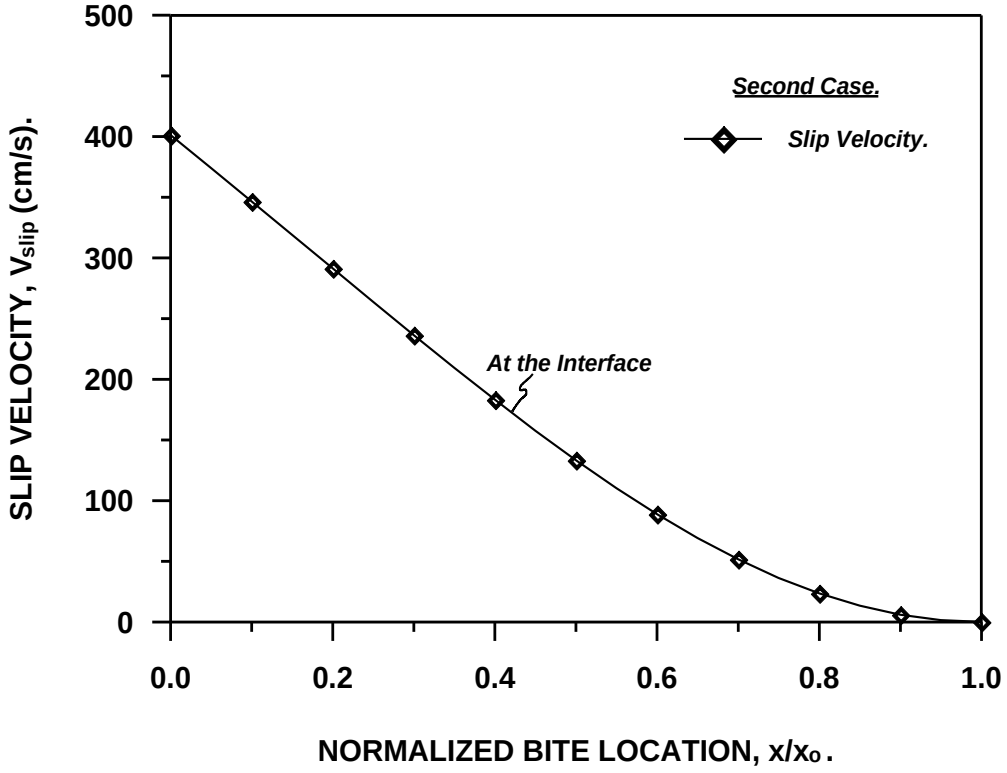

Fig. (٥-١٢): Slip Velocity at the interface.

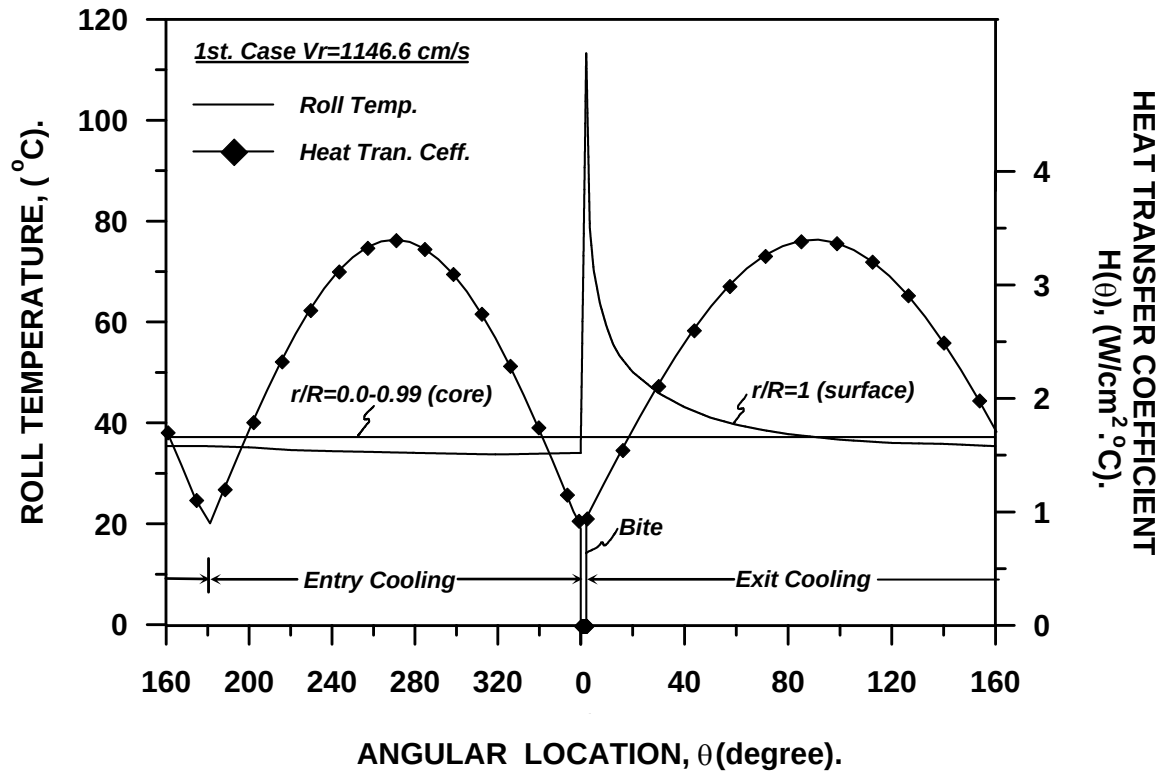

Fig. (٥-١٣): Heat Transfer Coefficient and Roll Temperature for Cold Rolling Case.

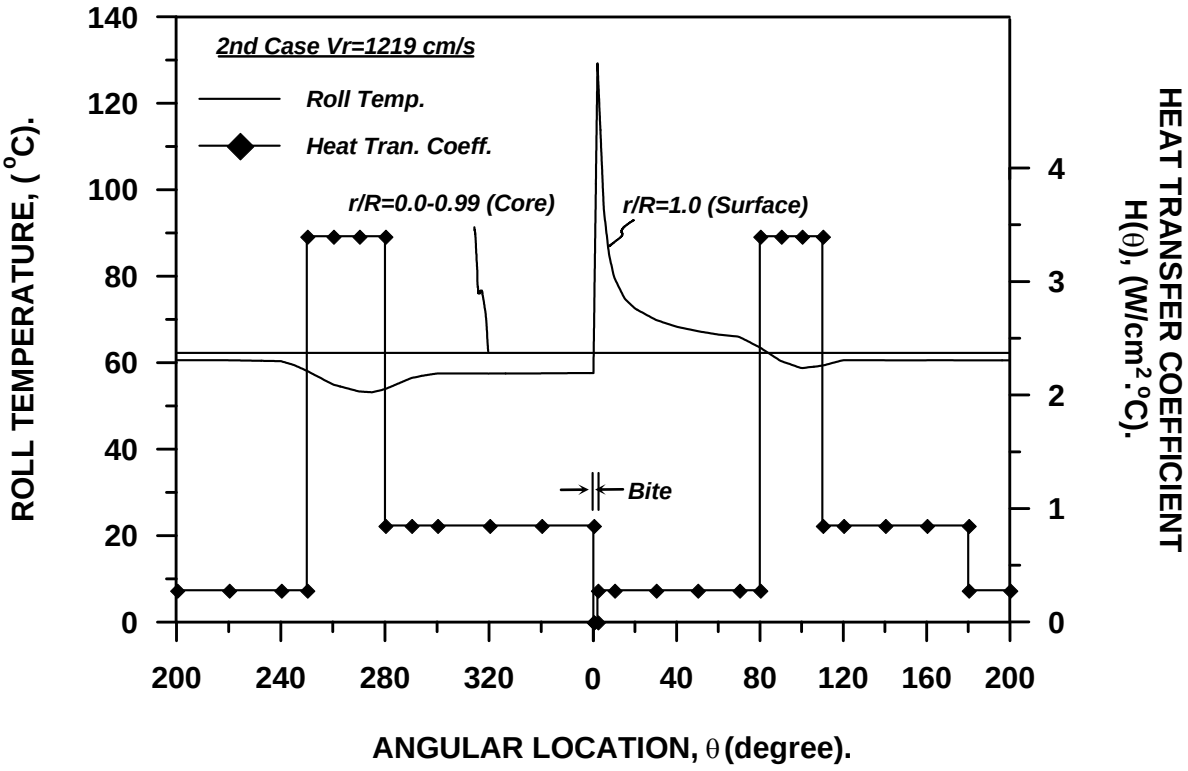

Fig. (٥-١٤): Heat Transfer Coefficient and Roll Temperature for Cold Rolling Case.

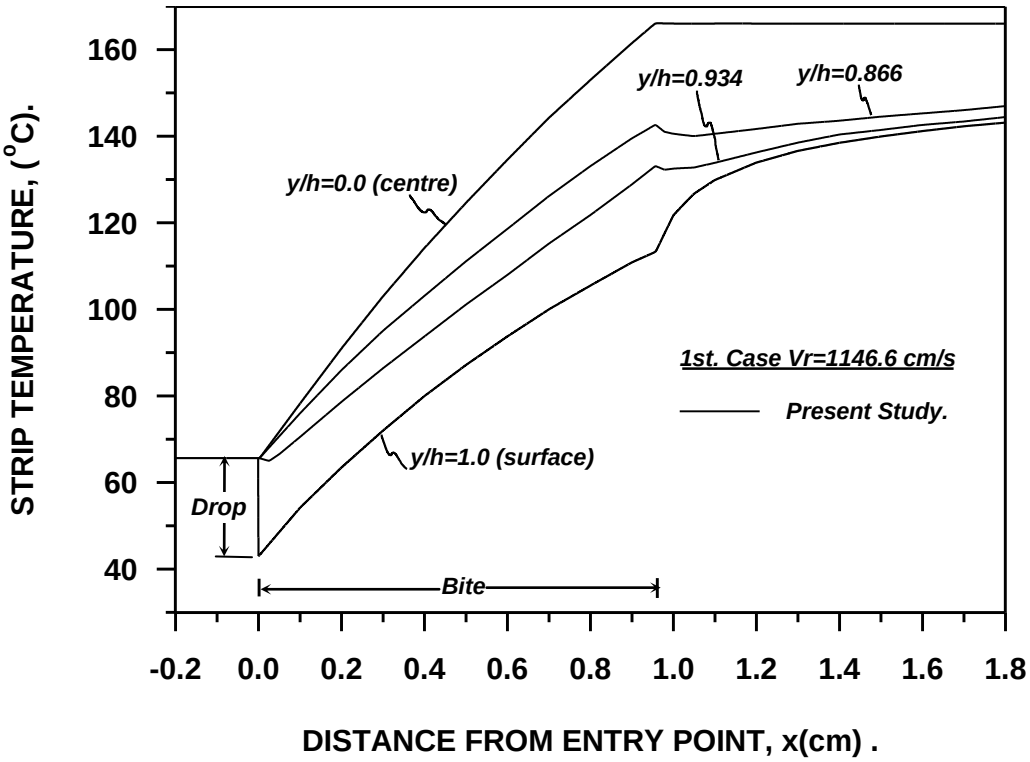

Fig. (٥-١٥): Strip Temperature for Cold Rolling Case.

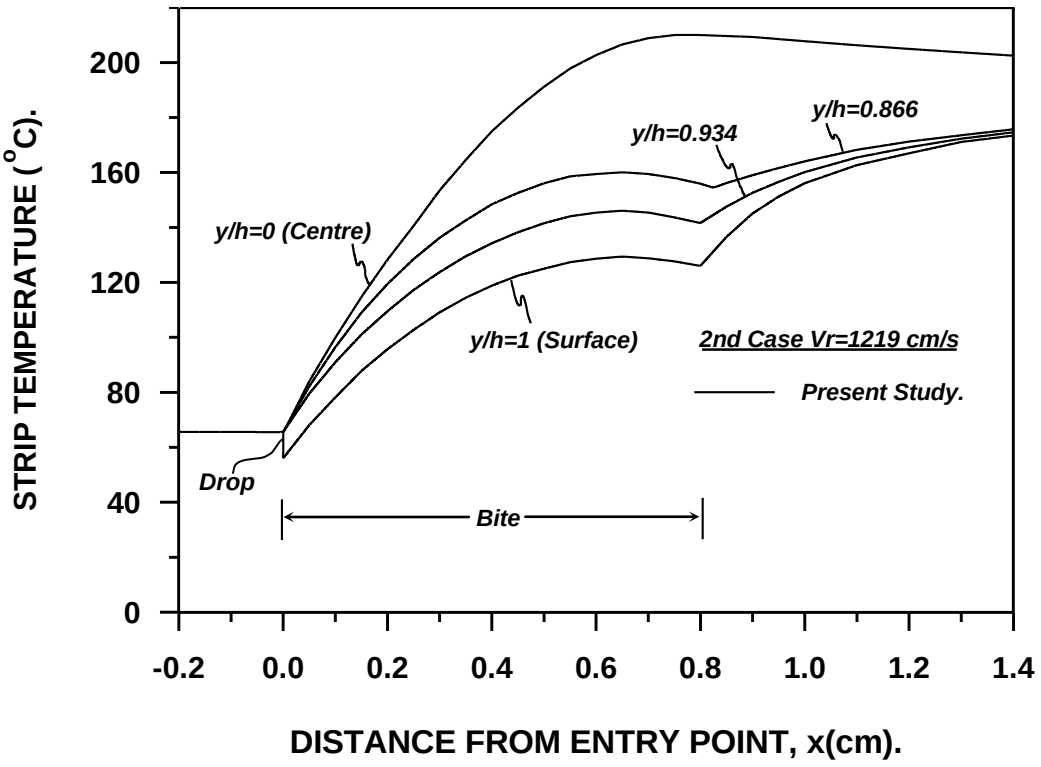

Fig. (٥-١٦): Strip Temperature for Cold Rolling Case.

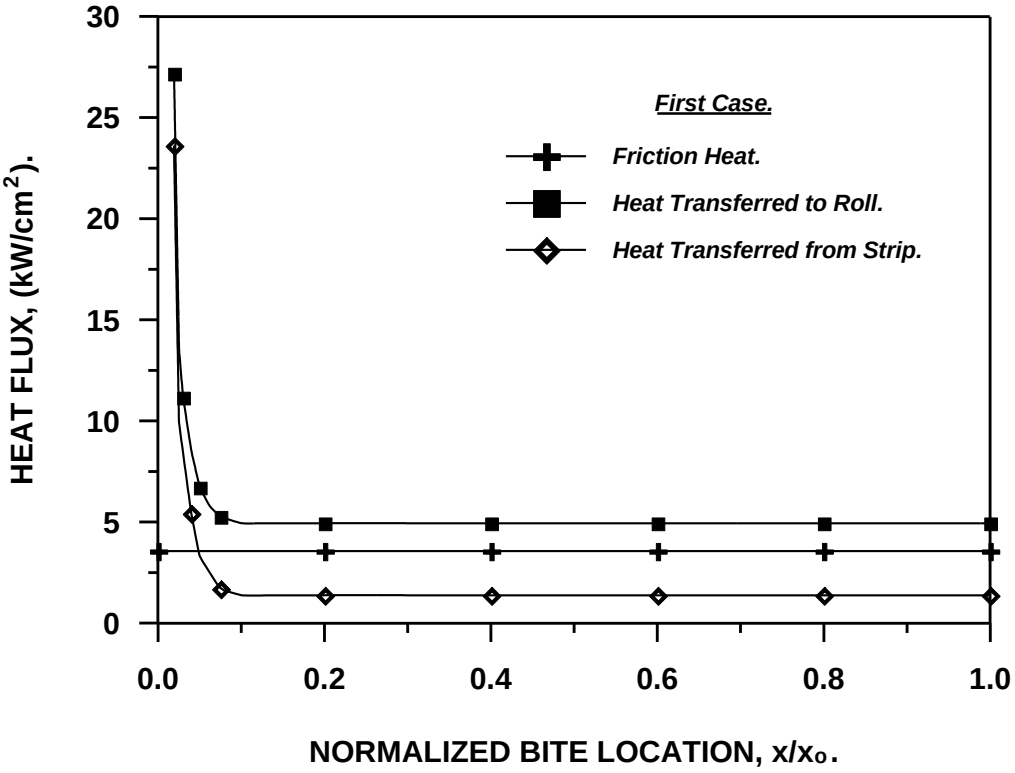

Fig. (٥-١٧): Distributions of the Interface Heat Flux.

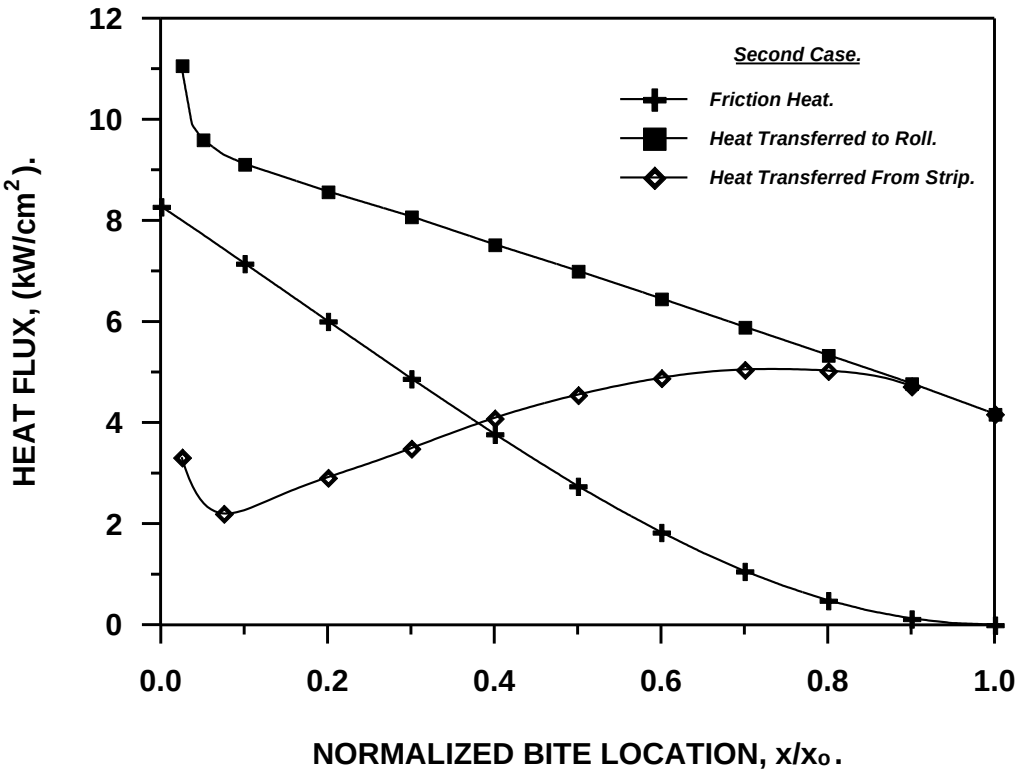

Fig. (٥-١٨): Distributions of the Interface Heat Flux.

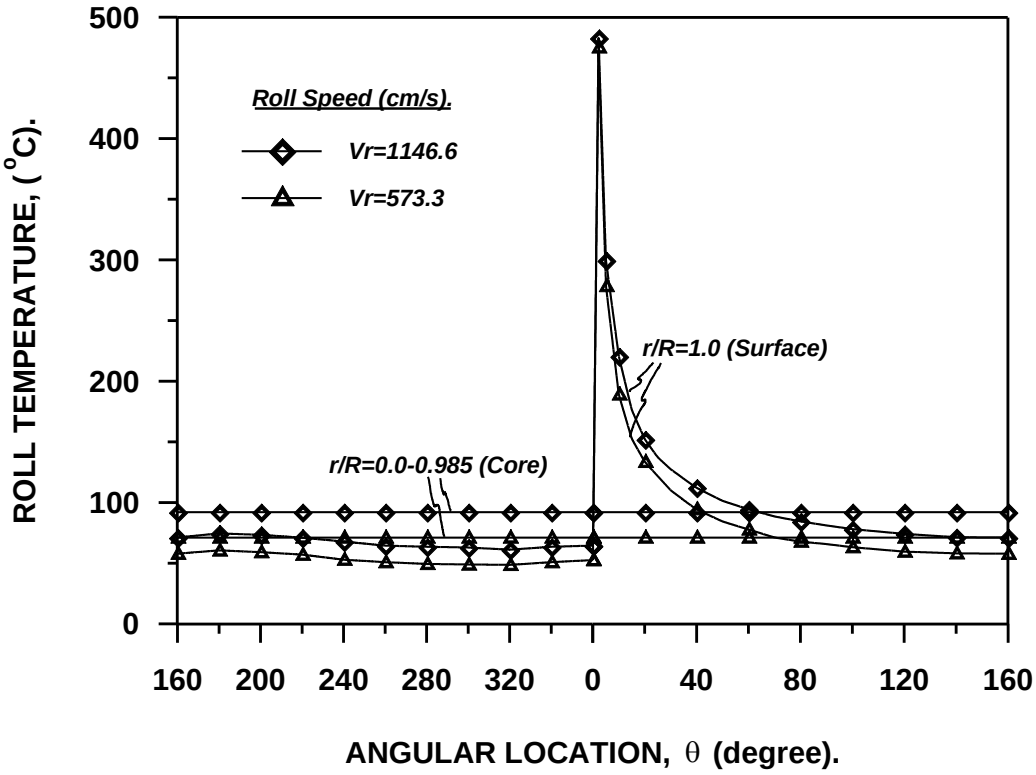

Fig. (٥-١٩): Roll Temperature for Hot Rolling Cases.

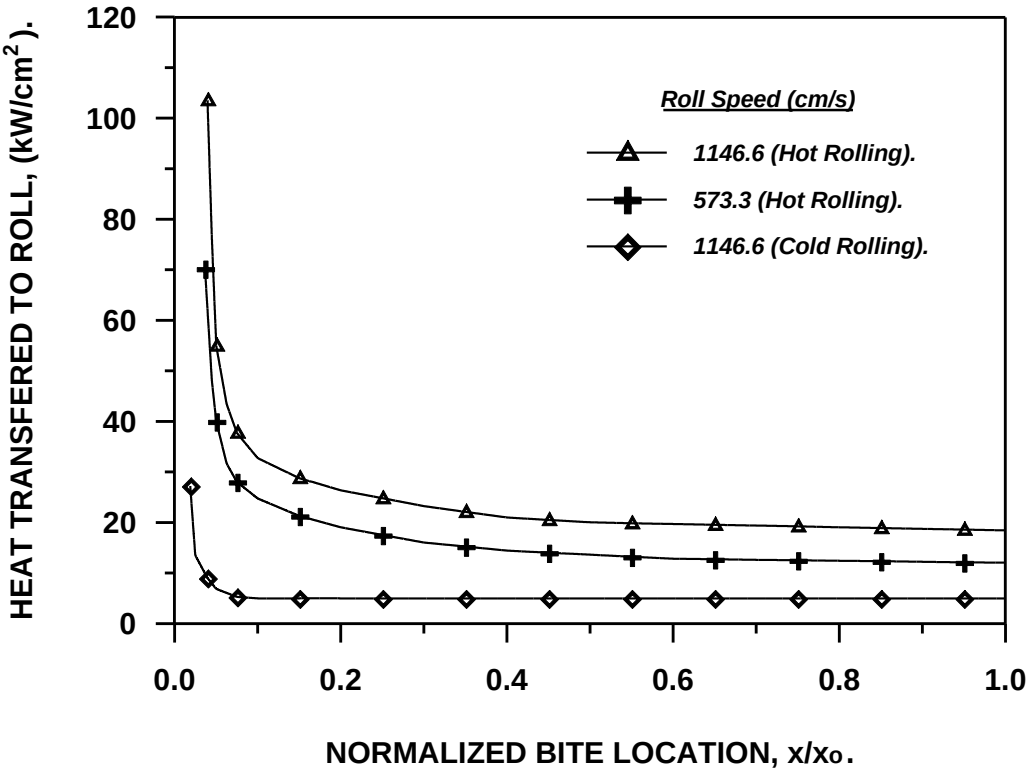

Fig. (٥-٢٠): Distributions of the Interface Heat Flux to Roll.

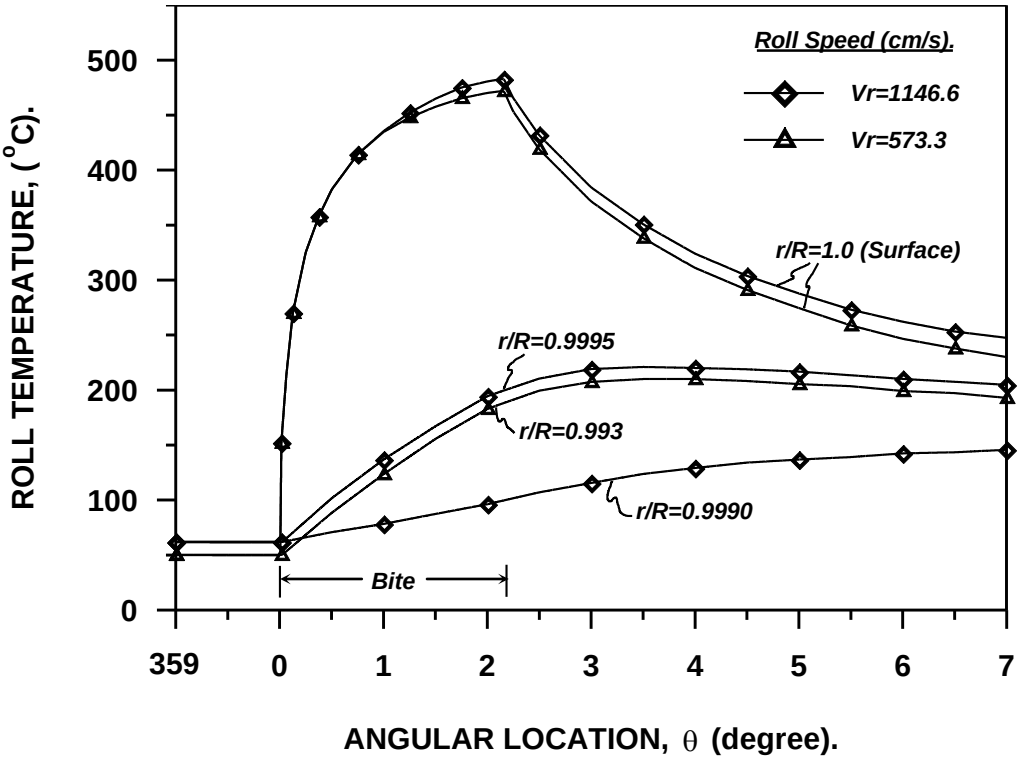

Fig. (٥-٢١): Roll Temperature near the Bite for Hot Rolling Cases.

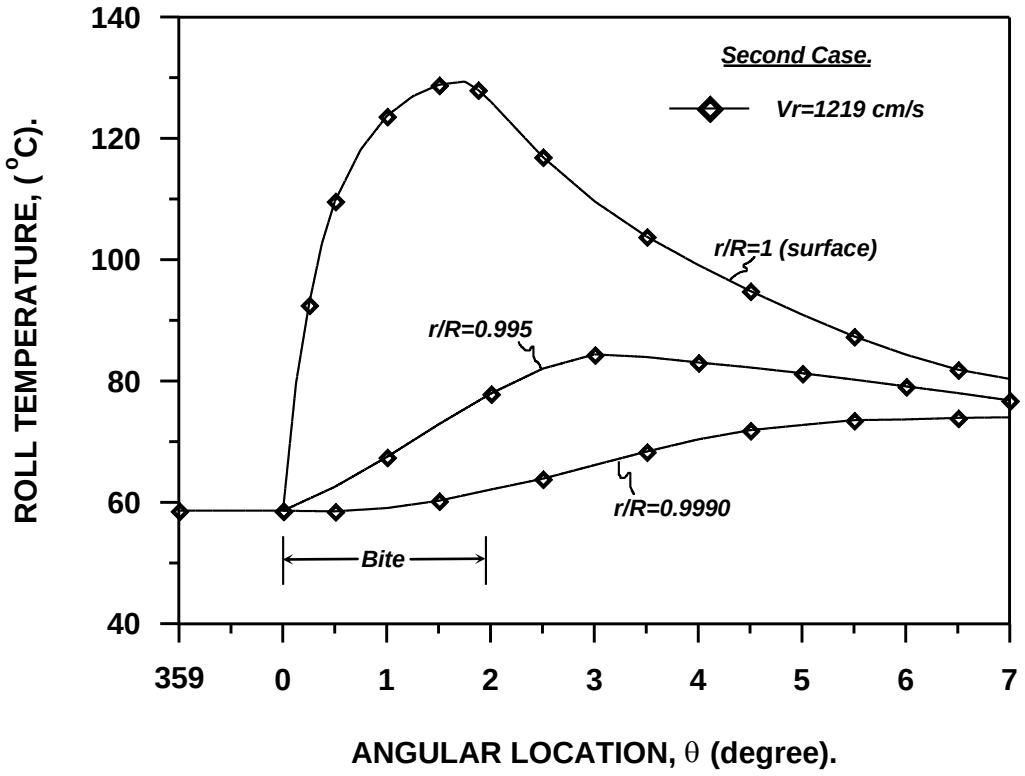

Fig. (٥-٢٢): Roll Temperature near the Bite for Cold Rolling Case.

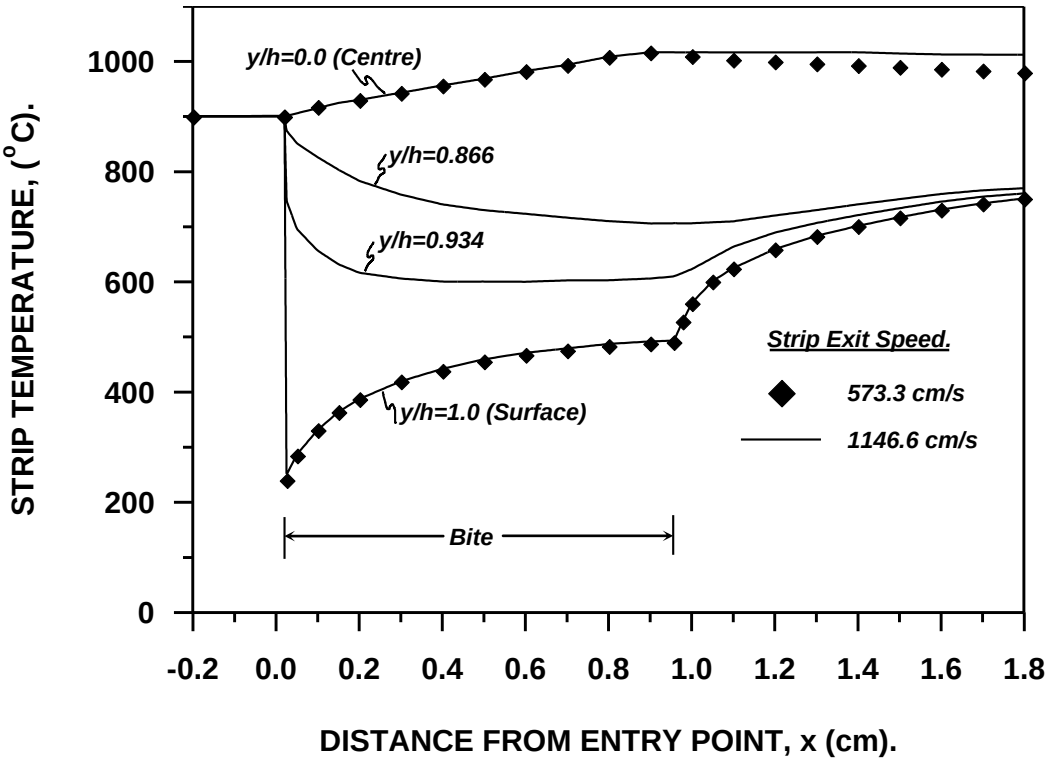

Fig. (٥-٢٣): Strip Temperature for Hot Rolling Cases.

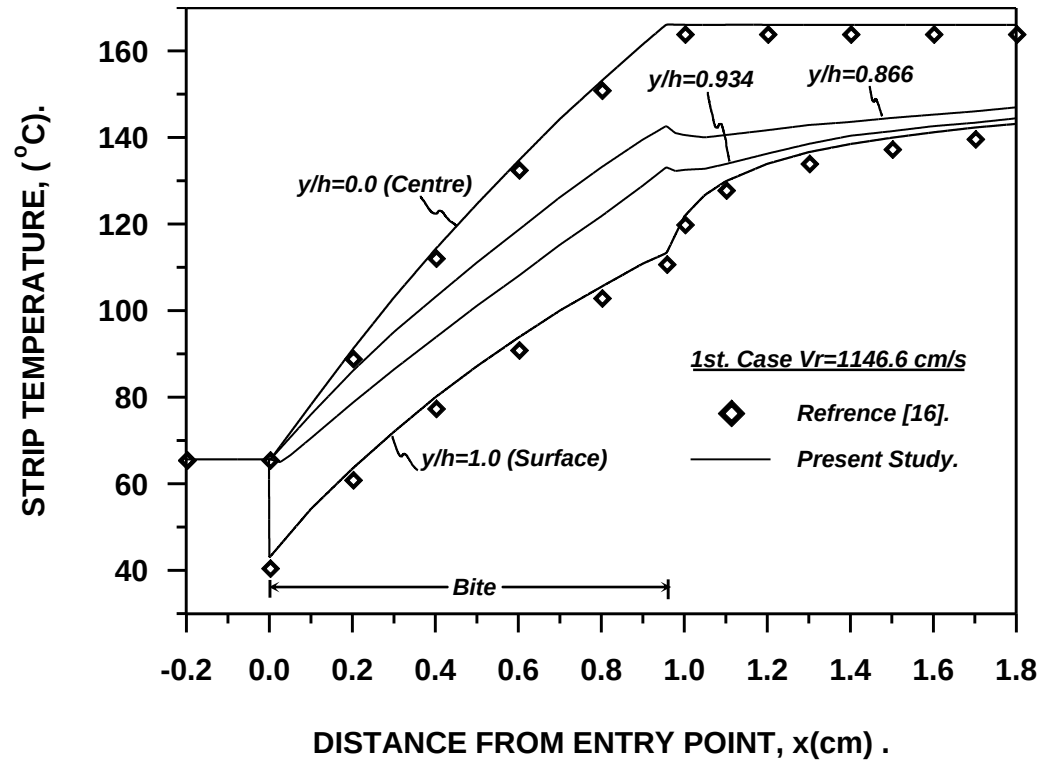

Fig. (٥-٢٤): Comparison of the Strip Temperature for Cold Rolling.

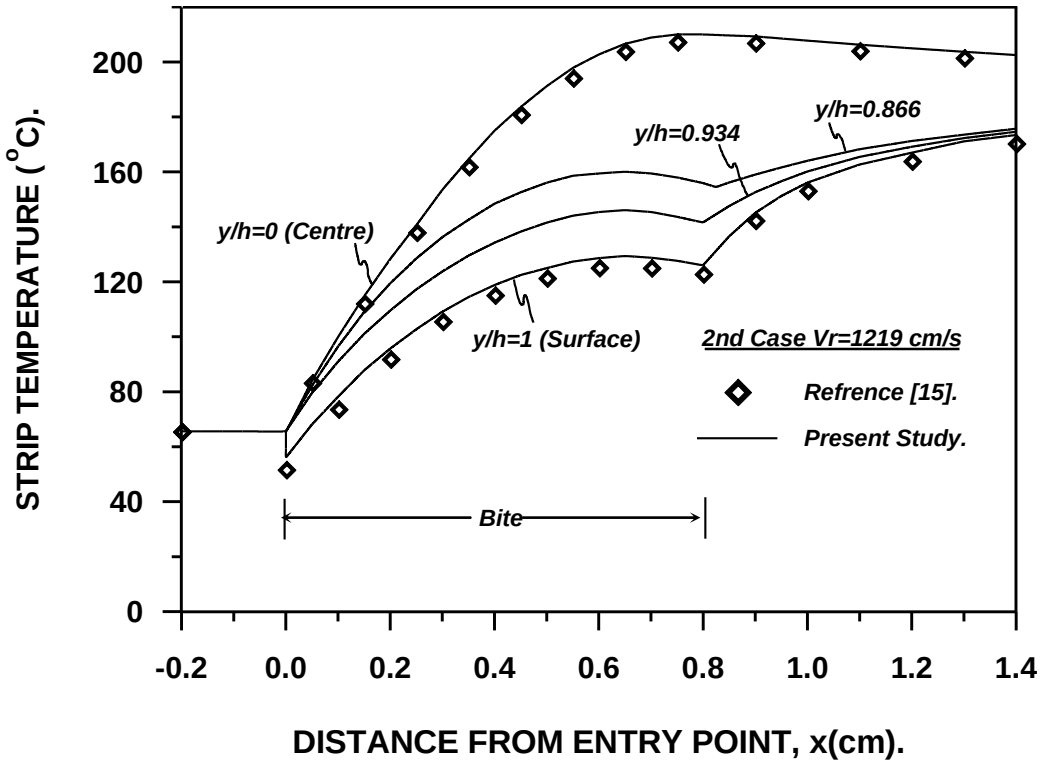

Fig. (٥-٢٥): Comparison of the Strip Temperature for Cold Rolling.

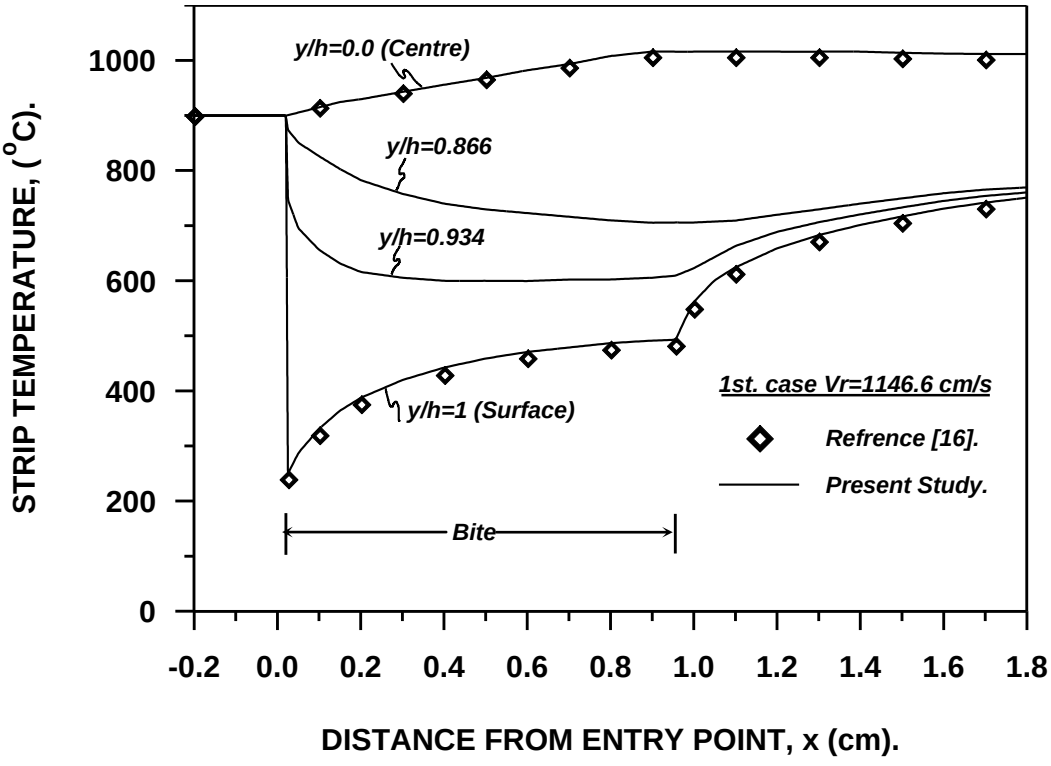

Fig. (٥-٢٦): Comparison of the Strip Temperature for Hot Rolling.

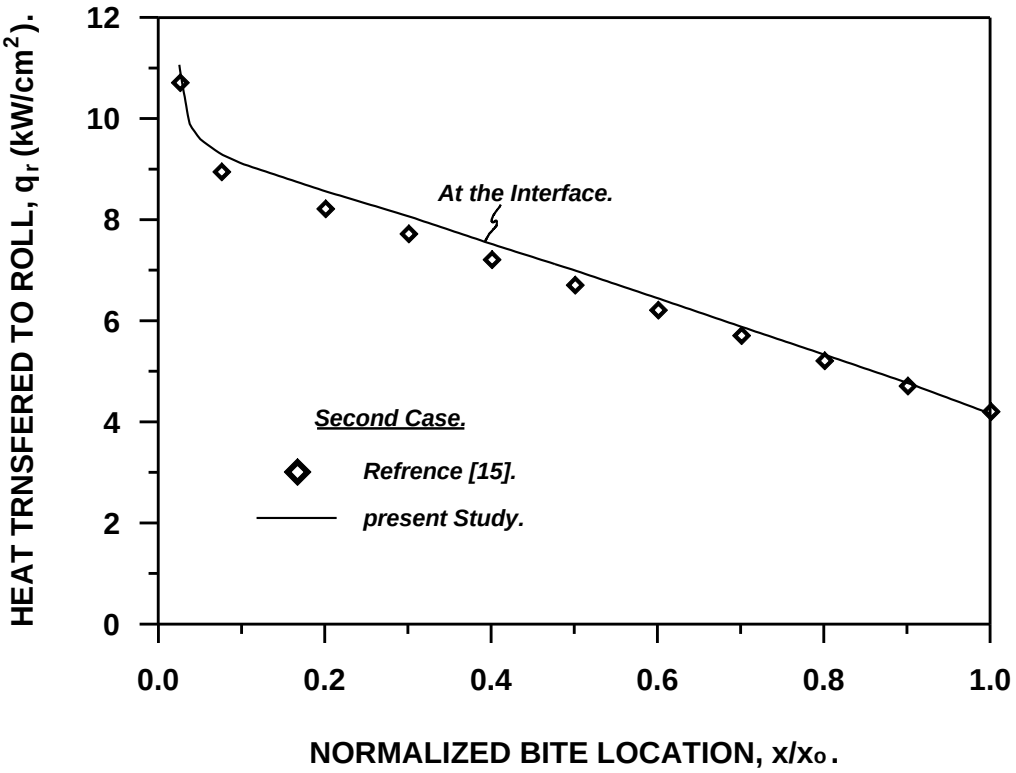

Fig. (٥-٢٧): Comparison of the Heat Transferred to Roll for Cold Rolling.

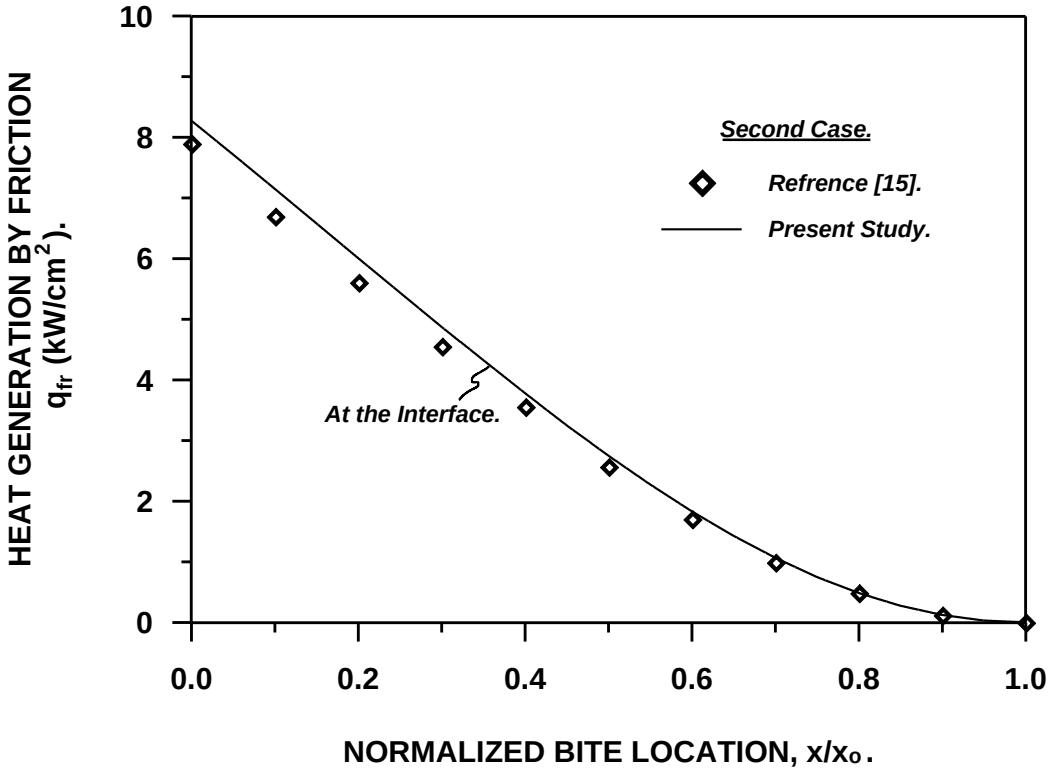

Fig. (٥-٢٨): Comparison of the Heat Generation by Friction for Cold Rolling.

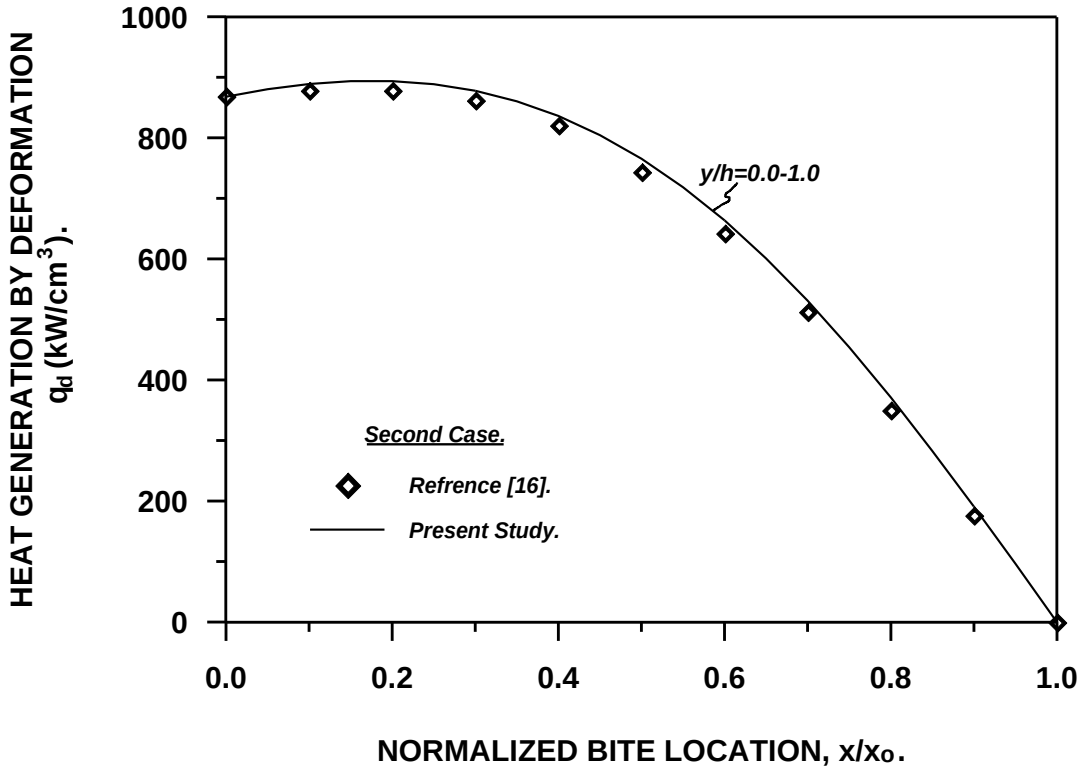

Fig. (٥-٢٩): Comparison of the Heat Generation by Deformation for Cold Rolling.

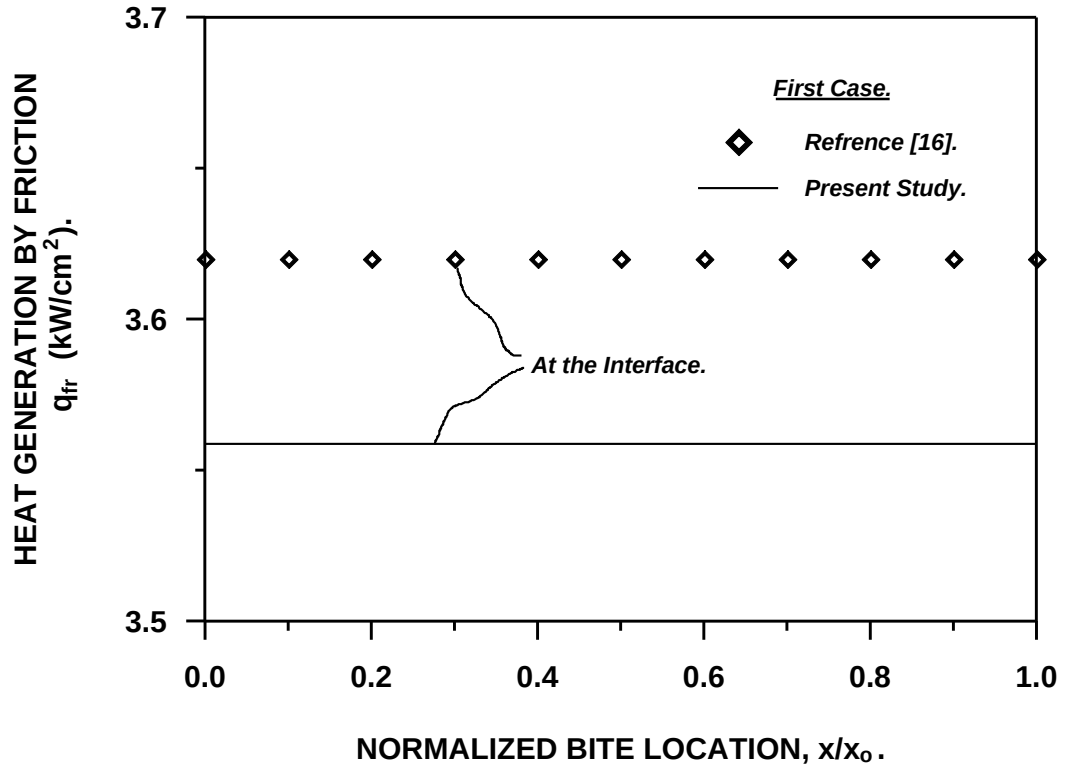

Fig. (٥-٣٠): Comparison of the Heat Generation by Friction for Cold Rolling.

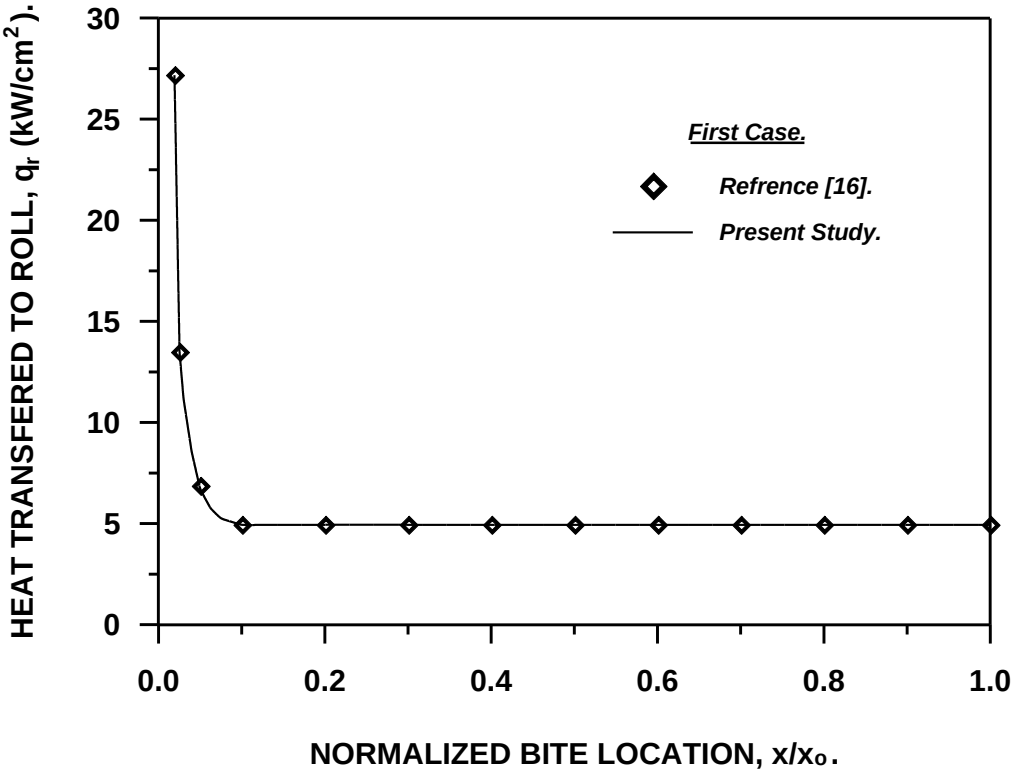

Fig. (٥-٣١): Comparison of the Heat Transferred to the Roll for Cold Rolling.

References

١. Dieter, "*Metals Metallurgy*," Mc Graw-George, E-Hill Book, Dieter company, Third addition, ١٩٨٦.

٢. Guo, J. L. and Kobayashi, S., "*Rigid-Plastic Finite Element Analysis of Plain Strain Rolling*," ASME, Journal of Engineering for Industry, ١٩٨٢, Vol. ١٠٤, pp.٥٥-٦٤.

٣. Lahoti, G. D., Shah S. N. and Altan, T., "*Computer Aided Heat Transfer Analysis of the Deformation and Temperatures in Strip Rolling*," ASME, Journal of Engineering for Industry, ١٩٧٨, Vol. ١٠٠, pp. ١٥٩-١٦٦.

٤. Remn-Min Guo, " *Two Dimensional Transient Thermal Behavior of Work Rolls*," ASME, Journal of Manufacturing Science and Technology, ١٩٩٨, Vol. ١٢٠, pp. ٢٨-٣٣.

٥. Lahoti, G. D. and Altan, T., "*Predication of the Temperature Distribution in Axi-Symmetric Compression and Torsion*," ASME, Journal of Engineering Materials and Technology, ١٩٧٥, Vol. ٩٧, pp.١١٣-١٢٠.

٦. Karagiozis, A. N. and Lenard, J. G., "*Temperature Distribution in A Slab During Hot Rolling*," ASME, Journal of Engineering Materials and Technology, ١٩٨٨, Vol. ١١٠, pp.١٧-٢١.

٧. Johnson, W. and Kudo, H., "*The Use of Upper-Bound Solutions for the Determination of Temperature Distributions in Fast Hot Rolling and Axi-Symmetric Extrusion Process,"* International Journal of Mechanical Science, ١٩٦٠, Vol. ١, PP. ١٧٥-١٩١.

٨. Cornfield, G. C. and Johnson, R. H., "*Theoretical Predications of Plastic Flow in Hot Rolling Including the Effect of the Various Temperature Distributions*," Journal of Iron and Steel Institute, ١٩٧٣, Vol.٢١١, pp. ٥٦٧-٥٧٣.

٩. Sheppard, T. and Wright, D. S., "*Structural and Temperature Variations During Rolling of Aluminum Slabs*," Metals Technology, ١٩٨٠, Vol. ٧, pp. ٢٧٤-٢٨١.

١٠. Zienkiewicz, O. C., Onate, E. and Heinrich, J. C., "*A General Formulation for Coupled Thermal Flow of Metals Using Finite Elements*," International Journal for Numerical Method in Engineering, ١٩٨١, Vol. ١٧, pp. ١٤٩٧-١٥١٤.

١١. Patula, E. T., " *Steady-State Temperature Distribution in A Rotating Roll Subjected to Surface Heat Fluxes and Convective Cooling*," ASME, Journal of Heat Transfer, ١٩٨١, Vol. ١٠٣, pp. ٣٦-٤١.

١٢. Bryant, G. F. and Heselton, M. O., "*Roll Gap Temperature Models for Hot Mills*," Metals Technology, ١٩٨٢, Vol. ٩, pp. ٤٦٩-٤٧٦.

١٣. Bryant, G. F. and Chiu, T. S. L., "*Simplified Roll Temperature Model (Convective Model)*," Metals Technology, ١٩٨٢, Vol. ٩, pp. ٤٧٧-٤٨٤.

١٤. Bryant, G. F. and Chiu, T. S. L., "*Simplified Roll Temperature Model (Spray Cooling and Stress Effects)*," Metals Technology, ١٩٨٢, Vol. ٩, pp. ٤٨٥-٤٩٢.

١٥. Tseng, A. A., "*A Generalized Finite Difference Scheme for Convection Dominated Metal Forming Problems*," International Journal for Numerical Methods in Engineering, ١٩٨٤, Vol.٢٠, pp. ١٨٨٥-١٩٠٠.

١٦. Tseng, A. A., "*A Numerical Heat Transfer Analysis of Strip Rolling*," ASME, Journal of Heat Transfer, ١٩٨٤, Vol. ١٠٦, PP. ٥١٢-٥١٧.

١٧. Dadras, P. and Wells, W. R., " *Heat Transfer Aspects of Non-Isothermal Axi-Symmetric Upset Forging*," Journal of Engineering for Industry, ١٩٨٤, Vol. ١٠٦, pp. ١٨٧-١٩٥.

١٨. Tseng, A. A., Tong, S. X., Maslen, S. H. and Mills, J. J., " *Thermal Behavior of Aluminum Rolling*," ASME, Journal of Heat Transfer, ١٩٩٠, Vol. ١١٢, pp. ٣٠١-٣٠٨.

١٩. Chang, D. F., " *An Efficient Way of Calculating Temperatures in the Strip Rolling process*," ASME, Journal of Manufacturing Science and Engineering, ١٩٩٨, Vol. ١٢٠, pp. ٩٣-١٠٠.

٢٠. Lee, P. W., Sims, R. B. and Wright, H., *"A Method for Predicting Temperatures in Continuos Hot Strip Mills*," Journal of the Iron and Steel Institute, ١٩٦٣, Vol. ٢٠١, pp. ٢٧٠-٢٧٤.

٢١. Gecim, B. and Winer, W. O., "*Steady-State Temperature in a Rotating Cylinder Subjected to a Surface Heating and Cooling*," ASME, Journal of Tribology, ١٩٨٤, Vol. ١٠٦, pp. ١٢٠-١٢٧.

٢٢. Roberts, W. L., "*Cold Rolling of Steel*," Marcel Dekker, New York, ١٩٧٨.

٢٣. Yun, I. S., Wilson, W. R. D. and Ehmann, K. F., "*Chatter in the Strip Rolling Process, Part ١: Dynamic Model of Rolling*," ASME, Journal of Manufacturing Science and Engineering, ١٩٩٨, Vol. ١٢٠, pp. ٣٣٠-٣٣٦.

٢٤. Saeed, U. and Lenard, J. G., "*A Comparison of Cold Rolling Theories Based on Equilibrium Approach*," ASME, Journal of Manufacturing Science and Technology, ١٩٨٠, Vol. ١٠٢, pp. ٢٢٣-٢٢٨.

٢٥. Barber, J. R., "*The Conduction of Heat from Sliding Solids*," International Journal of Mass and Heat Transfer, ١٩٧٠, Vol. ١٣, pp. ٨٥٧-٨٦٩.

٢٦. Wilson, W. R. D. and Sheu, S., "*Real Area of Contact and Boundary Friction in Metal Forming*," International Journal of Mechanical Science, ١٩٨٨, Vol. ٣٠, pp. ٤٧٥-٤٨٩.

٢٧. Kannel, J. W. and Dow, T. A., "*The Evolution of Surface Pressure and Temperature Measurement Techniques for Use in the Study of Lubricant in Metals Rolling*," ASME, Journal of Lubrication Technology, ١٩٧٤, Vol. ٧, pp. ٦١١-٦١٦.

٢٨. Gopta, M. M. and Manohar, R. P., "*A Critique of a Second-Order Upwind Scheme for Viscous Flow Problem*," A.I.A.A. Journal, ١٩٧٨, Vol. ١٦, pp. ٧٥٩-٧٦١.

٢٩. Roach, P. J., "*Computational Fluid Dynamic*," Hermosa Publishers, Albuquerque, New Mexico, ١٩٧٢.

٣٠. Anderson, D. A., Tannehill, J. C. and Pletcher, R. H., "*Computational Fluid Mechanics and Heat Transfer*," Mc Graw-Hill, ١٩٨٤.

٣١. Liszka, T. and Orkisz, J., "*The Finite Difference at Arbitrary Irregular Grids and It's Application in Applied Mechanics*," Journal of Computers and Structure, ١٩٨٠, Vol. ١١, pp. ٨٣-٩٥.

٣٢. Perrone, N. and Kao, R., "*A General Finite Difference Method for Arbitrary Meshes*," Journal of Computers and Structure, ١٩٧٥, Vol. ٥, pp. ٤٥-٥٨.

٣٣. Chapra, S. C. and Canale, R. P., "*Numerical Method for Engineers*," WCB/Mc Graw-Hill, Third Edition, ١٩٩٨.